

**Design, Synthesis, and Biological Evaluation of
Selective Estrogen Receptor Modulator/Histone
Deacetylase Inhibitor Hybrid Drug Molecules**

Yufei Wang

Supervised by Dr. James Gleason

Department of Chemistry, McGill University

Montréal, Québec, Canada

December 2019

A thesis submitted to McGill University in partial fulfillment of the requirements of a
Master of Science

© Yufei Wang 2019

Table of Contents

Abstract	III
Resumé	V
Acknowledgements	VII
List of Figures	IX
List of Schemes	XI
List of Tables	XII
List of Abbreviations	XIII
Contributions of Authors	XVII
Chapter 1: Introduction	1
1.1 Breast Cancer and the Estrogen Receptor	2
1.1.1 Estrogen Receptor α	2
1.1.2 Structure of the Estrogen Receptor	3
1.1.3 Mechanism of Estrogen Receptor Signalling	5
1.2 Agonists and Antagonists of the Estrogen Receptor	6
1.2.1 Agonists	6
1.2.2 Selective Estrogen Receptor Modulators	10
1.2.3 Selective Estrogen Receptor Downregulators	13
1.3 Endocrine Resistance in Breast Cancer	15
1.4 Histone Deacetylase and Breast Cancer	16
1.4.1 Structure and Function of Histone Deacetylases	16
1.4.2 Histone Deacetylase Inhibitors and Breast Cancer	19
1.5 Hybrid Molecules	21
1.5.1 Previous Examples of Hybrid Drugs	22
1.5.2 Hybrid SERM/HDACi Molecules	24
Chapter 2: Design, Synthesis, and Biology of Hybrid Molecules	35
2.1 Strategies for Bifunctional Hybrid Molecules	35
2.2 Hybrid Design and Molecular Docking Using FITTED	38

2.3 Design of SERM/HDACi Hybrids	47
2.4 Synthesis of SERM/HDACi Hybrids	48
2.5 Biological Assays	66
2.5.1 Fluorogenic HDACi Assay	67
2.5.2 ER Assays	68
2.6 Biological Activity and Discussion	69
2.6.1 HDAC inhibition	69
2.6.2 ER antagonism	74
2.7 Summary and Conclusions	75
Chapter 3: Experimental Procedures	80
3.1 Chemical Syntheses	80
3.2 HDAC Assay Protocol	117
3.3 ER Assay Protocols	119

Abstract

The prognosis for those diagnosed with breast cancer has dramatically improved since the 1980's, primarily due to improved diagnostic and treatment methods. One such treatment is a class of drugs called selective estrogen receptor modulators (SERMs). SERMs are a popular treatment option for breast cancer, commonly employed as adjuvant therapy. Prototypical examples of SERMs are tamoxifen and raloxifene.

Despite their widespread success, breast cancers can often develop resistance to SERMs. As a result, other biological targets which may mitigate this resistance have been identified. Recent interest in the field has arisen around histone deacetylases (HDACs), which are a class of enzymes that have been implicated in promoting resistance in breast carcinoma. Studies have demonstrated the combination treatment of SERMs and HDAC inhibitors (HDACi's) elicits a cooperative effect in enhancing cytotoxicity and resensitizing resistant breast cancers. In an effort to maximize the cooperative effects of SERMs and HDACi's, the project detailed in this thesis describes the design, synthesis, and biological evaluation of a series of hybrid raloxifene/HDACi molecules that combine the pharmacophores of both drug classes.

Previous work by the Gleason laboratory found tamoxifen/HDACi hybrids to exhibit potent biological activity, but further exploration of these would be laborious due to their inherent instability. As a result, a synthesis of raloxifene/HDACi hybrids was developed. Significant synthetic challenges resulted from the comparatively electron-deficient nature of key intermediates, making known methods used for raloxifene inapplicable towards these targets. After notable route scouting and reaction optimization, these challenges were resolved and a small library of seven hybrid drug molecules were successfully synthesized and purified prior to biological evaluation.

Fluorogenic HDACi assays determined the IC_{50} values of the raloxifene/HDACi hybrids against HDAC1 and HDAC6. All hybrids demonstrated sub-micromolar IC_{50} values for HDAC1. For HDAC6, one hybrid showed low micromolar potency for HDAC6, while all others had sub-micromolar values. Generally, carbon-linked hybrids were more potent than oxygen-linked hybrids against HDAC1, while the reverse was true for HDAC6.

Preliminary biological assays performed by the Mader lab at the Université de Montréal demonstrate all hybrids antagonize the ER at a low micromolar dose, both in the presence and in the absence of E2. A more conclusive result of the SERM/HDACi hybrids can be drawn once further biological testing has been completed by the Mader lab.

Resumé

Le pronostic pour les personnes diagnostiquées avec un cancer du sein s'est considérablement amélioré depuis les années 1980, principalement en raison de l'amélioration des méthodes de diagnostic et de traitement. Un de ces traitements est une classe de médicaments appelés modulateurs sélectifs des récepteurs aux œstrogènes (MSROs). Les MSROs sont une option de traitement populaire pour le cancer du sein, couramment utilisée comme thérapie adjuvante. Des exemples prototypes de MSROs sont le tamoxifène et le raloxifène.

Malgré leur succès généralisé, les cancers du sein peuvent souvent développer une résistance aux MSROs. En conséquence, d'autres cibles biologiques susceptibles d'atténuer cette résistance ont été identifiées. Un intérêt récent dans le domaine est apparu autour des histones désacétylases (HDACs), qui sont une classe d'enzymes qui ont été impliquées dans la promotion de la résistance au cancer du sein. Des études ont démontré que le traitement combiné des MSROs et des inhibiteurs de HDAC (iHDAC) induit un effet coopératif pour augmenter la cytotoxicité et resensibiliser les cancers du sein résistants. Dans un effort pour maximiser les effets coopératifs des SERM et des iHDAC, le projet détaillé dans cette thèse décrit la conception, la synthèse et l'évaluation biologique d'une série de molécules hybrides raloxifène / iHDAC qui combinent les pharmacophores des deux classes de médicaments.

Des travaux antérieurs du laboratoire Gleason ont révélé que les hybrides tamoxifène / iHDAC présentent une activité biologique puissante, mais une exploration plus approfondie de ceux-ci serait laborieuse en raison de leur instabilité inhérente. En conséquence, une synthèse d'hybrides raloxifène / iHDAC a été développée. Des défis de synthèse importants ont résulté de la nature relativement déficiente en électrons des intermédiaires clés, rendant les méthodes connues utilisées pour le raloxifène inapplicables à ces cibles. Après un repérage notable des routes et une optimisation de la réaction, ces défis ont été résolus et une petite bibliothèque de sept molécules de médicaments hybrides a été synthétisée et purifiée avec succès avant l'évaluation biologique.

Les tests fluorogènes iHDAC ont déterminé les valeurs IC_{50} des hybrides raloxifène / HDACi contre HDAC1 et HDAC6. Tous les hybrides ont démontré des valeurs IC_{50} sous-micromolaires pour HDAC1. Pour HDAC6, un hybride a montré une faible puissance micromolaire pour HDAC6, tandis que tous les autres avaient des valeurs sous-micromolaires. En général, les hybrides liés au carbone étaient plus puissants que les hybrides liés à l'oxygène contre HDAC1, tandis que l'inverse était vrai pour HDAC6.

Les résultats préliminaires du laboratoire Mader de l'Université de Montréal démontrent que tous les hybrides antagonisent le récepteur d'oestrogène à la faible dose micromolaire, à la fois en présence et en l'absence d'estradiol. Un résultat plus concluant des hybrides SERM / HDACi peut être tiré une fois que d'autres tests biologiques ont été effectués par le laboratoire Mader.

Acknowledgements

I would first like to thank my supervisor, Dr. Jim Gleason for the opportunity to be a part of his research group, and for the patience and guidance he provided throughout my studies at McGill. His knowledge and passion for chemistry were incredibly influential. In fact, his lectures for CHEM 302 were one of reasons I was inspired to pursue chemistry further in graduate school. I am grateful to him for the invaluable skills that I gained during my graduate studies, not only pertaining to organic synthesis but in problem solving of all nature.

Funding from FRQNT is gratefully acknowledged. I would like to thank Dr. Nicolas Moitessier for letting me conduct research in his laboratory in the summer before I started graduate school, and for providing me access to the FITTED docking program during my graduate studies. Credit goes to Jessica Plesica for her mentorship during my time in the Moitessier lab and beyond. I would like to express my gratitude for Dr. Youla Tsantrizos for the instruments she made available to me, and members of the Tsantrizos lab for taking the time to show me how to use them. I truly appreciate Drs. Nadim Saade and Alex Wahba for their efforts in the mass spectrometry facility, and Drs. Robin Stein and Tara Sprules for their assistance in the NMR facility. A huge thank you goes to Chantal Marotte for always having an open door, reminding us about deadlines, and ensuring our paperwork is complete. I would like to thank my undergraduate supervisor, Dr. Paul Clarke for his kindness and wisdom, and for passing onto me valuable advice on scientific writing and statistics.

During my time in the Gleason lab, I have had the privilege to work alongside some incredibly bright and hard-working colleagues. I would like to thank Dr. Jonathon Hughes, Sam Plamondon, Josie Warnica, Donald Campbell, David Scarlata, and HyunJune Jun for everything they taught me. To the newer members of the lab, Anthony Izzotti and Zhizhong Gao, good luck in your graduate studies. I am grateful to Ryan Barrett for his help with the biological assays. Ali Mansour- thank you for always laughing at my jokes and listening to my stories. Lastly, I would like to thank Adam Elmehriki for being a great mentor and friend, and for always humouring my endless questions, whether it was about

chemistry, Marxist theory, personal finances, astrology, current affairs, or anything in between.

Of course, none of this would have been possible without the support of my parents, Shuqin Zhou and Minji Wang, from whom I first learned by example about hard work and sacrifice. I am forever indebted to you for providing me the opportunities you did not have. I am incredibly grateful to all the friends who kept my interests and hobbies outside of the lab alive. Finally, I would like to thank Gianni Pampagnin for his love and support, which was always inexhaustible, even when things were not easy.

List of Figures

Figure 1.1 Domains of the ER	4
Figure 1.2 Crystal structure PDB: 1ERE	4
Figure 1.3 Simplified classical ER signalling	6
Figure 1.4 Hypothalamus-pituitary-gonadotropin axis	7
Figure 1.5 Common ER agonists	8
Figure 1.6 PDB: 1ERE	9
Figure 1.7 PDB: 4ZN7	9
Figure 1.8 Raloxifene ER-binding mode	11
Figure 1.9 Tamoxifen ER-binding mode	12
Figure 1.10 Fulvestrant and ICI-164,384	13
Figure 1.11 PDB: 1HJ1	14
Figure 1.12 HAT/HDAC cooperative opposition	16
Figure 1.13 Structure of SAHA and TSA	17
Figure 1.14 HDAC catalytic channel	19
Figure 1.15 HDAC inhibition leading to tumour death	20
Figure 1.16 Triceferol	22
Figure 1.17 SERMostat	24
Figure 1.18 Previous 4-OHT/HDACi C- and A-ring hybrids by the Gleason lab	26
Figure 1.19 Potent B-ring substituted analogues	27
Figure 1.20 4-OHT/HDACi vs. raloxifene/HDACi hybrid	28
Figure 2.1 Comparison of 4-OHT and raloxifene	36
Figure 2.2 Raloxifene/HDACi hybrids	37
Figure 2.3 FITTED virtual library	39
Figure 2.4 Rank scores for PDB: 1ERA	40
Figure 2.5 Docking pose of YW13-Ben with PDB:1ERa	41
Figure 2.6 Sensical docking poses with PDB:1ERa	42
Figure 2.7 Rank scores for PDB: 4LXZ	42
Figure 2.8 Docking poses with PDB:4LXZ	43

Figure 2.9 Rank scores for PDB: 5EDU	44
Figure 2.10 Non-sensical docking poses with PDB:5EDU	45
Figure 2.11 Sensical docking poses with PDB:5EDU	45
Figure 2.12 Hybrids selected for synthesis	47
Figure 2.13 Common retrosynthetic strategies towards the raloxifene	48
Figure 2.14 Select literature examples of phenyl-shift	49
Figure 2.15 Two-stage enzymatic HDAC assay	67
Figure 2.16 Original HDAC substrate and modified HDAC substrate	68
Figure 2.17 Dose-response curves of C- and O-linked hybrids against HDAC1	70
Figure 2.18 Dose-response curves of C- and O-linked hybrids against HDAC6	72
Figure 2.19 Single-dose BRET assay results	75

List of Schemes

Scheme 1.1 Prototypical SERMs, tamoxifen and raloxifene	10
Scheme 2.1 The retrosynthetic analysis to key intermediate	48
Scheme 2.2 Retrosynthetic analysis of the key synthetic intermediate	49
Scheme 2.3 Acid-catalyzed cyclization and phenyl shift	50
Scheme 2.4 A second strategy via a Suzuki cross-coupling	51
Scheme 2.5 Successful synthesis of 11	51
Scheme 2.6 Poor regioselectivity observed in Friedel-Crafts acylation of 11	54
Scheme 2.7 Acetyl-protected aryl bromide does not undergo acylation	54
Scheme 2.8 Styrene intermediate not amenable to Friedel-Crafts acylation	56
Scheme 2.9 Acylation of 27 and 17	56
Scheme 2.10 Oxygen-containing functionality at B-ring <i>para</i> position	57
Scheme 2.11 Regioselective acylation with B-ring oxygen substitution	59
Scheme 2.12 Synthesis and acylation of benzyl-protected intermediate	60
Scheme 2.13 Synthesis of styrene 46	62
Scheme 2.14 Completion of 1 (YW359) and 2 (YW471)	63
Scheme 2.15 Completion of 3 (YW490) and 4 (YW466)	64
Scheme 2.16 Synthesis of O-linked intermediate 49	64
Scheme 2.17 Completion of 5 (YW472), 6 (YW486), 7 (YW487)	66

List of Tables

Table 1.1 SERD/HDACi hybrids derived from ICI-164,384	23
Table 2.1 Select literature examples of Friedel-Crafts acylations	53
Table 2.2 Screening Suzuki cross-coupling conditions to construct 28	55
Table 2.3 Screening conditions to effect the Suzuki cross-coupling of 27	58
Table 2.4 Effect of AlCl ₃ in Friedel-Crafts acylation	61
Table 2.5 HDAC1 IC ₅₀ values of all inhibitors tested	71
Table 2.6 HDAC6 IC ₅₀ values of all inhibitors tested	73

List of Abbreviations

1,25D	1 α ,25-dihydroxy-vitamin D ₃
4-OHT	4-hydroxytamoxifen
5-aza-dC	azacitidine
Ag ₂ O	silver(I) oxide
AlCl ₃	aluminum chloride
AF-1	transcription activation factor 1
AF-2	transcription activation factor 2
AMC	7-amino-4-methylcoumarin
BBr ₃	boron tribromide
BF ₃ .OEt ₂	boron trifluoride etherate
BnBr	benzyl bromide
Boc	tert-butyloxycarbonyl
BRET	bioluminescence resonance energy transfer
c-MYC	c- master regulator of cell cycle entry and proliferative metabolism
CaH ₂	calcium hydride
CDC6	cell division cycle 6
CMZ	cytomegalovirus
CSA	camphorsulfonic acid
DCM	dichloromethane
DES	diethylstilbestrol
DBD	DNA-binding domain
DME	1,2-dimethoxyethane
DMF	N,N-dimethylformamide
DNA	deoxyribonucleic acid
DNMT1	DNA methyltransferase 1
E2	17 β -estradiol
EGFR	epidermal growth factor receptor
ER	estrogen receptor

ERE	estrogen response element
EtOAc	ethyl acetate
EtOH	ethanol
ER+	ER-positive
ER-	ER-negative
FITTED	Flexibility Induced Through Targeted Evolutionary Description
FSH	follicle stimulating hormone
GnRH	gonadotropin release hormone
GPCR	G-protein coupled receptor
H ₂ O	dihydrogen monoxide
HATs	histone acetyltransferases
HCl	hydrochloric acid
HDACs	histone deacetylases
HDACi's	histone deacetylase inhibitors
HER2	human epidermal growth factor receptor 2
H-bond(ing)	hydrogen-bond(ing)
HGII	Hoveyda-Grubbs II catalyst
HPLC	high-performance liquid chromatography
IC ₅₀	Inhibitory concentration 50
IR	infrared
K ₂ CO ₃	potassium carbonate
K _D	dissociation constant
KOH	potassium hydroxide
LBD	ligand binding domain
LDL	low-density lipoprotein
LH	lutening hormone
MDA-MB-231	MD Anderson-Metastatic Breast-231 cell line
MDA-MD-468	MD Anderson-Metastatic Breast-468 cell line
MeCN	acetonitrile

MEF-2	myocyte enhancer factor-2
MeOH	methanol
MCF-7	Michigan Cancer Foundation-7
MOM	methoxy methyl ether
NCOA2	Nuclear Receptor Coactivator 2
Na ₂ CO ₃	sodium carbonate
NaH	sodium hydride
<i>n</i> BuLi	<i>n</i> -butyllithium
NLS	nuclear localization signal
o/n	overnight
p53	tumour protein 53
PCy ₃	tricyclohexylphosphine
Pd(dba) ₂	tris(dibenzylideneacetone)dipalladium(0)
Pd(dppf)Cl ₂	[1,1'-bis(diphenylphosphino)ferrocene]dichloropalladium(II)
PhMe	toluene
Pd(OAc) ₂	palladium(II) acetate
Pd(PPh ₃) ₄	palladium tetrakis
PPA	polyphosphoric acid
RLucII	Renilla luciferase
SAHA	suberoylanilide hydroxamic acid
SERDs	selective estrogen receptor downregulators
SERMs	selective estrogen receptor modulators
SM	starting material
S _N Ar	nucleophilic aromatic substitution
SRC1	steroid receptor coactivator 1
SRC3	steroid receptor coactivator 3
STAR	Study of Tamoxifen and Raloxifene
<i>t</i> BuXPhos	2-di-tert-butylphosphino-2',4',6'-triisopropylbiphenyl
TFA	trifluoroacetic acid

THF	tetrahydrofuran
TLC	thin-layer chromatography
TSA	trichostatin A
XPhos	2-Dicyclohexylphosphino-2',4',6'-triisopropylbiphenyl
YFP	yellow fluorescent protein

Contributions of Authors

This thesis contains three original chapters. Collaborative research is presented in Chapter 2 and Chapter 3. *In silico* docking studies using the program FITTED were performed by the thesis author and Jessica Plesica, a graduate student in the Moitessier lab. The FITTED program was developed by Dr. Nicolas Moitessier at McGill University. All chemical syntheses were performed by the thesis author, with the exception of the HDAC peptide substrate, which had been previously synthesized by Adam Elmehriki, a former graduate student in the Gleason lab. All HDAC enzymatic assays were performed by the thesis author. Collaborators at Université de Montréal in Dr. Sylvie Mader's lab (Marine Diennet, Mohamed El Ezzy, Dr. David Cotnoir-White) developed and performed the cell-based ER antagonism assays.

Chapter 1: Introduction

Since 1989, the prognosis for those diagnosed with breast cancer has improved dramatically, with the death rate having dropped by 40% as of 2016,¹ primarily as a function of improved diagnostic and treatment methods. Despite this, the lifetime risk of a woman in the United States being diagnosed with breast cancer has risen from 1-in-11 to 1-in-8 since the 1970's,² and continues to increase incrementally as of 2019¹. This results in part from an increase in life expectancy, but also from an overall increase in breast cancer incidence. In the female population, breast cancer alone represents 30% of all new cancer diagnoses and is the second-largest cause of cancer-related deaths. While the 5-year survival rate is 98% for women diagnosed with localized disease, and 84% for those with regionally spread breast cancer, the rate drops to only 23% for those with distant metastases.³

Our understanding of the biology of breast cancer has largely been shaped by our discovery of sex hormones and their proliferative effects in breast tissue mediated by estrogen receptor (ER) signalling.⁴ In turn, these discoveries have led to the development of synthetic estrogen antagonists as therapeutics in breast cancer, including selective estrogen receptor modulators (SERMs) and selective estrogen receptor downregulators (SERDs). Commonly, SERMs are used in combination with radio- or chemotherapy in breast cancers that express the estrogen receptor (ER+) and are endocrine-responsive. Since the introduction of SERM co-therapy in endocrine-responsive breast cancers, significant reductions in both recurrence and death in those diagnosed with breast cancer has been observed.⁵ Despite the widespread success of adjuvant therapy, resistance is known to develop in many cases, in which the tumour no longer responds to endocrine treatment and tumour growth becomes hormone-independent. In these cases, treatment options become very limited, and often involves the use of SERDs, which act in a fully antiestrogenic fashion distinct from SERMs. Unfortunately, resistance to SERDs can also develop. As a result, other biological targets have been identified for breast cancer therapy, including histone deacetylases (HDACs), which are a class of enzymes responsible for deacetylating the chromatin around DNA, thereby facilitating the

expression of specific genes. There are many hypotheses for their exact role in mediating endocrine resistance in breast cancer, but it has been shown that combining histone deacetylase inhibitors (HDACi's) with SERMs is effective in resensitizing endocrine-resistant breast cancers towards endocrine-based therapy.⁶

Briefly, this chapter will discuss: 1) our current understanding of the fundamental role of estrogen signalling in endocrine-responsive breast cancer, 2) breast cancer treatments targeting estrogen-dependency, 3) the ability of tumours to acquire resistance to endocrine treatments, 4) the potential role of histone deacetylases in treating endocrine-resistant breast cancers, and 5) the rationale behind the design of hybrid SERM/HDACi drug molecules that are hypothesized to combine the cooperative behaviour of these two distinct drug classes.

1.1 Breast Cancer and the Estrogen Receptor

1.1.1 Estrogen Receptor α

The link between breast cancer and sex hormones was first suggested almost 120 years ago, when Schinzinger first proposed the idea of removing the ovaries for the treatment of breast cancer.⁴ The surgery itself was not actually performed until 1895, when George Beatson performed the operation on three menopausal patients diagnosed with breast cancer.⁷ Unfortunately, only one of three women seemed to benefit,⁸ but he has since been considered the father of the anti-hormonal treatment of breast cancer. Subsequent work in animal models confirmed the importance of ovarian hormones to breast cancer development.⁹

A major advancement came 1966 when the estrogen receptor was isolated by Toft et al., during their efforts to produce a cell-free method for studying the proliferative effects of estrogens.¹⁰ In spite of this, investigations in the field remained slow due to the laborious methods used to extract the ER from tissue samples. The ER was sequenced and successfully cloned by Green et al. in 1986,¹¹ leading to rapid advances in our understanding of the mechanism by which the ER regulates gene expression. In 1997, the crystal structures of the ER α ligand binding domain (LBD) bound to an agonist (17 β -

estradiol) and an antagonist (raloxifene), respectively, was resolved by Brzozowski et al.,¹² allowing for the first molecular understanding of ER activation and deactivation.

A second isoform of the ER, ER β was identified in 1996.¹³ ER β has structural similarities to ER α in the LBD and DNA-binding domain (DBD), and can also bind 17 β -estradiol (E2). The exact role of the ER β is not well-studied, but one hypothesis is that unbound ER β regulates ER α -mediated gene transcription in the presence of E2, with varying relative levels of ER isoforms thereby providing a more fine-tuned local control of ER signalling.

The GPR30 is another receptor which is responsive to E2 signalling. It is a transmembrane G-protein coupled receptor (GPCR) located on the nuclear envelope, Golgi body, and the endoplasmic reticulum. It is thought to mediate the rapid non-genomic actions attributed to E2 signalling,¹⁴ and likely has an independent influence on E2 responsiveness in breast carcinoma.¹⁵ While the existence of the ER β and the GPR30 introduces additional complexity to our understanding of ER signaling, this thesis will limit the discussion of the ER to the better-understood ER α , although there are several excellent reviews on both the ER β ^{13, 16-17} and the GPR30.^{14, 18-19}

1.1.2 Structure of the Estrogen Receptor

The ER is expressed throughout the body in various tissues. The function of the ER varies depending on the tissue it is expressed in. Its endocrine function arises from its expression in the hypothalamus-pituitary-gonadotropic axis,²⁰⁻²¹ thereby regulating the endogenous production of E2. More locally, the ER plays a key role in the regulation of: adipocytes in fat tissues,²² osteoblasts and chondrocytes of bone, vascular endothelium and aortic smooth muscle cells, and numerous sites in the brain.²³

The ER is a 595 amino-acid residue nuclear receptor protein consisting of 6 domains (Figure 1.1). The A/B domain at the amino terminus houses the Transcription Activation Factor 1 (AF-1), which mediates ligand-independent activity and is regulated by phosphorylation. Domain C contains a highly-conserved DBD and houses two zinc-fingers that are responsible for recognizing the estrogen response element (ERE), a promoter gene sequence, upon ER activation.²⁴ Domain D contains the hinge region and

is where dimerization of activated ER monomers occurs. The carboxy terminus, domains E and F, houses the LBD and Transcription Activation Factor 2 (AF-2) which are directly involved in ligand-induced activation and transcription regulation.²⁴ AF-1 and AF-2 are able to function independently or synergistically, depending on cell type and target promoter.²⁵⁻²⁶

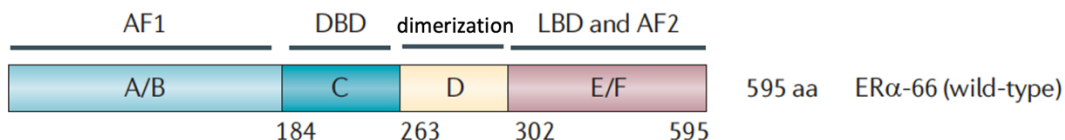


Figure 1.1 Domains of the ER.²⁷

The LBD (Figure 1.2) is a three-layered antiparallel α -helical sandwich with a central core composed of H5/6, H9 and H10 (yellow). Two additional layers of helices H1-4 (purple), and H7, H8, and H11 (red) flank the sides of the core. The front and the back of the binding pocket are blocked off by a two-stranded antiparallel β -sheet (orange), and H12 (pink) seals the opening of the ligand-binding cavity.

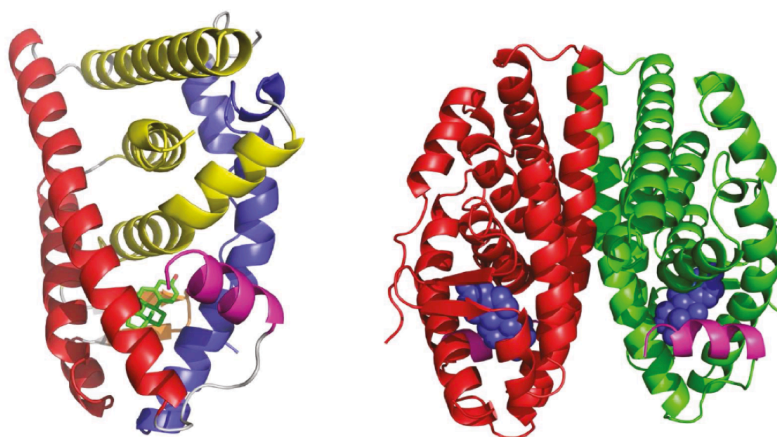


Figure 1.2. Crystal structure of the LBD of ER bound to E2 (PDB: 1ERE). Left: ER monomer bound to E2. H7, H8, H11 are shown in red. H5/6, H9, and H10 shown in yellow. H1-4 shown in purple. H12 shown in pink. Right: active ER dimer, with the key H12 of each monomer shown in pink.²⁸

This helical arrangement of the LBD creates a “wedge-shaped” scaffold. Even at the more narrow end of the domain, the ligand binding cavity remains quite large. In fact, the ER is described as being quite promiscuous, since its ligand binding pocket is almost twice the size (450 Å) of its endogenous ligand (245 Å). The LBD is able to receive non-steroidal compounds, but the A-ring of these compounds must contain an aromatic moiety due to the “pincer-like” arrangement of the LBD.²⁸

1.1.3 Mechanism of Estrogen Receptor Signalling

In the absence of any ligands, the ER exists as a monomer, stabilized by heat shock proteins Hsp56, Hsp70, and Hsp90, which dissociate once a ligand has been bound.²⁹ In healthy breast cells, endogenous E2 enters the cytosol and binds the inactive, monomeric ER (Figure 1.3). Upon E2 binding, a conformation change is elicited which allows the monomers to dimerize at the H8/H11 interface. This conformational change reveals a nuclear localization signal (NLS) locating the ER complex to the cell nucleus.³⁰ The active dimeric ER then associates with the estrogen response elements (ERE), which are 13 bp palindromic inverted repeat sequences (5'-GGTCAnnnTGACC-3') in the promoters of ER-regulated genes.³¹⁻³² Once assembled, the ER-coregulator complex then recognizes and binds the ERE using the pair of zinc-fingers found within the DBD³³. Transcription activation requires association with a large number of transcriptional coregulators,³⁴ among which include SRC1 and SRC3 (steroid receptor coactivators),³⁵ and chromatin remodelling proteins such as histone acetyl transferases (HAT) or histone deacetylases (HDAC).³⁶⁻³⁷ The formation of the ER-coregulator complex is then followed by recruitment of the general transcription machinery to the promoter site, where DNA transcription is initiated.

In healthy breast tissue, ER signalling leads to the transcription of genes that maintain regular tissue growth and function. In ER+ breast carcinoma, notable nuclear targets of ER signalling consist of several notorious oncogenes including: *c-MYC* (a cell apoptosis regulator),³⁸ cyclin D1 (a cell-cycle check protein),³⁹⁻⁴⁰ CDC6 (a cell-cycle check protein),⁴¹ HER2 (a breast cancer biomarker), and the ER itself.⁴²

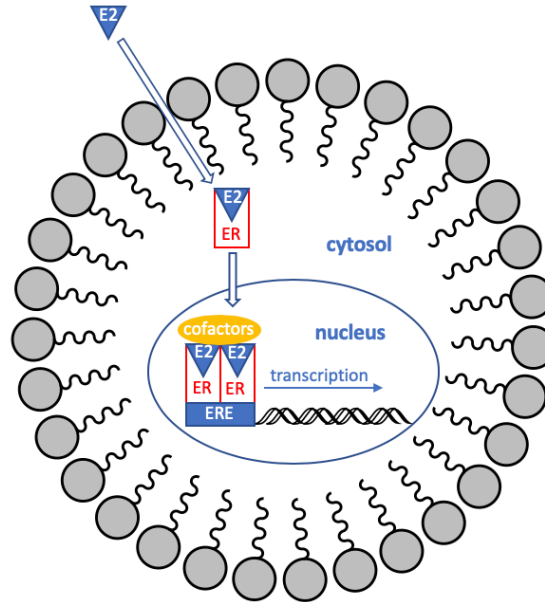


Figure 1.3 A simplified version of classical ER signalling: 1) E2 freely diffuses across plasma membrane, 2) binds monomeric ER, causing dimerization, 3) translocation into the nucleus, 4) ER-complex binds ERE's and activates transcriptional activation.

1.2 Agonists and Antagonists of the Estrogen Receptor

1.2.1 Agonists

The endogenous agonist of the ER is E2, the predominant sex hormone involved in regulating normal tissue function throughout the body. E2 levels are tightly controlled by a set of feedback and feedforward loops within the hypothalamus-pituitary-gonadotropin axis. Briefly, gonadotropin release hormone (GnRH) is secreted by the hypothalamus (Figure 1.4). GnRH signals to the anterior pituitary, which releases follicle stimulating hormone (FSH) and lutenizing hormone (LH). FSH and LH promote the secretion of androgens from the theca cells of the ovaries, and simultaneously inhibit the secretion of GnRH from the hypothalamus. Within the ovaries, the local enzyme aromatase then converts the androgens into E2, which feedback inhibits the secretion of GnRH and LH. This complex set of feedback and feedforward loops helps regulate homeostatic levels of estrogen present in the body. In premenopausal women, the ovaries

are the main source of estrogens. In post-menopausal women, ovarian production of E2 slows to a halt, and adipose tissues become the primary source of E2 until death.²³ Other endogenous estrogens include estrone and estriol (Figure 1.5), but these bind to ER with far less potency than E2.⁴³ There are several hormonal breast cancer treatments which target the hypothalamus-pituitary-gonadotropin axis, but these will not be discussed in great detail.

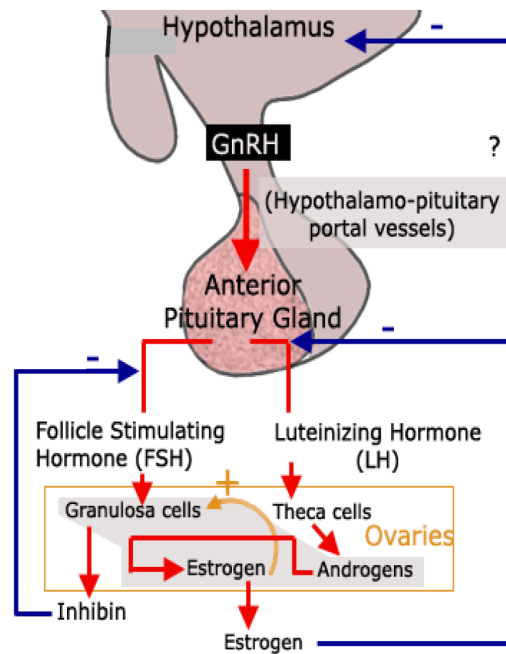


Figure 1.4 A diagram representation of the hypothalamus-pituitary-gonadotropin axis with feedback and feedforward loops.⁴⁴

The ER recognizes E2 within a hydrophobic pocket inside the LBD. The phenolic moiety of E2 (highlighted in red in Figure 1.5) makes a key hydrogen bonding network between E2 and Glu353, Arg394, and a molecule of water within the hydrophobic cleft (Figure 1.6). Another important hydrogen bonding interaction occurs between the 17β -hydroxyl of E2 with His 524. The lipophilic hormone core is stabilized by hydrophobic interactions with the rest of the binding pocket. Once bound to E2, H12 folds over the ligand binding pocket,²⁸ like a container lid, with its hydrophobic residues projecting perpendicular to the receptor dimerization surface. This conformational change allows

AF-2 to interact with various coactivators, allowing nuclear translocation and DNA transcription to begin. It would appear that H12 adopting this conformation over ligand binding cavity is both necessary and sufficient for AF-2 activation, and mutations of H12 can cause the ER to become estrogen-insensitive.⁴⁵ The mechanism of ER activation is well-conserved amongst other members of the nuclear hormone receptor superfamily.⁴⁶⁻
⁴⁸ Our molecular understanding of ER activation has shaped the way we design synthetic compounds which aim to modulate it.

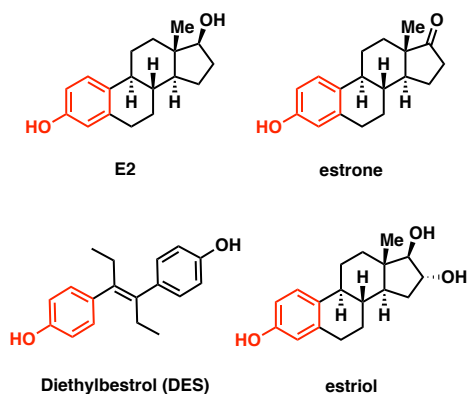


Figure 1.5 A selection of common ER agonists. The key phenolic moiety required in ER agonist pharmacophores for ER binding is highlighted in red.

Synthetic ER agonists possess a similar pharmacophore to E2 (Figure 1.5), and activate the ER in a similar fashion. Of the synthetic ER agonists, diethylstilbestrol (DES) is most well-known, due to its notorious history as a potent endocrine disruptor. Initially prescribed during the 1940-1970's as a therapeutic for the prevention of adverse pregnancy outcomes, it was later revealed to increase the risk of a rare vaginal clear cell carcinoma in females who had been exposed to it *in utero*.⁴⁹⁻⁵⁰ Unfortunately, it was also later discovered that diethylstilbestrol had no real therapeutic value for treating adverse pregnancies.⁵¹⁻⁵² Since these discoveries, prescription and marketing of DES has been largely discontinued.

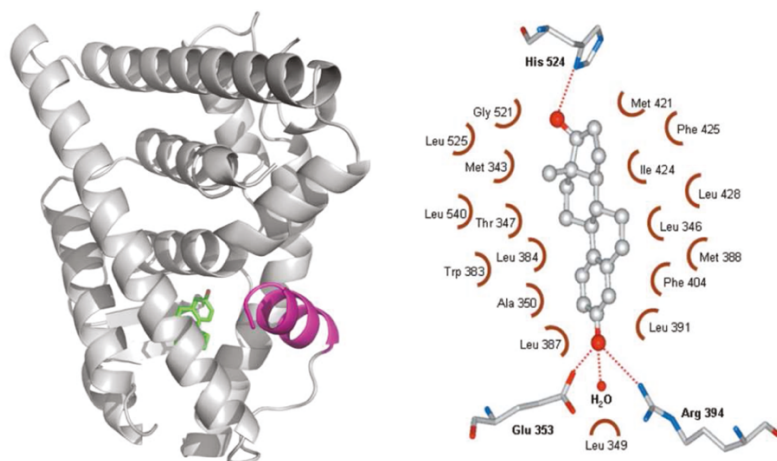


Figure 1.6 PDB: 1ERE Left: E2 bound to the LBD of the ER, with H12 (pink) folded over the cavity.²⁸ Right: E2 binds to residues inside the ER.⁵³

DES is a trans-stilbene derivative containing two ethyl groups bound to tetra-substituted olefin core. The phenolic moieties of DES make similar contacts with the ER ligand binding pocket as seen with E2 (Figure 1.7), including that with His524, Glu353, and Arg394. The rest of the molecule is stabilized by hydrophobic interactions with the rest of the pocket. Importantly, DES is held within the ligand binding cavity, and H12 is able to fold over the opening, leading to the activation of the ER.

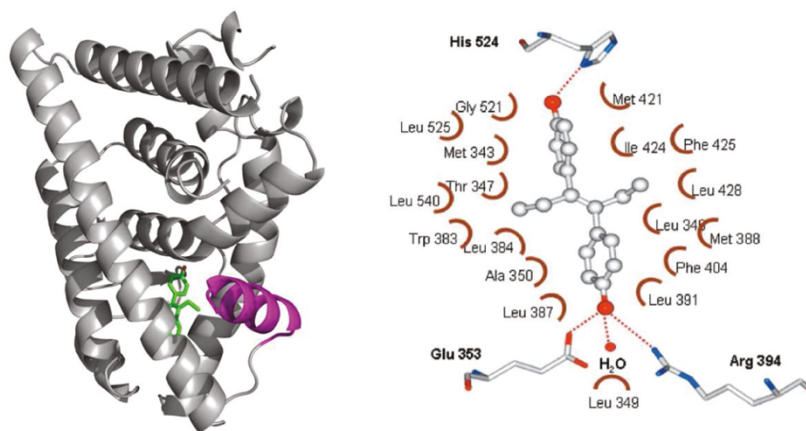
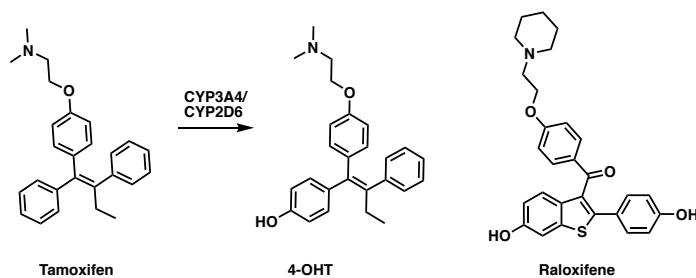


Figure 1.7 PDB: 4ZN7 Left: DES bound to the ligand binding pocket of the ER, with H12 (pink) folded over the cavity.⁵⁴ Right: DES binds to residues inside the ER.⁵³

1.2.2 Selective Estrogen Receptor Modulators

Tamoxifen is the most well-known SERM, and is currently the first-in-line treatment used in conjunction with chemo- or radio-therapy in ER+ breast cancer, with typical treatment lasting five years.⁵⁵ It has been used for ER+ breast cancer since the 1970's, and gained approval as a preventative treatment in 1977.⁵⁶⁻⁵⁷

Several well-characterized metabolites of tamoxifen are formed by CYP enzymes in the liver.⁵⁸ Of these, the most notable is 4-hydroxytamoxifen (4-OHT). 4-OHT has a much higher affinity for the ER than the parent molecule with a K_D of 0.15 nM, compared to the tamoxifen K_D of 8 nM.⁵⁹ As a result, 4-OHT is 100 times more potent than tamoxifen,⁶⁰⁻⁶¹ which has an IC_{50} of 400 nM (in MCF-7 cells).⁶² This difference in affinity and potency for the ER is due to the critical phenolic residue, which is key for good recognition of the ER ligand binding cavity. As such, tamoxifen can be considered as a prodrug for 4-OHT.



Scheme 1.1. Prototypical SERMs, tamoxifen and raloxifene. Tamoxifen becomes converted in vivo to the more potent metabolite 4-OHT.

Tamoxifen acts as a ER antagonist in breast tissues, but possess estrogenic properties in bone⁶³ and endometrial tissue. Its agonist effects in endometrial tissue are significant because administration of tamoxifen can increase the risk of uterine cancers by 3-4 fold.⁶⁴⁻⁶⁵ The increased risk of endometrial cancer eventually led to the development of second- and third-generation SERMs.

One well-known second-generation SERMs is raloxifene. Raloxifene was originally developed with the specific goal of enhancing ER antagonism while minimizing the inherent estrogenicity that tamoxifen suffers from.⁶⁶ In rats, raloxifene is able to prevent

the development and growth of induced mammary carcinomas⁶⁷⁻⁶⁸ while maintaining bone density in ovariectomized subjects.⁶³ In humans, raloxifene is able to significantly reduce the risk of invasive breast cancer,⁶⁹ increase bone mineral density, lower serum LDL cholesterol, and does not stimulate the endometrium.⁷⁰ Interestingly, the endometrial stimulation effects observed with estrogen and tamoxifen are blocked by treatment with raloxifene.⁶⁶ Data from the Study of Tamoxifen and Raloxifene (STAR) clinical trial, which directly compared raloxifene to tamoxifen, indicated raloxifene has equal chemopreventative properties as tamoxifen but with a better safety profile.⁷¹ Metabolic studies of raloxifene show that it suffers from poor oral bioavailability owing to its high first-pass metabolism, which results in glucuronidation at the two phenols.⁷² Despite this, the proportion of ingested raloxifene that does manage to enter the bloodstream is effective, likely owing to its incredibly potent IC_{50} of 0.2 nM (in MCF-7 cells).⁶²

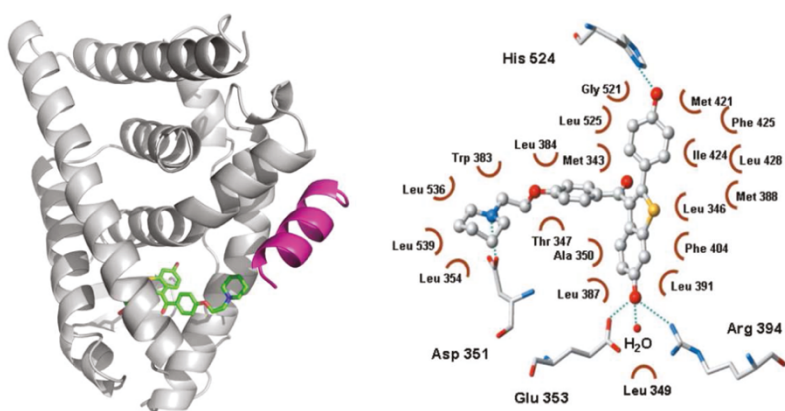


Figure 1.8 PDB: 1ERR. Left: raloxifene's piperazine tail inhibits H12 (pink) from folding over the LBD. Right: raloxifene binds to residues inside the LBD.⁵³

Both raloxifene and tamoxifen bind to the ER ligand binding pocket in a manner that mimics the binding mode of E2. The benzothiophene phenol of raloxifene mimics the E2 phenol by making H-bonds with Glu353, Arg 394, and a molecule of water (Figure 1.8). Raloxifene's distal phenol makes a H-bonding contact with His524, mimicking the 17 β -hydroxyl of E2. Hydrophobic residues stabilize the binding conformation of the rest

of the relatively lipophilic molecule. Tamoxifen makes similar contacts within the ligand binding cavity, with the exception of the H-bond with His524, because it lacks a H-bonding moiety at that position (Figure 1.9).

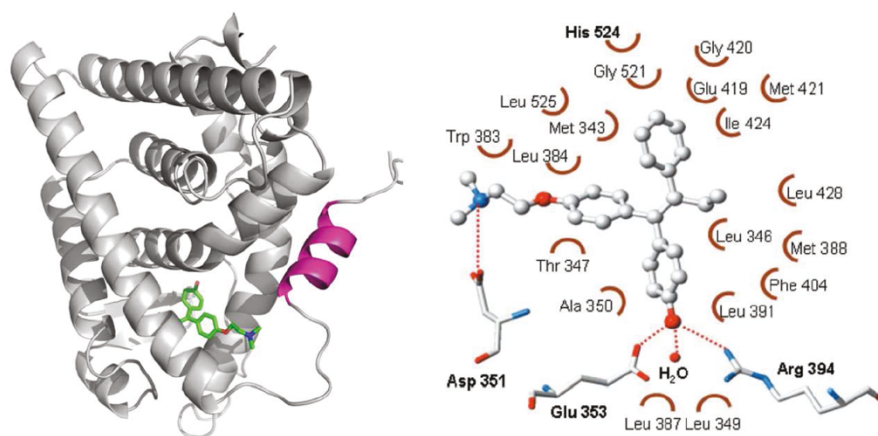


Figure 1.9 PDB: 1ERT. Left: tamoxifen's N,N-dimethylamino tail inhibits H12 (pink) from folding over the LBD. Right: tamoxifen binds to residues inside the LBD.⁵³

On a molecular scale, both tamoxifen and raloxifene antagonize the ER in a comparable fashion. While they both recognize and bind the LBD of the ER, they inhibit the critical H12 folding event, which is required for ER dimerization and activation. In both raloxifene and tamoxifen's binding modes, the amino-containing side chains form a salt bridge with Asp351 and protrude from the binding cavity (Figure 1.7 and 1.8). The protrusion of the aminoalkoxy tails force H12 to adopt a conformation where the hydrophobic inner residues of H12 complement the hydrophobic residues of a groove between H3 and H5,¹² and prevents AF-2 from interacting with various coactivators to initial nuclear translocation and DNA transcription. In fact, the aminoalkoxy chain is essential for antiestrogenic activity⁷³ – changes in the distance between the oxygen and nitrogen,⁷⁴ restriction of the side chain conformation,⁷⁵ decreasing the basicity of the nitrogen,⁷⁶ or replacing the basic nitrogen with a carbon⁷⁷ all decrease the antiestrogenic properties of their respective analogues.

There are two predominant hypotheses regarding the dual antiestrogenic/estrogenic nature of SERMs. One idea is that they are able to differentially recruit a variety of coregulators in a tissue-dependent manner.⁷⁸ In turn, the recruited coregulators either abrogate or promote the activity of the ER.⁷⁹⁻⁸⁰ The other hypothesis suggests that variation in the relative levels of ER α vs ER β expression in different tissues lead to distinct ER responses in a tissue-dependent manner.⁷⁸

1.2.3 Selective Estrogen Receptor Downregulators

SERDs act as anti-estrogens in all tissues, which can lead to undesirable side effects as estrogen is required for maintain a variety of bodily functions. Owing to their global antiestrogenic nature, they are typically used as last resort, reserved for patients with breast cancers that are either non-responsive to SERMs or become resistant to them.⁴ The steroidal core of SERDs are modelled after E2, with a long alkyl chain, which is required for antiestrogenic activity. Two prominent examples of SERDs are fulvestrant and ICI-164,384 (Figure 1.10).

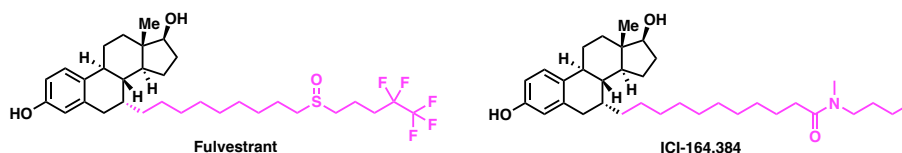


Figure 1.10 SERDs fulvestrant and ICI-164,384. Steroid core shown in black and antiestrogenic alkyl chain shown in pink.

Fulvestrant was derived from ICI-164,384,⁸¹ and has an in vivo potency an order of magnitude greater in MCF-7 cells and in mice.⁸² It was approved for express purpose of treating advanced breast cancer in patients who were unresponsive to endocrine therapy.⁸³

The binding mode of SERDs to the ER was revealed by the crystal structure of ICI-164,384 bound to the ER β (Figure 1.11).²⁸ The complex was resolved as a homodimer with the ligand bound within the binding cavity. A set of antiparallel helices analogous to those seen in ER surround the binding cavity. Within the ligand binding cavity, the

steroidal core is flipped 180° relative to E2 bound in the ER cavity in order to accommodate the long alkyl chain. Resemblances to the E2 binding mode include the H-bonding interactions between the phenol of ICI-164,384 with Glu260 and Arg301, and the 17β-hydroxyl makes a contact with His430. In contrast to SERM binding, there is no salt bridge formation with Asp258. The most striking difference between the SERM and the SERD binding modes is the position of H12. The long alkyl chain of ICI-164,384 protrudes from the binding cavity and occupies the hydrophobic groove that H12 normally occupies when the receptor is antagonized by a SERM. It is unclear from the crystal structure where H12 is located. This appears to be highly disordered and completely deregulates the protein, and likely accounts for the differences observed in the biological activities of SERMs and SERDs.

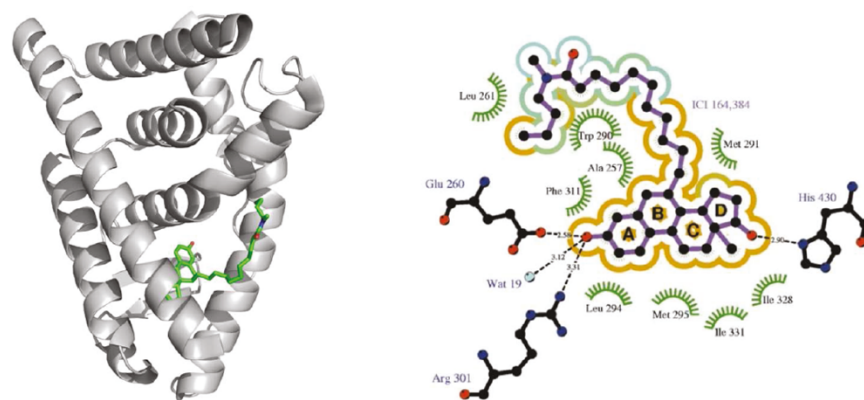


Figure 1.11 PDB: 1HJ1. Left: crystal structure of ICI-164,384 bound to ERβ, with the location of H12 unresolved.²⁸ Right: ICI-164,384 making critical contacts within the ligand binding cavity.

While SERMs nullify AF-2 mediated ER signalling, SERDs completely antagonize the ER in a number of ways that are distinct from SERMs. SERDs act as full anti-estrogens by blocking the activation of both AF-1 and AF-2, as well as by reducing the half-life of the ER.⁸⁴ This likely occurs via promotion of ER degradation⁸⁵ and turnover⁸⁶ because

binding of anti-estrogens to the ER marks the protein via SUMO-ylation or ubiquitination for proteasomal degradation.⁸⁷⁻⁸⁹

1.3 Endocrine Resistance in Breast Cancer

Despite the wide variety of breast cancer therapies targeting the ER, resistance often occurs. Only 30% of patients undergoing endocrine therapy experience tumour regression, and 20% stabilize over a prolonged period of time. The remainder are unresponsive or develop resistance to endocrine therapy. Of the 30-40% of ER+ breast cancers who do not respond to endocrine therapy, 2/3 of patients will respond to fulvestrant. However, response rates to full antiestrogens are only slightly better than those of SERMs⁹⁰ and acquired resistance after an initial response is common.

Acquired resistance to SERMs occurs after long-term treatment, and is subdivided into three phases.⁹¹ During phase I, a dual signal transduction process develops, in which both SERMs and (once administration of SERMs has been stopped) endogenous estrogen stimulates tumour growth. Aromatase inhibitors and fulvestrant are both effective during this phase of resistance. The transition into phase II is marked by a striking mechanism that causes apoptosis rather than growth in response to physiologic levels of estrogen. Continued exposure to SERMs will then lead to phase III of resistance, in which the tumor achieves autonomous growth, and becomes unresponsive to fulvestrant or aromatase inhibitors.

There are several mechanisms which underlie acquired resistance. Mutations in ER structure and function can lead to the ER being constitutively active.⁹²⁻⁹⁴ Changes in post-receptor interactions can dissociate growth from receptor response. There can be changes in paracrine interactions. Pharmacological changes, such as increases in estrogen-like metabolite production or biological mechanisms which lead to decreases in intracellular drug concentrations, can occur.⁹⁵⁻⁹⁶ Often it is a combination of several factors that play into hormone resistance.⁹⁷

Due to the high prevalence of hormone therapy resistance and the difficulty with which it is to overcome, several biological targets involved in this process have been identified and investigated.

1.4 Histone Deacetylase and Breast Cancer

1.4.1 Structure and Function of Histone Deacetylases

One target class that has attracted recent attention for its potential role in cancer are the HDACs. Amongst their many functions, HDACs are most well known as epigenetic factors which work in cooperative opposition to histone acetyltransferases (HATs). HDACs are metalloproteins that condense chromatin by deacetylating lysine residues on histone proteins in order to restrict access of general transcription machinery to DNA. Typically, HDACs are recruited at the end of DNA transcription cycle, to zip the chromatin back up around a gene that has just been transcribed, while HATs are associated with the beginning of DNA transcription (Figure 1.12). HDACs and HATs are catalytic units that make up larger protein complexes.⁹⁸

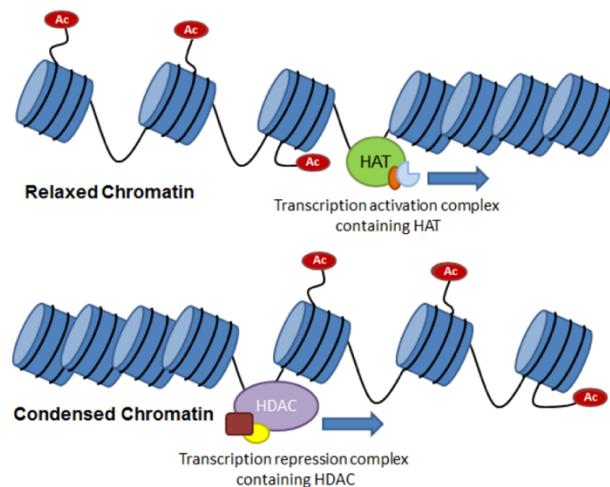


Figure 1.12 Transcription is promoted HATs and repressed by HDACs.⁹⁹

There are two main types of HDACs: zinc-dependent and sirtuins.¹⁰⁰ These are further organized into four different classes, organized mostly by their function and tissue and cellular localization. The sirtuins, which are not zinc-dependent, compose class III. They are structurally, mechanistically, and functionally very different from the zinc-dependent HDACs,¹⁰¹ and will be excluded from further discussion. Within the zinc-dependent HDACs, there are three classes of enzymes: class I, II, and IV. Class I comprises HDAC1, 2, 3, and 8, and are typically found in the cell nucleus. They form a variety of important DNA transcription repression complexes.¹⁰²⁻¹⁰³ Class II is further divided into class IIa and IIb. Class IIa contains HDAC4, 5, 7, and 9. They are considered as signal transducers because they can move freely between the nucleus and the cytoplasm. In addition to their ability to deacetylate histone, they can deacetylate other proteins,¹⁰³ and bind transcription factor enhancer MEF-2.¹⁰⁴ HDAC 6 and 10 are located in the cytoplasm only, and thus are considered Class IIb. The only enzyme in class IV is HDAC11, whose function is largely unknown.¹⁰⁵

From a clinical standpoint, HDAC inhibitors (HDACi's) have garnered the most interest for their potential application in the treatment of a variety of cancers. Prototypical HDACi's include suberoylanilide hydroxamic acid (SAHA) and trichostatin A (TSA) (Figure 1.13).¹⁰⁶ SAHA is currently on the market as a treatment for cutaneous T-cell lymphoma.¹⁰⁷



Figure 1.13 Structure of SAHA and TSA with key pharmacophore feature highlighted: aryl cap (red), aliphatic linker (black), and Zn²⁺-binding group (blue).

The typical pharmacophore of a HDACi consists of an aryl cap, an aliphatic linker, and a Zn²⁺ binding group (Figure 1.13).⁹⁸ The aryl cap is thought to bind to the rim of a substrate channel, conveying inhibitor specificity. The long aliphatic linker spans the long and narrow substrate binding channel in the enzyme. A large variety of capping groups

and aliphatic linkers are tolerated by HDACs, and variations can help to induce HDAC isoform selectivity.¹⁰⁸ The Zn²⁺ binding group binds the Zn²⁺ atom coordinated at the base of the catalytic channel, rendering the enzyme inactive. Zn²⁺ binding moieties can include hydroxamic acids, benzamides, thiols, electrophilic ketones, and silanediols,¹⁰⁹⁻¹¹² although the most clinically-relevant groups are hydroxamic acids or benzamides. Due to their relatively simple structures, a variety of compounds can act as HDACi's, even though they may not have been originally made for that purpose (e.g. valproic acid). A commonly-encountered problem is non-specificity of HDACi's, which can result in toxic side-effects. Unfortunately, HDACi's have had limited clinical applications and (apart from lymphomas) have performed underwhelmingly in cancer treatment as monotherapies.

A bacterial acetylase HDAC1 homologue was co-crystallized with SAHA and TSA in 1999,¹¹³ giving insight into the structure of HDACs (Figure 1.14). While there is considerable structural variation amongst the zinc-dependent metalloproteases, they share a common catalytic domain. The catalytic pocket is composed of 7 loops which extend and form a deep narrow channel leading to the Zn²⁺ atom. The channel is predominantly composed of hydrophobic residues and has a depth of 11 Å and is 7.5 Å at its narrowest point. The Zn²⁺ is coordinated at the base by Asp168, His170, Asp258, and a molecule of water in a tetrahedral coordination environment. SAHA and TSA coordinate Zn²⁺ by displacing the water molecule to give pentacoordinated Zn²⁺. Their aliphatic linkers are stabilized by Van der Waals interactions, and their aryl groups give specificity by interacting with the protein surface.

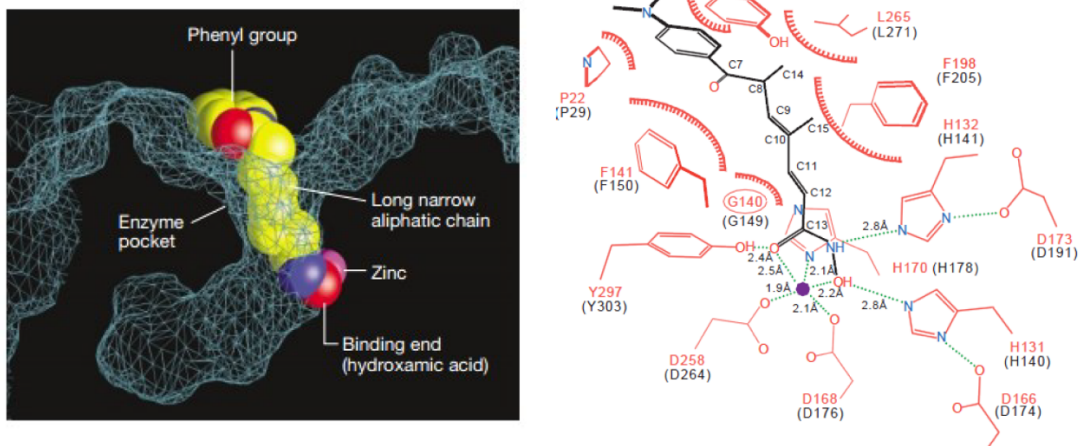


Figure 1.14 Left: space-filling model of the HDAC catalytic channel occupied by TSA. Right: coordination of zinc by TSA.

1.4.2 Histone Deacetylase Inhibitors and Breast Cancer

The exact relationship between HDACs and tumorigenesis is unclear. It has been suggested that inhibition of HDAC's (leading to increased open forms of chromatin) would drive the transcription of specific genes that result in cell growth arrest, differentiation, and/or apoptotic cell death, culminating in tumor shrinkage (Figure 1.15).⁴ While there is no direct link between HDAC overexpression and tumorigenesis, aberrant expression and activity seem to play a role. While Class I HDACs are suggested to be the most clinically relevant in cancer therapy, HDAC6 is also emerging as a potential target of interest.¹¹⁴

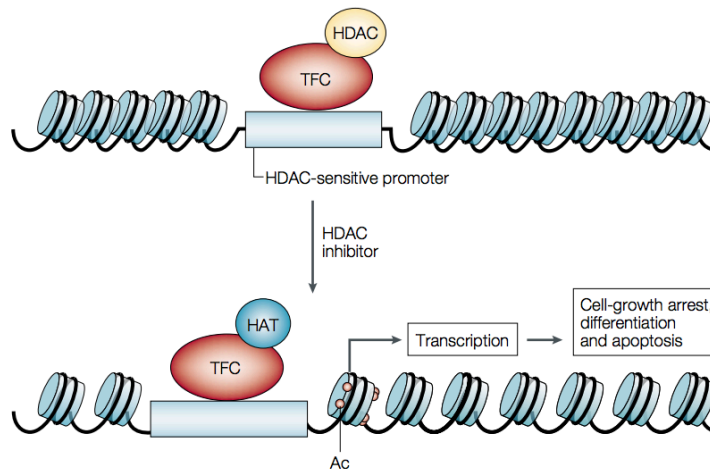


Figure 1.15 Working hypothesis for HDAC inhibition leading to tumor death.⁴ TFC= transcription factor coactivators.

While inhibition of ER signalling prevents the growth of ER+ tumors, the loss of ER expression appears to be paradoxically critical for tumor progression and endocrine-resistance. In endocrine-unresponsive tumours, the ER gene silencing does not appear to be not due to mutations within the ER gene itself, but is rather attributed (at least in part) to epigenetic regulation of the ER gene promoter. This is supported by the observation that methylation of ER promoters occurs commonly in ER- breast cancers, but is not seen in ER+ or healthy breast tissue.¹¹⁵ The activation of the ER occurs concomitantly with partial demethylation of the ER promoter, and increased acetylation of both histone 3 and histone 4, suggesting both DNA methyltransferase 1 (DNMT1) and HDAC may play a role in ER gene silencing.¹¹⁶ The first study directly linking epigenetic ER silencing in ER- genes was demonstrated by Sharma et al. In ER- cells, they showed that silenced genes associated with endocrine resistance, including the gene encoding the ER, could be turned back on by treatment with a combination of TSA and 5-aza-dC (a DNMT1 inhibitor). These previously endocrine-resistant cells then became resensitized to tamoxifen treatment.

Other studies have shown a similar concomitant link in HDAC inhibition with either re-expression of ER and/or resensitization to endocrine therapy. In MCF-7 cells which were made to overexpress HDAC1, a loss of ER with an accompanying increase in cell

proliferation were observed. Treatment with TSA restored ER levels, and decreased cellular proliferation, suggesting HDAC1 may increase tumor cell proliferation and suppress ER transcription.¹¹⁷ Both HDAC1 and HDAC2 have been linked to deacetylation and downregulation of the tumor suppressor gene p53, which in turn decrease its ability to modulate cell growth and induce tumor apoptosis.¹¹⁸⁻¹¹⁹ Treatment of MDA-MD-468 cells (an ER- breast cancer cell line) with SAHA led to a decrease in cell proliferation and an increase in tumour cell differentiation.¹²⁰ In cell samples collected from breast cancer patients, HDAC1 served as a potential marker for endocrine-responsive patients in cells that co-expressed HDAC1 and ER, with higher levels associated with prolonged disease-free survival.¹²¹⁻¹²² The most promising link between HDAC inhibition and hormone resensitization comes from a Phase II clinical trial.⁶ The subjects were patients who had previously undergone endocrine and chemotherapies for breast cancer, and had developed resistance to them. A SERM/HDACi combination therapy was found to be beneficial in 40% of these patients, with benefit being either tumour regression or prolonged disease stabilization.

Taken together, these studies point towards combination therapy of SERM and HDACi being a very promising solution to endocrine resistance in breast cancer.

1.5 Hybrid Molecules

Combination therapy is a classic method of combatting resistance in many diseases. However, it is associated with several well-known issues, including decreased patient compliance, increased pharmacokinetic interactions, difficulties associated with dose optimization, and increased drug manufacturing costs. These problems can be addressed with hybrid drugs.

Hybrid molecules are small molecules whose structure is an overlap of the distinct domains of two biologically active molecules and can modulate two different protein targets.¹²³ In addition to the aforementioned issues, hybrid drugs are able to exploit the inherent uptake capacity of one parent molecule to improve the uptake of the added pharmacophore.¹²³ Hybrid drug designs tend to be maximally beneficial when exploiting a 1:1 relationship in the combination of drugs.

1.5.1 Previous Examples of Hybrid Drugs

The use of HDACi in hybrid drug molecules have become more popular in recent history. One clinical example is CUDC-101, a multi-targeted inhibitor of HDACi, epidermal growth factor receptor (EGFR), and human epidermal growth factor receptor 2 (HER2).¹²⁴ They have also been explored in many academic publications. In the Gleason lab, the main theme of the medicinal chemistry program is the incorporation of HDACi functionality into nuclear receptor-targeting drug scaffolds.

An early successful example of a hybrid drug molecule published by the Gleason lab was triceferol. Triceferol was made by combining the scaffolds of $1\alpha,25$ -dihydroxy-vitamin D₃ (1,25D) and TSA (Figure 1.16). 1,25D is an agonist at the vitamin D receptor, which attenuates cell proliferation in a number of cancers. Previous studies showed combination treatment with TSA and 1,25D was effective in treating cancer

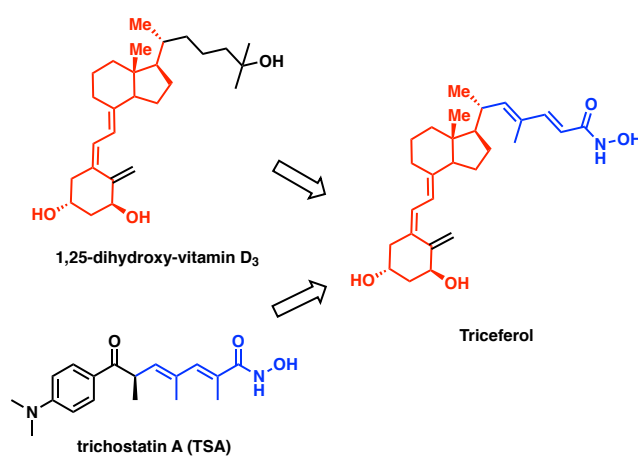


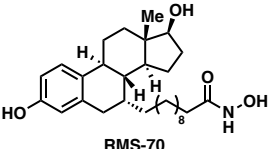
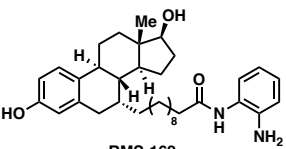
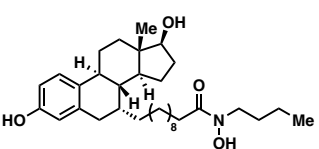
Figure 1.16 Triceferol is made by incorporating 1,25D and TSA scaffolds.

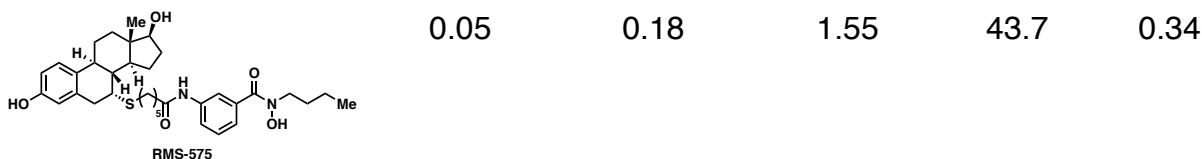
cells which had become resistant to 1,25D. Compared to combination treatment of the two drugs, the hybrid molecule triceferol demonstrated greater cytotoxicity in poorly differentiated breast and squamous carcinoma lines. This project was not only a proof of concept for the hybrid drug paradigm, but gave valuable insight into molecule design.¹²⁵

Another example published by the Gleason lab more relevant to this thesis was the synthesis of SERD/HDACi hybrid inhibitors derived from ICI-164,384 in 2015.¹²⁶ All the hybrids had low micromolar to high nanomolar activity against both ER+ MCF-7 and ER- MDA-MB-231 breast cancer cell lines. While all the hybrids performed well in cytotoxic assays, it was noteworthy that the most successful compounds did not necessarily exhibit the most potent activity in single-target assays (Table 1.1). RMS-70 was the most potent synthesized hybrid in enzymatic HDACi assays, with an IC₅₀= 0.96

μM against HDAC3 and was within one order of magnitude of the SAHA IC_{50} against HDAC6. Remarkably, in BRET (Bioluminescence Resonance Energy Transfer) and luciferase assays measuring ER activity, the most successful of the synthesized hybrids was RMS-575, which was a hybrid of ICI164,384 and entinostat, a benzamide HDACi. RMS-575 possessed an IC_{50} of $0.34 \mu\text{M}$ against ER+ MCF-7, which was similar to those of SAHA, entinostat, ICI-164,384, and 4-OHT. In ER- MDA-MB-231 cells, RMS-575 had an IC_{50} value within one order of magnitude of SAHA.

Table 1.1 SERD/HDACi hybrids derived from ICI-164,384 and their summarized biological activities compared to SAHA, entinostat, and ICI-164,384.

Compound	ER BRET (IC_{50} in μM)	ER Luciferase (IC_{50} in μM)	HDAC3 (IC_{50} in μM)	HDAC6 (IC_{50} in μM)	MCF7 (IC_{50} in μM)
SAHA	ND	ND	0.17	0.35	0.32
entinostat	ND	ND	0.31	ND	0.35
ICI-164,384	0.34	0.05	ND	ND	0.93
 RMS-70	0.51	1.06	0.96	1.15	2.93
 RMS-162	0.21	0.72	3.18	>50.0	1.90
 RMS-234	2.55	2.10	>5.0	>50.0	9.11



1.5.2 Hybrid SERM/HDACi Molecules

There has been one previous example of raloxifene/HDACi hybrids, which was published by Patel et al. in 2014,¹²⁷ where they attached multiple HDACi functionalities to the 3-position of the benzothiophene core. These hybrid molecules were termed “SERMostats” by the authors. The most successful of SERMostat showed IC₅₀ values of 1-3 μM in HDACs 1-3 and was capable of inducing apoptosis in an ER- cell line (Figure 1.17). The extend of cytotoxicity was comparable to the cytotoxicity induced by combination treatments of 4-OHT, raloxifene, or DMA. The authors also demonstrated cytotoxic cargo could be conjugated onto the benzothiophene scaffold and localized to the nucleus of ER+ breast cancer cell lines.

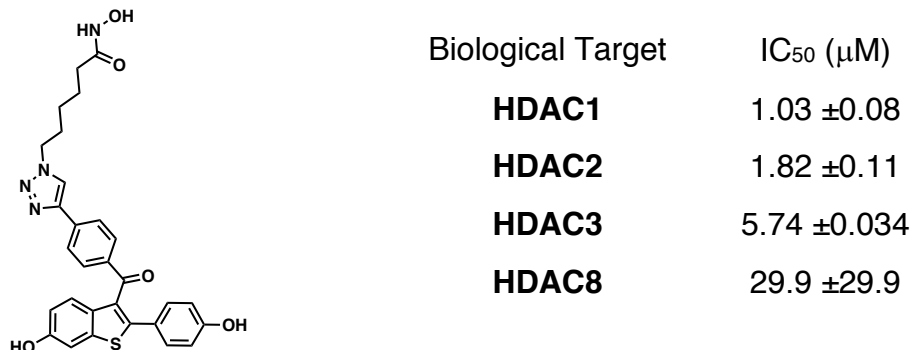


Figure 1.17 Most successful SERMostat published by Patel et al.¹²⁷ and its associated biological data.

Previous published work in the Gleason lab on SERM/HDACi hybrids incorporated the SAHA alkyl chain and hydroxamic acid into the 4-OHT scaffold.¹²⁸ Initial efforts by former Gleason lab graduate students Laurie Lim¹²⁹ and Benjamin Williams¹³⁰ were focused on constructing C-ring analogues (Figure 1.18). These analogues replaced the

antiestrogenic side chain of tamoxifen with alkyl chain of varying chain lengths bearing a terminal hydroxamic acid. It was hoped that this aliphatic linker would mimic the antiestrogenic character of the N,N-dimethylaminoethyl side chain due to the polarity of the hydroxamic acid and the retention of the ether functionality. While some of these hybrids demonstrated sub-micromolar binding of the ER and of HDAC6, they demonstrated incomplete ER inhibition and many failed to act as antagonists at all concentrations. Next, a series of A-ring substituted analogues were made. These were largely unsuccessful in binding the ER due to the removal of the phenolic moiety, which is required for a key interaction within the ER ligand binding cavity. Finally, a B-ring substituted analogue was synthesized and showed modest micromolar affinities for both the ER and HDAC6, and demonstrated full antiestrogenicity, in contrast to the A-ring hybrids.

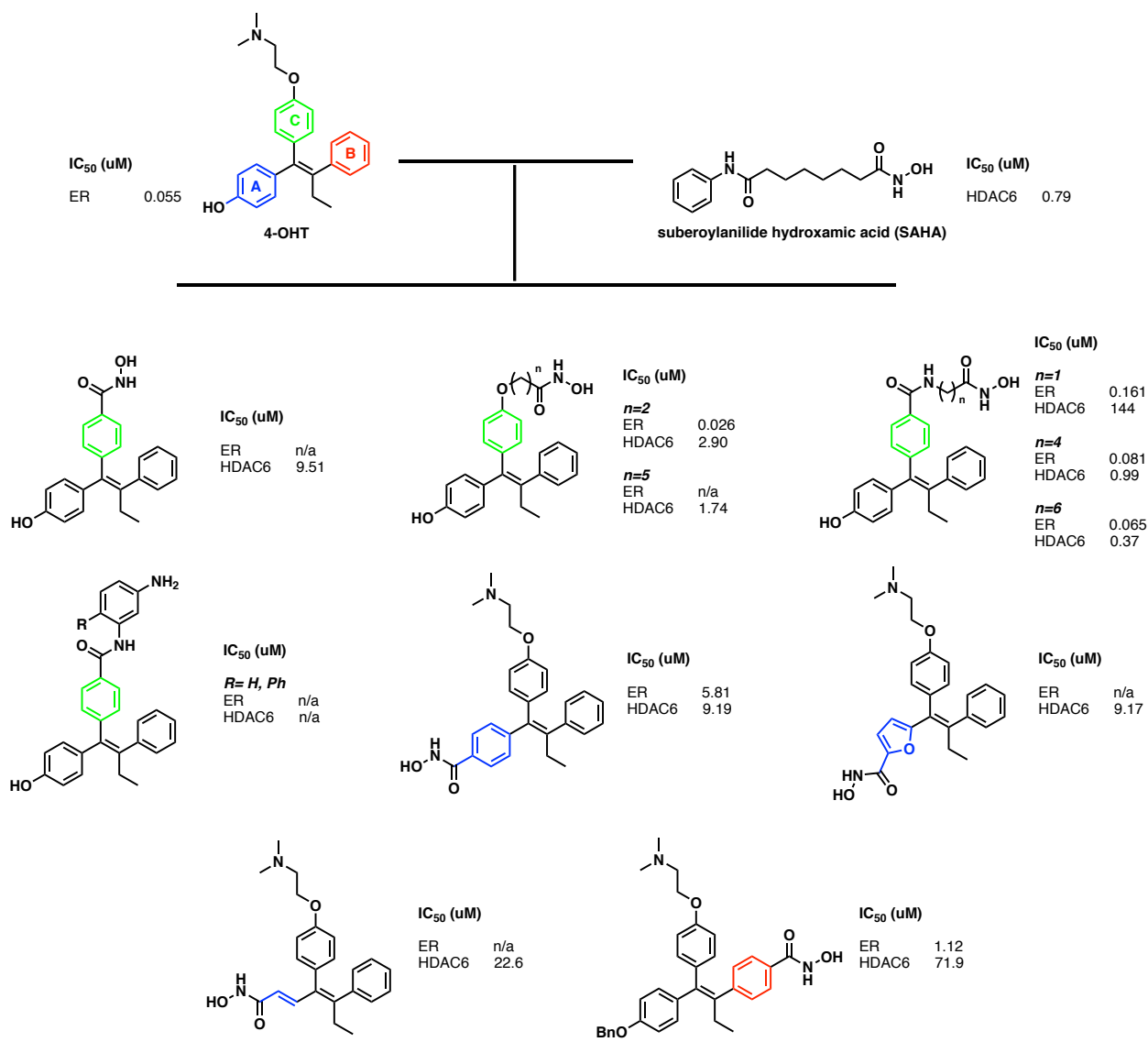


Figure 1.18 Previous 4-OHT/HDACi C- and A-ring hybrids by the Gleason lab.¹²⁹⁻¹³⁰

Biological results were mostly unfruitful, but one B-ring analogue promising.

Further exploration of the B-ring substituted analogues ensued with Anthony Palermo (Figure 1.19), another former Gleason lab graduate student. The B-ring hybrids demonstrated IC_{50} values ranging 0.69-5.64 μ M against HDAC3, 0.25-0.37 μ M against HDAC6, and 0.802-1.94 μ M against the ER. Of these, AFP-477 demonstrated the most potent cytotoxicity in cell-based assays, outcompeting both SAHA and 4-OHT in suppressing four- and seven-day growth in MCF-7 cells.¹²⁸ The potent antiproliferative

effects of AFP-477 was satisfying, given the 60% difference in IC₅₀ values (0.502 μM for 4-OHT vs. 0.818 μM for AFP-477). While gratifying, these observations were not entirely surprising, because they were in keeping with the expected outcome of a functional dual inhibitor capable of acting on several different pathways of MCF-7 cells.

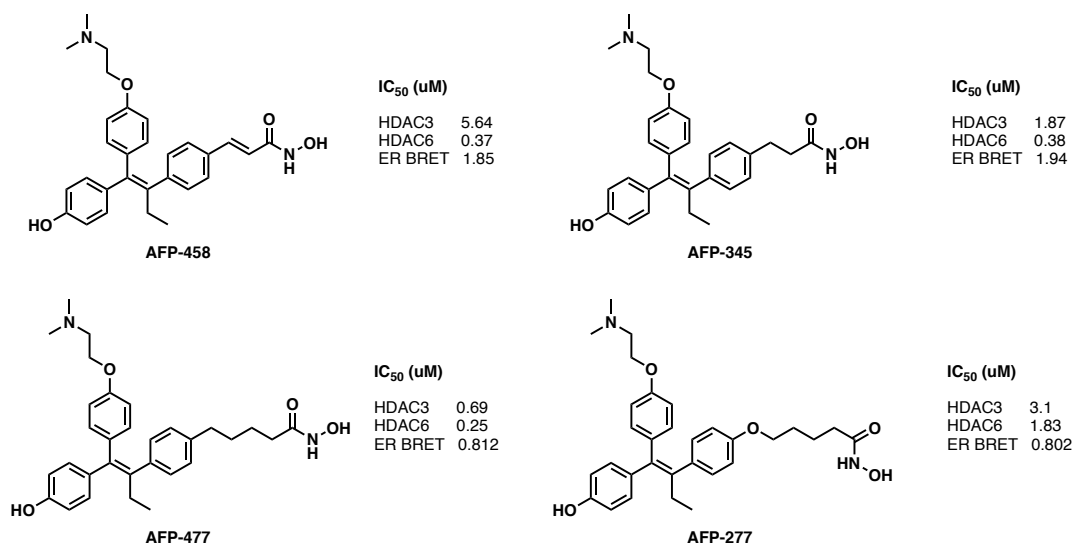


Figure 1.19 Potent B-ring substituted analogues made by Anthony Palermo.¹²⁸

While these compounds were very promising, there is still room for improvement to their cytotoxicity. One strategy for this could be the addition of a long SERD aliphatic chain in place of the N,N-dimethylaminoethyl moiety on the 4-OHT scaffold. Unfortunately, all three former graduate students had difficulties controlling the E/Z isomerization of the central olefin in both the synthetic intermediates and the final compounds themselves, even under the most stringent acid-free conditions. The tendency for the central olefin to isomerize is likely due to the additional electron-donating groups on the hybrids, which are not present on the parent tamoxifen structure. So while the 4-OHT/HDACi hybrids were encouraging, further investigations into the 4-OHT/HDACi hybrids (e.g. incorporating SERD activity) would be extremely laborious.

With this in mind, efforts were turned towards making raloxifene/HDACi hybrids that could effect the same potent biological activity as the 4-OHT/HDACi hybrids, with hopefully better inherent stability. These hybrids could eventually be made into analogues

incorporating the SERD side chains to maximize cytotoxic properties. In the raloxifene scaffold, the problematic tamoxifen alkene is locked in place by a sulfur atom, via the benzothiophene core, which has added stability owing to its aromaticity (Figure 1.20). The research described in this thesis will describe the design, synthesis, and biological evaluation of a series of these raloxifene/HDACi hybrid molecules. These hybrids will be used to test the hypothesis that drug molecules incorporating dual inhibitory activity are beneficial in the treatment of breast cancers that have become resistant to traditional hormone-based therapies.

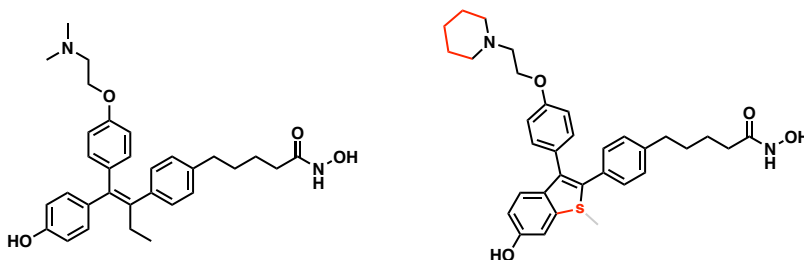


Figure 1.20 Left: A 4-OHT/HDACi hybrid,¹²⁸ unfortunately highly unstable and prone to alkene isomerization. Right: proposed raloxifene analogue of the same hybrid.

References

1. Siegel, R. L.; Miller, K. D.; Jemal, A., *CA Cancer J Clin* **2019**, *69* (1), 7-34.
2. DeSantis, C.; Ma, J.; Bryan, L.; Jemal, A., *CA Cancer J Clin* **2014**, *64* (1), 52-62.
3. Jemal, A.; Siegel, R.; Xu, J.; Ward, E., *CA Cancer J Clin* **2010**, *60*, 277-300.
4. Ali, S.; Coombes, R. C., *Nat. Rev. Cancer* **2002**, *2* (2), 101-12.
5. Osborne, K., *N. Engl. J. Med.* **1998**, *339* (22), 1609-1618.
6. Munster, P. N.; Thurn, K. T.; Thomas, S.; Raha, P.; Lacey, M.; Miller, A.; Melisko, M.; Ismail-Khan, R.; Rugo, H.; Moasser, M.; Minton, S. E., *Br. J. Cancer* **2011**, *104* (12), 1828-35.
7. Beatson, G., *Lancet* **1896**, *148*, 162-165.
8. Boyd, S., *Br. Med. J.* **1900**, *2* (2077), 1161-1167.
9. Lathrop, A. E. C.; Loeb, L., *J. Cancer Res.* **1916**, *1*, 1-16.
10. Toft, D.; Gorski, J., *Proc. Natl. Acad. Sci. U.S.A* **1966**, *55*, 1574-1581.
11. Green, S.; Walter, P.; Kumar, V.; Krust, A.; Bornert, J.-M.; Argos, P.; Chambon, P., *Nature* **1986**, *320*, 134-139.
12. Brzozowski, A. M.; Pike, A. C. W.; Dauter, Z.; Hubbard, R. E.; Bonn, T.; Engstro, O.; Ohman, L.; Greene, G. L.; Gustafsson, J.-A.; Carlquistumoto, M., *Nature* **1997**, *389*, 753-758.
13. Kuiper, G. G. J. M.; Enmark, E.; Peltö-Kuikko, M.; Nilson, S.; Gustafsson, J.-A., *Proc. Natl. Acad. Sci. U.S.A* **1996**, *93*, 5925-5930.
14. Revankar, C. M.; Cimino, D. F.; Sklar, L. A.; Arterburn, J. B.; Prossnitz, E. R., *Science* **2005**, *307* (5715), 1625-1630.
15. Filardo, E. J.; Graeber, C. T.; Quinn, J. A.; Resnick, M. B.; Giri, D.; DeLellis, R. A.; Steinhoff, M. M.; Sabo, E., *Clin. Cancer Res.* **2006**, *12* (21), 6359-66.
16. Speirs, V., *J. Pathol.* **2002**, *197* (2), 143-7.
17. Hall, J. M.; McDonnell, D. P., *Endocrinology* **1999**, *140*, 5566-5578.
18. Langer, G.; Bader, B.; Meoli, L.; Isensee, J.; Delbeck, M.; Noppinger, P. R.; Otto, C., *Steroids* **2010**, *75* (8-9), 603-10.
19. Prossnitz, E. R.; Oprea, T. I.; Sklar, L. A.; Arterburn, J. B., *J. Steroid Biochem. Mol. Biol.* **2008**, *109* (3-5), 350-3.
20. Glidewell-Kenney, C.; Hurley, L. A.; Pfaff, L.; Weiss, J.; Levine, J. E.; Jameson, J. L., *Proc. Natl. Acad. Sci. U.S.A* **2007**, *104* (19), 8173-7.
21. Dorling, A. A.; Todman, M. G.; Korach, K. S.; Herbison, A. E., *Neuroendocrinology* **2003**, *78* (4), 204-209.
22. Cooke, P. S.; Naaz, A., *Exp. Biol. Med.* **2004**, *229* (11), 1127-1135.
23. Simpson, E. R., *J. Steroid Biochem. Mol. Biol.* **2003**, *86* (3-5), 225-230.
24. Kumar, V.; Green, S.; Stack, G.; Berry, M.; Jin, J.-R.; Chambon, P., *Cell* **1987**, *51*, 941-951.
25. Lees, J. A.; Fawell, S. E.; Parker, M. G., *Nucleic Acids Res.* **1989**, *17*, 5477-5488.
26. Tora, L.; White, J.; Brou, C.; Tasset, D.; Webster, N.; Scheer, E.; Chambon, P., *Cell* **1989**, *59*, 477-487.

27. Thomas, C.; Gustafsson, J. A., *Nat. Rev. Cancer* **2011**, *11* (8), 597-608.
28. Pike, A.; Brzozowski, A.; Walton, J.; Hubbard, R.; Thorsell, A.; Li, Y.; Gustafsson, J., *Structure* **2001**, *9*, 145-153.
29. Whitley, D.; Goldberg, S. P.; Jordan, W. D., *J. Vasc. Surg.* **1999**, *29* (4), 748-751.
30. McDonnell, D. P.; Norris, J. D., *Science* **2002**, *296* (5573), 1642-1644.
31. Bjornstrom, L.; Sjoberg, M., *Nuclear Receptor* **2004**, *2* (3), 1-11.
32. Rosenblum, J. S.; Kozarich, J. W., *Curr. Opin. Chem. Biol.* **2003**, *7* (4), 496-504.
33. Klinge, C. M.; 2001, 2905-2919., *Nucleic Acids Res.* **2001**, *29*, 2905-2919.
34. Nilsson, S.; Makela, S.; Treuter, E.; Tujague, M.; Thomsen, J.; Andersson, G.; Pettersson, K.; Warner, M.; Gustafsson, J.-A., *Physiol. Rev.* **2001**, *81* (4), 1535-1565.
35. Kalkhoven, E.; Valentine, J. E.; Heery, D. M.; Parker, M. G., *EMBO* **1998**, *17* (1), 232-243.
36. Voegel, J. J.; Heine, M. J. S.; Tini, M.; Vivat, V.; Chambon, P.; Gronemeyer, H., *EMBO* **1998**, *17* (2), 507-519.
37. Rosenfeld, M. G.; Glass, C. K., *J. Biol. Chem.* **2001**, *276*, 36865-36868.
38. Dubik, D.; Dembinski, T. C.; Shiu, R. P. C., *Cancer Res.* **1987**, *47*, 6517-6521.
39. Altucci, L.; Addeo, R.; Cicatiello, L.; Dauvois, S.; Parker, M. G.; Truss, M.; Beato, M.; Sica, V.; Bresciani, F.; Weisz, A., *Oncogene* **1996**, *12* (11), 2315-2324.
40. Roy, P. G.; Pratt, N.; Purdie, C. A.; Baker, L.; Ashfield, A.; Quinlan, P.; Thompson, A. M., *Int. J. Cancer* **2010**, *127* (2), 355-60.
41. Akman, B. H.; Can, T.; Erson-Bensan, A. E., *Nucleic Acids Res.* **2012**, *40* (21), 10679-10688.
42. Inoue, K.; Fry, E. A., *Biomark Cancer* **2016**, *8*, 25-42.
43. Anstead, G. M.; Carlson, K. E.; Katzenellenbogen, J. A., *Steroids* **1997**, *62*, 268-303.
44. White, J. H., 2015.
45. Danielian, P. S.; White, R.; Hoare, S. A.; Fawell, S. E.; Parker, M. G., *Mol. Endocrinol.* **1993**, *7*, 232-240.
46. Renaud, J. P.; Rochel, N.; Ruff, M.; Vivat, V.; Chambon, P.; Gronemeyer, H.; Moras, D., *Nature* **1995**, *378* (6558), 681-9.
47. Bourguet, W.; Ruff, M.; Chambon, P.; Gronemeyer, H.; Moras, D., *Nature* **1995**, *375*, 377-382.
48. Wagner, R. L.; Apriletti, J. W.; McGrath, M. E.; West, B. L.; Baxter, J. D.; Fletterick, R. J., *Nature* **1995**, *378*, 690-697.
49. Giusti, R. M.; Iwamoto, K.; Hatch, E. E., *Ann. Intern. Med.* **1995**, *122* (10), 778-788.
50. Herbst, A.; Ulfelder, H.; Poskanzer, D.; N. Engl. J. Med. 1971, 878-881., *N. Engl. J. Med.* **1971**, *284*, 878-881.
51. Ferguson, J. H., *AJOG* **1953**, *65* (3), 592-601.
52. Swyer, G.; Law, R. In *An evaluation of the prophylactic ante-natal use of stilboestrol- preliminary report* Journal of Endocrinology, 1954; pp R6-R7.
53. Bai, Z.; Gust, R., *Arch Pharm (Weinheim)* **2009**, *342* (3), 133-49.

54. Nwachukwu, J. C.; Srinivasan, S.; Zheng, Y.; Wang, S.; Min, J.; Dong, C.; Liao, Z.; Nowak, J.; Wright, N. J.; Houtman, R.; Carlson, K. E.; Josan, J. S.; Elemento, O.; Katzenellenbogen, J. A.; Zhou, H. B.; Nettles, K. W., *Mol. Sys. Biol.* **2016**, *12* (4), 864.
55. Stewart, H.; Prescott, R.; Forrest, A.; *J. Natl. Cancer Inst.* 2001, 456-462., *J. Natl. Cancer Inst.* **2001**, *93*, 456-462.
56. Cole, M.; Jones, C.; Todd, I., *Br. J. Cancer* **1971**, *25*, 270-275.
57. Ward, H. W. C., *Br. Med. J.* **1973**, *1*, 13-14.
58. Borgna, J.-L.; Rochefort, H., *J. Biol. Chem.* **1981**, *256*, 859-868.
59. Coezy, E.; Borgna, J.-L.; Rochefort, H., *Cancer Res.* **2009**, *342*, 133-149.
60. K., A. H.; J., D. E.; V., K. J., *Biochem. Pharmacol.* **1979**, *28*, 145-147.
61. Desta, Z.; Ward, B. A.; Soukhova, N. V.; Flockhart, D. A., *J. Pharmacol. Exp. Ther.* **2004**, *310* (3), 1062-75.
62. Sato, M.; Glasebrook, A. L.; Bryant, H. U., *J. Bone Miner. Metab.* **1994**, *12*, S9-S20.
63. Jordan, V.; Phelps, E.; Lindgren, J., *Breast Cancer Res. Treat.* **1987**, *10*, 31-35.
64. Cosman, F.; Lindsay, R., *Endocr. Rev.* **1999**, *20*, 418-434.
65. Grady, D.; Gebretsadik, T.; Kerlikowske, K.; Ernster, V.; Petitti, D., *Obstet. Gynecol.* **1995**, *85* (2), 304-313.
66. Jones, C. D.; Jevnikar, M. G.; Pike, A. J.; Peters, M. K.; Black, L. J.; Thompson, A. R.; Falcone, J. F.; Clemens, J. A., *J. Med. Chem.* **1984**, *27*, 1057-1066.
67. Clemens, J. A.; Bennett, D. R.; Black, L. J.; Jones, C. D., *Life Sci.* **1983**, *32*, 2869-2875.
68. Gottardis, M. M.; Jordan, V. C., *Cancer Res.* **1987**, *47*, 4020-4024.
69. Cummings, S. R.; Eckert, S.; Krueger, K. A.; Grady, D.; Powles, T. J.; Cualey, J. A.; Norton, L.; Nickelsen, T.; Bjarnason, N. H.; Morrow, M.; Lippman, M. E.; Glusman, J. E.; Costa, A.; Jordan, V. C., *JAMA* **1999**, *281* (23), 2189-2197.
70. Delmas, P. D.; Bjarnason, N. H.; Mitlak, B.; Ravoux, A.-C.; Shah, A. S.; Huster, W. J.; Draper, M.; Christiansen, C., *JAMA* **1999**, *281* (23), 1641-1647.
71. Vogel, V. G.; Costantino, J. P.; Wickerham, D. L.; Cronin, W. M.; Cecchini, R. S.; Atkins, J. N.; Bevers, T. B.; Fehrenbacher, L.; Pajon, J., Eduardo R. ; Wade III, J. L.; Robidoux, A.; Margolese, R. G.; James, J.; Lippman, S. M.; Runowicz, C. D.; Ganz, P. A.; Reis, S. E.; McCaskill-Stevens, W.; Ford, L. G.; Jordan, V. C.; Wolmark, N., *JAMA* **2006**, *295* (23), 2727-2741.
72. Kemp, D. C.; Fan, P. W.; Stevens, J. C., *Drug Metab. Dispos.* **2002**, *6* (694-700).
73. Jordan, V. C., *Pharmacol. Rev.* **1984**, *36*, 245-276.
74. Lednicer, D.; Lyster, S. C.; Asperoren, B. D.; Duncan, G. W., *J. Med. Chem.* **1996**, *9*, 172-176.
75. Clark, E. R.; Jordan, V. C., *Br. J. Pharmacol.* **1976**, *157*, 487-493.
76. Robertson, D. W.; Katzenellenbogen, J. A.; Hayes, J. R.; Katzenellenbogen, B. S., *J. Med. Chem.* **1982**, *25*, 167-171.
77. Grese, T. A.; Cho, S.; Finley, D. R.; Godfrey, A. G.; Jones, C. D.; Lugar, C. W. I.; Martin, M. J.; Matsumoto, K., J. G.; Pennington, L. D.; Winter, M. A.; Adrian, M. D.; Cole, H. W.; Magee, D. E.; Phillips, D. L.; Rowley, E. R.; Short, L. L.; Glasebrook, A. L.; Bryant, H. U., *J. Med. Chem.* **1997**, *40*, 146-167.

78. Shao, W.; Brown, M., *Breast Cancer Res.* **2004**, *6* (1), 39-52.
79. Shang, Y.; Brown, M., *Science* **2002**, *295*, 2465-2468.
80. Shang, Y.; Hu, X.; DiRenzo, J.; Lazar, M. A.; Brown, M., *Cell* **2000**, *103*, 843-852.
81. Wakeling, A.; Dukes, M.; Bowler, M., *J. Cancer Res.* **1991**, *51*, 3867-3873.
82. Robertson, J. F. R.; Cheung, K. L., *Expert Opin. Investig. Drugs* **2005**, *11* (2), 303-308.
83. Howell, A.; DeFriend, D.; Robertson, J.; Blamey, R.; Anderson, L.; Anderson, E.; Sutcliffe, F.; Walton, P., *Br. J. Cancer* **1996**, *74*, 300-308.
84. Gibson, M. K.; Nemmers, L. A.; Beckam, W. C. J.; Davis, V. L.; Curtis, S. W.; Korach, K. S., *Endocrinology* **1991**, *129*, 2000-2010.
85. Long, X.; Nephew, K. P., *J. Biol. Chem.* **2006**, *281* (14), 9607-9615.
86. Dauvois, S.; Danielian, P. S.; White, R.; Parker, M. G., *Proc. Natl. Acad. Sci. U.S.A* **1992**, *89*, 4037-4041.
87. Hilmi, K.; Hussein, N.; Mendoza-Sanchez, R.; El-Ezzy, M.; Ismail, H.; Durette, C.; Bail, M.; Rozendaal, M. J.; Bouvier, M.; Thibault, P.; Gleason, J. L.; Mader, S., *Mol. Cell. Biol.* **2012**, *32* (19), 3823-37.
88. Traboulsi, T.; El Ezzy, M.; Gleason, J. L.; Mader, S., *J. Mol. Endocrinol.* **2017**, *58* (1), R15-R31.
89. Wijayaratne, A. L.; McDonnell, D. P., *J. Biol. Chem.* **2001**, *276* (38), 35684-92.
90. Kuukasjarvi, T.; Kononen, J.; Helin, H.; Holli, K.; Isola, J., *J. Clin. Oncol.* **1996**, *14*, 2584-2589.
91. Jordan, V. C., *Cancer Cell* **2004**, *5* (3), 207-213.
92. Levenson, A. S.; Jordan, V. C., *Cancer Res.* **1998**, *58*, 1872-1875.
93. Jordan, V. C.; Wolf, D. M., *Breast Cancer Res. Treat.* **1994**, *31*, 129-138.
94. Zhang, Q.; Borg, A.; Wolf, D.; Oesterreich, S.; Fuqua, S., *Cancer Res.* **1997**, *57*, 1244-1249.
95. Osborne, C. K.; Coronado, E.; Allred, D. C.; Wiebe, V.; DeGregorio, M., *J. Natl. Cancer Inst.* **1991**, *83* (20), 1477-1482.
96. van de Vijver, M. J.; He, Y. D.; van 't Veer, L. J.; Dai, H.; Hart, A. A. M.; Voskuil, D. W.; Schreiber, G. J.; Peterse, J. L.; Roberts, C.; Marton, M. J.; Parrish, M.; Atsma, D.; Witteveen, A.; Glas, A.; Delahaye, L.; van der Velde, T.; Bartelink, H.; Rodenhuis, S.; Rutgers, E. T.; Friend, S. H.; Bernards, R., *N. Engl. J. Med.* **2002**, *347*, 1999-2009.
97. Katzenellenbogen, B. S., *J. Natl. Cancer Inst.* **1991**, *83*, 1434-1435.
98. Bantscheff, M.; Hopf, C.; Savitski, M. M.; Dittmann, A.; Grandi, P.; Michon, A. M.; Schlegl, J.; Abraham, Y.; Becher, I.; Bergamini, G.; Boesche, M.; Delling, M.; Dumpelfeld, B.; Eberhard, D.; Huthmacher, C.; Mathieson, T.; PoECKel, D.; Reader, V.; Strunk, K.; Sweetman, G.; Kruse, U.; Neubauer, G.; Ramsden, N. G.; Drewes, G., *Nat. Biotechnol.* **2011**, *29* (3), 255-65.
99. De Ruijter, A. J.; Van Gennip, A. H.; Caron, H. N.; Kemp, S.; van Kuilenburg, A. B., *Biochem. J.* **2003**, *370*, 737-749.
100. Marks, P. A.; Rifkind, R. A.; Richon, V. M.; Breslow, R.; Miller, T.; Kelly, W. K., *Nat. Rev. Cancer* **2001**, *1*, 194-202.
101. Schwer, B.; Verdin, E., *Cell Metab.* **2008**, *7* (2), 104-12.

102. Yang, X. J.; Seto, E., *Nat. Rev. Mol. Cell. Biol.* **2008**, *9* (3), 206-18.
103. Yang, X.-J.; Seto, E., *Curr. Opin. Genet. Dev.* **2003**, *13* (2), 143-153.
104. Yang, X. J.; Gregoire, S., *Mol. Cell. Biol.* **2005**, *25* (8), 2873-2884.
105. Gregorette, I. V.; Lee, Y. M.; Goodson, H. V., *J. Mol. Biol.* **2004**, *338* (1), 17-31.
106. Marks, P. A.; Breslow, R., *Nat. Biotechnol.* **2007**, *25* (1), 84-90.
107. Duvic, M.; Talpur, R.; Ni, X.; Zhang, C.; Hazarika, P.; Kelly, C.; Chiao, J. H.; Reilly, J. F.; Ricker, J. L.; Richon, V. M.; Frankel, S. R., *Blood* **2007**, *109* (1), 31-39.
108. Falkenberg, K. J.; Johnstone, R. W., *Nat. Rev. Drug Discov.* **2014**, *13* (9), 673-91.
109. Yoshida, M.; Horinouchi, S.; Beppu, T.; 1995, 423-430., *BioEssays* **1995**, *17*, 423-430.
110. Cousens, L.; Gallwitz, D.; Alberts, B., *J. Biol. Chem.* **1979**, *254*, 1716-1723.
111. Drummond, D. C.; Noble, C. O.; Kirpotin, D. B.; Guo, Z.; Scott, G. K.; Benz, C. C., *Ann. Rev. Pharmacol. Toxicol.* **2005**, *45*, 495-528.
112. Madsen, A. S.; Kristensen, H. M.; Lanz, G.; Olsen, C. A., *ChemMedChem* **2014**, *9* (3), 614-26.
113. Finnin, M.; Donigian, J.; Cohen, A.; Richon, V.; Rifkind, R.; Marks, P.; Breslow, R.; Pavletich, N., *Nature* **1999**, *401*, 188-193.
114. Karagiannis, T. C.; El-Osta, A., *Leukemia* **2007**, *21* (1), 61-5.
115. Lapidus, R. G.; Ferguson, A. T.; Ottaviano, Y. L.; Parl, F. F.; Smith, H. S.; Weitzman, S. A.; Baylin, S. B.; Issa, J. P.; Davidson, N. E., *Clin. Cancer Res.* **1996**, *2*, 805-810.
116. Yang, X.; Phillips, D.; Ferguson, A.; Nelson, W.; Herman, J.; Davidson, N. E., *Cancer Res.* **2001**, *61*, 7025-7029.
117. Kawai, H.; Li, H.; Avraham, S.; Jiang, S.; Avraham, H. K., *Int. J. Cancer* **2003**, *107* (3), 353-8.
118. Luo, J.; Su, F.; Chen, D.; Shiloh, A.; Gu, W., *Nature* **2000**, *408*, 377-381.
119. Harms, K. L.; Chen, X., *Cancer Res.* **2007**, *67* (7), 3145-52.
120. Munster, P.; Troso-Sandoval, T.; Rosen, N.; Rifkind, R.; Marks, P.; Richon, V., *Cancer Res.* **2001**, *61*, 8492-8497.
121. Zhang, Z.; Yamashita, H.; Toyama, T.; Sugiura, H.; Ando, Y.; Mita, K.; Hamaguchi, M.; Hara, Y.; Kobayashi, S.; Iwase, H., *Breast Cancer Res Treat* **2005**, *94* (1), 11-6.
122. Krusche, C. A.; Wulfing, P.; Kersting, C.; Vloet, A.; Bocker, W.; Kiesel, L.; Beier, H. M.; Alfer, J., *Breast Cancer Res. Treat.* **2005**, *90*, 15-23.
123. Meunier, B., *Acc. Chem. Res.* **2008**, *41*, 69-77.
124. Lai, C. J.; Bao, R.; Tao, X.; Wang, J.; Atoyan, R.; Qu, H.; Wang, D. G.; Yin, L.; Samson, M.; Forrester, J.; Zifcak, B.; Xu, G. X.; DellaRocca, S.; Zhai, H. X.; Cai, X.; Munger, W. E.; Keegan, M.; Pepicelli, C. V.; Qian, C., *Cancer Res* **2010**, *70* (9), 3647-56.
125. Lamblin, M.; Dabbas, B.; Spingarn, R.; Mendoza-Sanchez, R.; Wang, T. T.; An, B. S.; Huang, D. C.; Kremer, R.; White, J. H.; Gleason, J. L., *Bioorg. Med. Chem.* **2010**, *18* (11), 4119-37.

126. Mendoza-Sanchez, R.; Cotnoir-White, D.; Kulpa, J.; Jutras, I.; Pottel, J.; Moitessier, N.; Mader, S.; Gleason, J. L., *Bioorg. Med. Chem.* **2015**, *23* (24), 7597-606.
127. Patel, H. K.; Siklos, M. I.; Abdelkarim, H.; Mendonca, E. L.; Vaidya, A.; Petukhov, P. A.; Thatcher, G. R., *ChemMedChem* **2014**, *9* (3), 602-13.
128. Palermo, A. F.; Diennet, M.; El Ezzy, M.; Williams, B. M.; Cotnoir-White, D.; Mader, S.; Gleason, J. L., *Bioorg. Med. Chem.* **2018**, *26* (15), 4428-4440.
129. Lim, L. Effects Towards the Design and Synthesis of Small Molecule Inhibitors of the Estrogen Receptor. MSc thesis, McGill University, Montreal, Canada, 2011.
130. Williams, B. Design, synthesis and evaluation of selective estrogen receptor modulator/histone deacetylase inhibitor merged bifunctional ligands. MSc thesis, McGill University, Montreal, Canada, 2014.

Chapter 2: Design, Synthesis, and Biology of Hybrid Molecules

2.1 Strategies for Bifunctional Hybrid Molecules

The incorporation of a HDACi hydroxamic acid side chain into 4-OHT was investigated by three former graduate students in the Gleason lab: Anthony Palermo, Ben Williams, and Laurie Lim. To summarize these efforts (which are covered in more depth in Chapter 1), a series of analogues were initially synthesized, which incorporated aliphatic side chains (with varying chain lengths), terminating in a hydroxamic acid into the C-ring of 4-OHT.¹⁻² The rationale for the C-ring analogues was that the aliphatic hydroxamic acid would resemble the antiestrogenic character of the N,N-dimethylamino ethyl side chain. Unfortunately, most of the hybrids failed to act as antagonists at any concentration tested. Anthony Palermo was able to make a more promising B-ring series, of which the most potent contained a four-carbon linker with a terminal hydroxamic acid.³ The impressive antiproliferative potency of the B-ring analogues was attributed to its dual-nature design, and its ability to inhibit multiple biological pathways. While these hybrids were potent, their cytotoxicity could be improved upon by further modification of their structures, such as in the incorporation of the antiestrogenic long aliphatic chain of SERDs.

Unfortunately, all three former graduate students had difficulties controlling the E/Z isomerization of the intermediates involved in the synthesis and the final compounds themselves. So while their findings were encouraging, further investigation of the 4-OHT/HDACi hybrids would be extremely laborious.

Given this, efforts were redirected into designing a synthesis of raloxifene/HDACi hybrids that could effect the same potent biological activity as the 4-OHT/HDACi hybrids, with hopefully better inherent stability. The first goal of this project was to make a series of raloxifene/HDACi hybrids analogous to the successful B-ring 4-OHT/HDACi hybrids. A second goal was to develop and optimize a synthesis for these raloxifene/HDACi hybrids that could be easily amenable to further incorporation of more potent biological activity

(e.g. SERD pharmacophore) for a set of 2nd generation molecules to be made in the future.

The design of these molecules would build upon the findings from previous studies on the 4-OHT/HDACi hybrids. Several structural parallels are immediately obvious when comparing the 4-OHT and raloxifene structures (Figure 2.1). The A-ring of 4-OHT is translated into the phenolic ring of raloxifene's central benzothiophene. The C-ring of both 4-OHT and raloxifene is the ring which bears the critical aminoalkyl side chain responsible for antiestrogenic activity. The central alkene in 4-OHT is locked in place by the sulfur of the thiophene in raloxifene. Finally, the phenyl B-ring of 4-OHT is mirrored by the phenol ring of raloxifene.

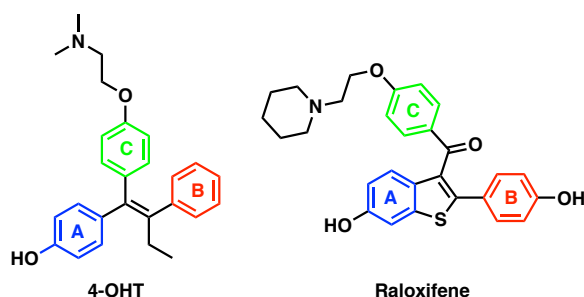


Figure 2.1 Comparison of the 4-OHT and raloxifene scaffold.

Since the primary goal of this project was to translate the successful B-ring 4-OHT/HDACi hybrids into raloxifene/HDACi hybrids, it was decided that the HDACi functionality would be introduced onto the raloxifene phenol ring, which is analogous to the 4-OHT B-ring. These bi-functional inhibitors would be made by combining or replacing the aryl cap of the HDACi pharmacophore with the aryl scaffold of raloxifene (Figure 2.2), while retaining the alkyl chain and HDACi moiety. The phenolic oxygen of raloxifene would be either removed or retained, giving rise to a set of C-linked hybrids and a set of O-linked hybrids.

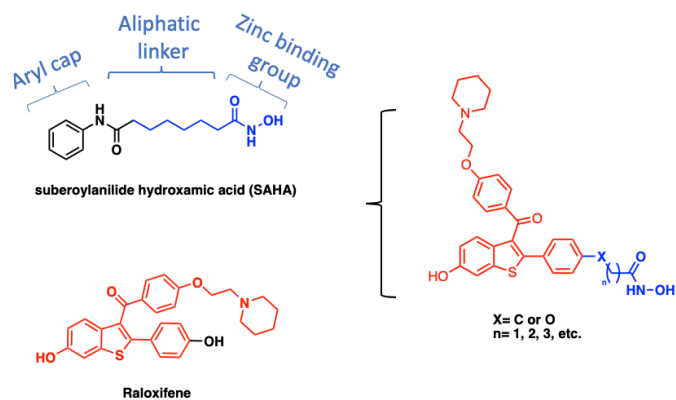


Figure 2.2 Raloxifene/HDACi hybrids made by replacing the aryl cap of HDACi's with raloxifene.

A main concern in designing hybrids was whether the modified scaffolds of the bifunctional molecules would still fit into the binding cavity of their intended biological targets. Given that the ER ligand binding cavity is 450 Å, almost twice the volume of its endogenous ligand E2, it was expected that adding an aliphatic side chain to raloxifene would be well-tolerated. This is supported by the success with the 4-OHT/HDACi B-ring series hybrids that incorporate the aliphatic side chain and hydroxamic acid at an analogous position on the raloxifene scaffold. More supporting evidence for this came in the form of computational docking of a series of proposed hybrids in the ER and HDAC binding pockets.

In silico techniques have been used extensively to discover and optimize drug pharmacophores in medicinal chemistry, leading to the discovery of several inhibitors across many drug classes. In the Department of Chemistry at McGill, the Moitessier lab has developed the molecular docking software platform called FITTED (Flexibility Induced Through Targeted Evolutionary Description). FITTED has played an important role in the development of prolyl oligopeptidase inhibitors from the Moitessier group,⁴⁻⁵ and has aided in the design of bifunctional drug molecules in the Gleason lab.⁶ FITTED uses a genetic algorithm to optimize the lowest energy conformation of a given ligand within a binding site, then outputs a score. The score is a measure of how well the docked ligand binds in the protein. It is calculated by taking into account a number of parameters

including London dispersion forces, van der Waals interactions, and H-bonding interactions.⁷

2.2 Hybrid Design and Molecular Docking Using FITTED

A small virtual library of hybrid raloxifene/HDACi hybrids was prepared for virtual docking (Figure 2.3). The library consisted of both carbon- and oxygen-linked hydroxamic acids with alkyl chain lengths of varying lengths. The molecules YW1-PhO-1, YW2-PhO-2, and YW3-PhO-3 all retained the raloxifene phenolic oxygen and built on either a one-, two-, or three- carbon aliphatic linker with a terminal hydroxamic acid. The molecules YW4-Ph-1, YW5-Ph-2, YW6-Ph-3 all discarded the phenolic oxygen, and respectively had either a one-, two-, or three- carbon aliphatic linker with a terminal hydroxamic acid. YW8-Ph had a hydroxamic acid directly attached to the phenyl ring without any alkyl linker. The scaffold of YW7-Ph-cin had the hydroxamic acid attached to the phenyl ring via a cinnamate. YW13-Ben was included as a benzamide analogue for variety in the HDACi moiety. YW12-Alkyl-3, YW10-Alkyl-1, YW11-Alkyl-2, and YW9-Alkyl were a final set of analogues with the alkyl chain attached directly to the raloxifene core, with the 2-phenyl ring missing. The rationale behind the final set of analogues being that the 2-phenyl ring with alkyl and cycloalkyl groups does not appear to alter the SERM profile of raloxifene both in vivo or in vitro.⁸

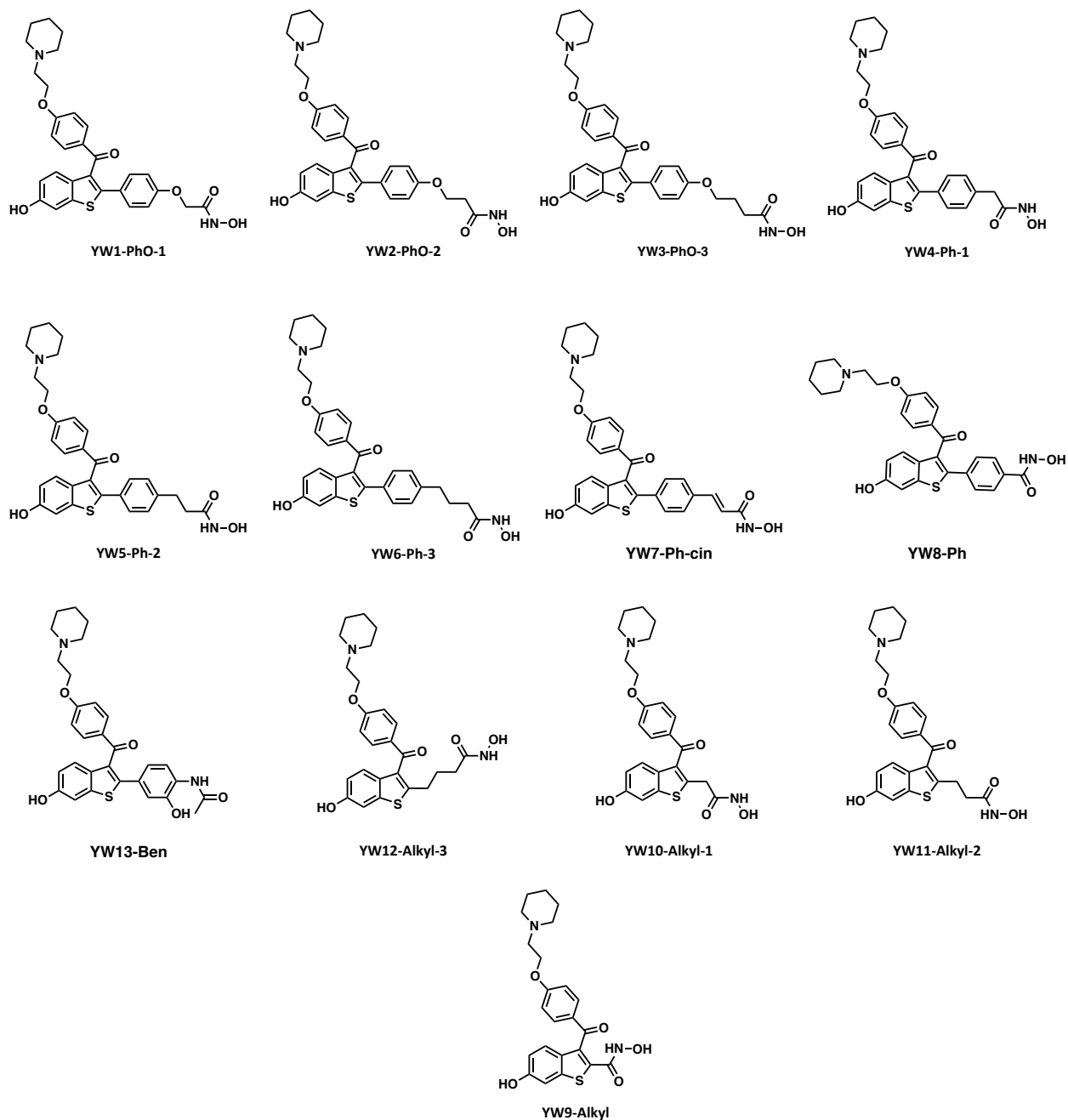


Figure 2.3 A virtual library of hybrid compounds for screening in FITTED.

Once uploaded, the hybrid library 2D file was converted to 3D structures. These were then docked into protein crystal structure PDB files. The PDB file 1ERa was chosen for docking into the ER because it is the crystal structure of raloxifene bound to the ER.⁹ Raloxifene itself was docked back into the 1ERa PDB file for comparison. The results of this computational comparison are represented in Figure 2.4, where the more negative a

score is, the better ligand-protein interaction there is predicted to be. Raloxifene itself scored the best at -25.038 , but the YW10-Alkyl-1 came at a close second, scoring -24.266 . Another hybrid that showed promise was YW6-Ph-3, which generated a rank score of -22.337 .

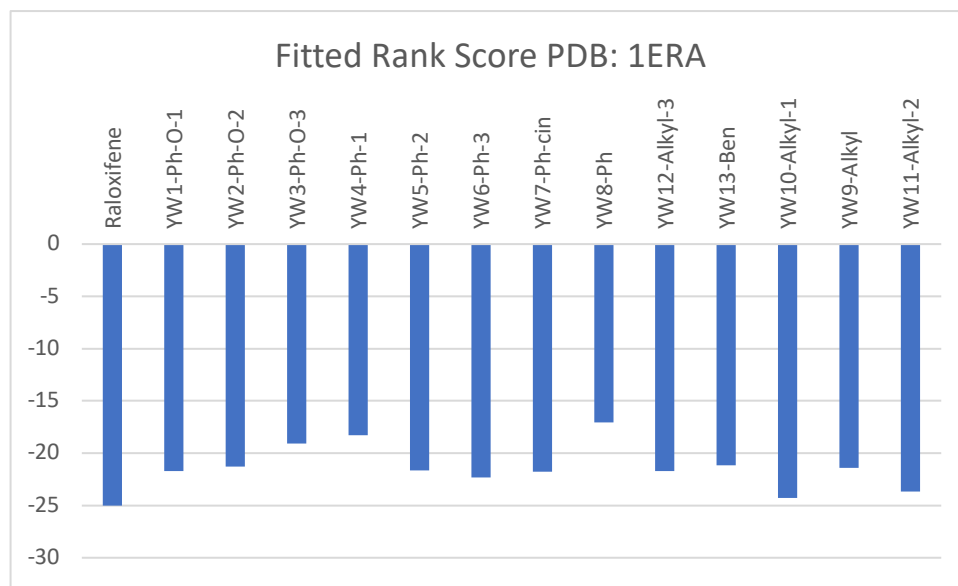


Figure 2.4 The FITTED-generated rank scores for raloxifene/HDACi hybrids docked into the ER (PDB: 1ERA).

While raloxifene was docked correctly back into the ER, many of the hybrids did not fit properly inside the ligand binding pocket of the ER. In many of these cases, the lipophilic cores of these molecules extended outside of the ER binding pocket with the piperidine side chain instead making contacts within the ligand binding cavity. These illogical docking poses were obtained from YW4-Ph-1, YW7-Ph-cin, YW8-Ph, and YW13-Ben. A general feature of hybrids with illogical 1ERA docking poses is that they contain either short alkyl chains (YW4-Ph-1 and YW7-Ph-cin) or no alkyl chain (YW8-Ph and YW13-Ben). The docking pose of YW13-Ben is shown as an example in Figure 2.5, where its lipophilic core of is extended outside of the ER ligand binding domain, while the piperidine side chain is extended into the protein core.

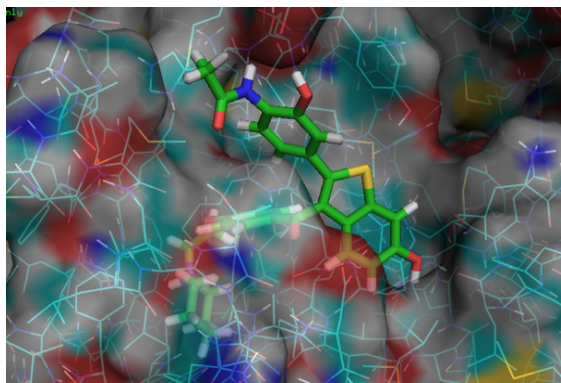


Figure 2.5 FITTED-generated non-sensical docking pose of YW13-Ben with PDB:1ERa.

In contrast, all other molecules in the virtual library generated sensible docking poses (YW1-Ph-O-1, YW2-Ph-O-2, YW3-Ph-O-3, YW5-Ph-2, YW6-Ph-3, YW12-Alkyl-3, YW10-Alkyl-1, YW9-Alkyl, YW11-Alkyl-2). Sensible docking poses were defined as molecules whose raloxifene cores were extended into the ER ligand binding cavity, where the same or similar H-bonding contacts were made as raloxifene. Generally, the benzothiophene phenolic ring of these molecules made at least two hydrogen-bonding interactions to protein residues within the ligand binding domain. Of these, the docking poses of YW10-Alkyl-1 and YW1-PhO-1 are shown in Figure 2.6. The raloxifene core of YW10-Alkyl-1 is clearly extended into the ER ligand binding cavity, and the A-ring phenolic residue makes H-bonding interactions with Arg3-306, Glu3-265, and Phe4-337. Another example demonstrating proper ligand conformation inside ER is YW1-PhO-1, where H-bonding interactions are made between its A-ring phenol and residues inside the ER ligand binding pocket (Glu3-265 and Arg3-306).

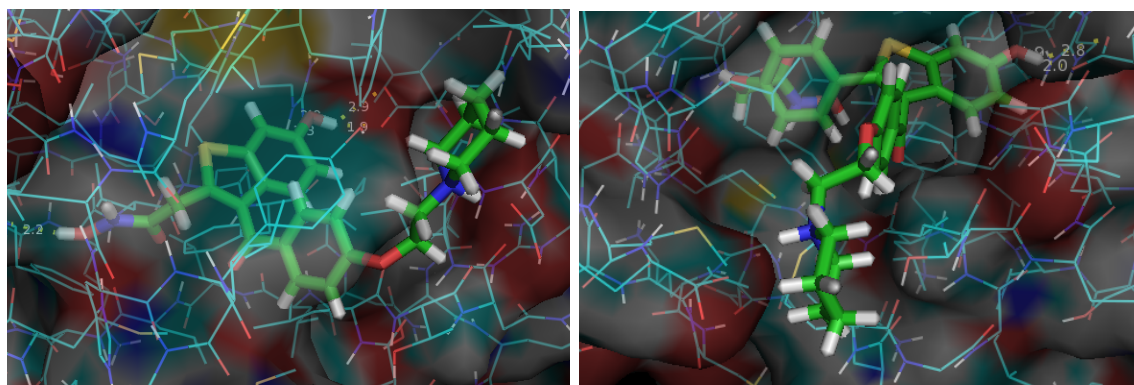


Figure 2.6 FITTED-generated sensical docking poses with PDB:1ERa. Left: YW10-Alkyl-1. Right: YW1-PhO-1.

The PDB file 4LX was used for docking the virtual library into HDAC2. 4LXZ is a X-ray crystal structure of HDAC2 in a complex with SAHA.¹⁰ All the hybrids, except for YW10-Alkyl-1 scored around -30 or lower (Figure 2.7). The best-scoring hybrids were YW7-Ph-cin, YW8-Ph, YW12-Alkyl-3, and YW11-Alkyl-2. There was no clear correlation between alkyl chain length and rank score.

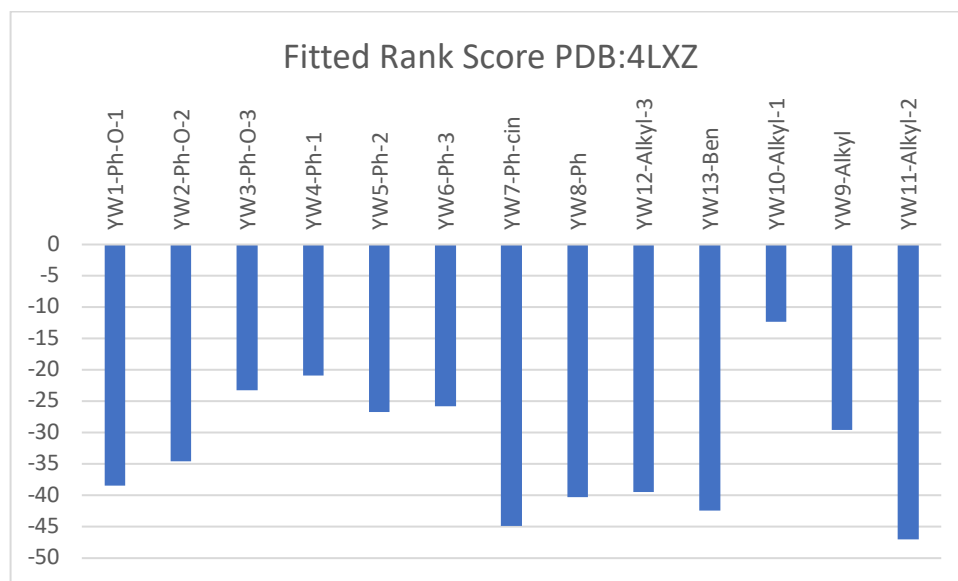


Figure 2.7 The FITTED-generated rank scores for raloxifene/HDACi hybrids docked into HDAC2 (PDB: 4LXZ).

Molecules missing the raloxifene B-ring (YW9-Alkyl, YW10-Alkyl-1, YW11-Alkyl-2, YW12-Alkyl-3) tended to exhibit poor docking poses, where the hydroxamic acid did not extend into the HDAC substrate binding pore. YW11-Alkyl-2, which had one of the best rank scores, did not in fact bind the HDAC substrate binding channel in a sensical manner (Figure 2.8). The benzamide-containing molecule (YW-13-Ben) also did not dock into 4LXZ in a sensical manner, where its Zn²⁺-binding benzamide extended exterior to the substrate binding channel (Figure 2.8). All other hybrids (YW1-Ph-O-1, YW2-Ph-O-2, YW3-Ph-O-3, YW4-Ph-1, YW5-Ph-2, YW6-Ph-3, YW7-Ph-cin, YW8-Ph) demonstrated the expected binding conformation, where the HDACi moiety extends into the HDAC substrate binding pore. Two examples (YW2-Ph-O-2, YW5-Ph-2) are shown in Figure 2.8. These data suggest that the B-ring is required for binding to HDAC2.

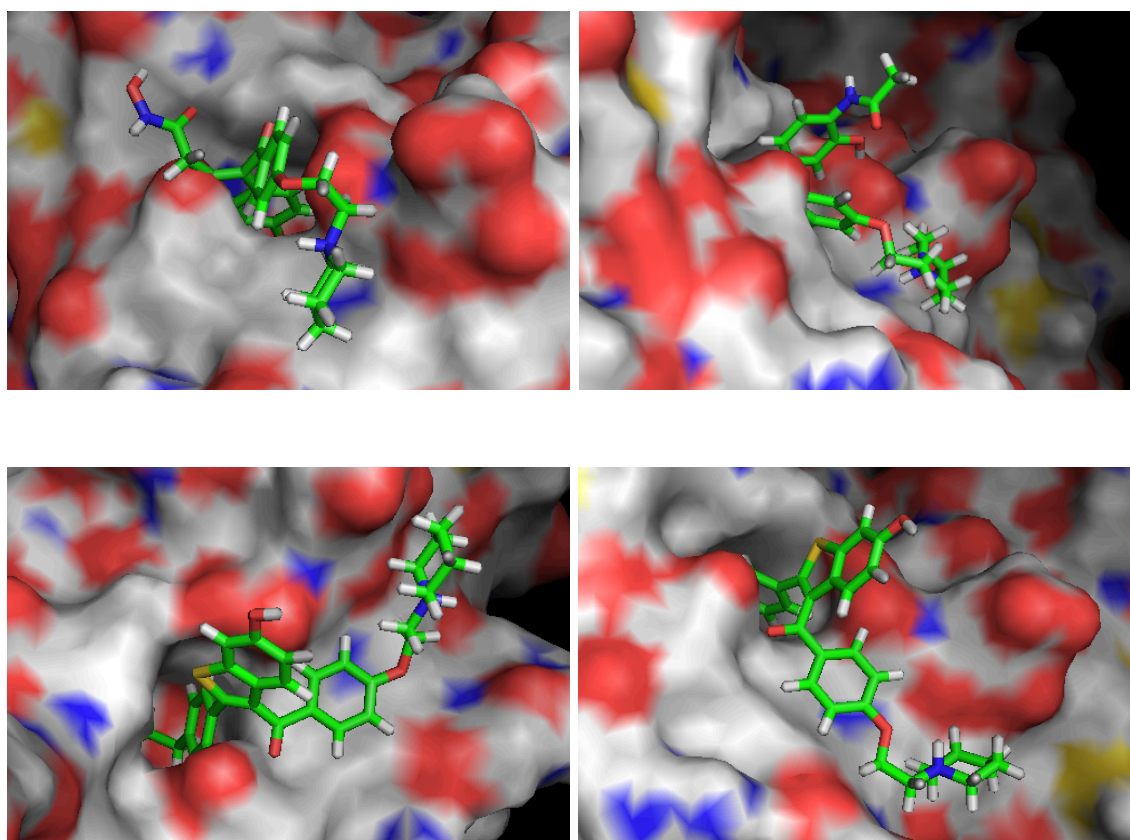


Figure 2.8 FITTED-generated docking poses with PDB:4LXZ. Top: non-sensical docking poses (left: YW11-Alkyl-2, right: YW13-Ben). Bottom: sensical docking poses (left: YW2-Ph-O-2, right: YW5-Ph-2).

The PDB file 5EDU was used for docking into HDAC6. 5EDU is a X-ray crystal structure of HDAC6 in complex with Trichostatin A.¹¹ All the hybrids, except YW13-Ben, had rank scores lower than -30. As shown in Figure 2.9, hybrids with the best rank scores were YW1-Ph-O-1, YW7-Ph-cin, and YW8-Ph. More generally, hybrids retaining the B-ring tended to score the best, whether they retained (YW1-Ph-O-1, YW2-Ph-O-2, YW3-Ph-O-3) or omitted (YW4-Ph-1, YW5-Ph-2, YW6-Ph-3) the phenolic oxygen, including the cinnamate-containing hybrid (YW7-Ph-cin). Within the sets of similar hybrids, there was no clear pattern of correlation between alkyl chain lengths and rank scores.

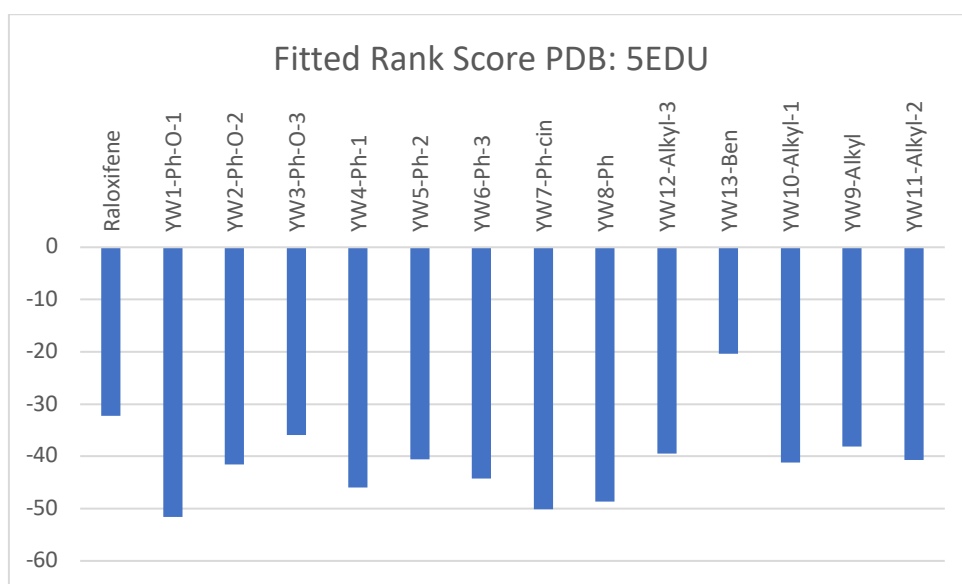


Figure 2.9 The FITTED-generated rank scores for raloxifene/HDACi hybrids docked into HDAC6 (PDB: 5EDU).

Despite many of the molecules missing the raloxifene B-ring (YW9-Alkyl, YW10-Alkyl-1, YW11-Alkyl-2, YW12-Alkyl-3) generating good rank scores, they tended to exhibit poor docking poses, where the hydroxamic acid did not extend into the HDAC substrate binding pore (Figure 2.10). The benzamide-containing molecule (YW-13-Ben) also did not dock into 5EDU in a promising manner (Figure 2.10). This is unsurprising, given the low rank score generated for this compound.

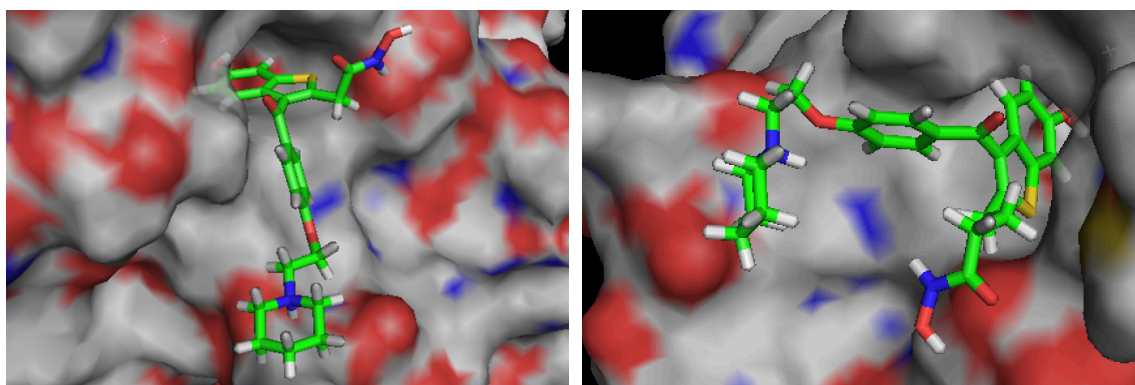


Figure 2.10 FITTED-generated non-sensical docking poses with PDB:5EDU. Left: docking pose for YW10-Alkyl-1. Right: docking pose for YW12-Alkyl-3.

All other hybrids demonstrated the expected binding conformation when docked into 5EDU, where the HDACi moiety extends into the HDAC substrate binding pore. The hybrids with sensical docking poses all retain the B-ring of raloxifene, and are all hydroxamic acid-based HDACi's, suggesting these are important features for binding HDAC6. Two examples are illustrated in Figure 2.11.

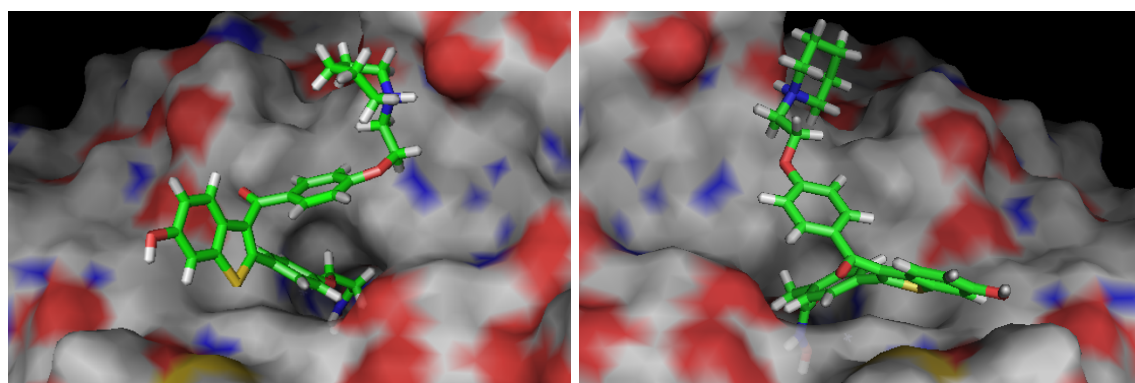


Figure 2.11 FITTED-generated sensical docking poses with PDB:5EDU. Left: YW2-Ph-O-1. Right: YW4-Ph-1.

While computational methods are fast and convenient, the results they generate must be interpreted carefully. Many hybrids which scored well had nonsensical binding poses or poses that contradicted the known raloxifene binding mode. While the rank

scores and binding modes generated by FITTED were taken into consideration when selecting hybrids for synthesis, greater weight was placed on the rationale developed from the extensive work done by previous graduate students who had worked on 4-OHT/HDACi hybrid molecules. The molecules that ended up being selected for synthesis are shown in Figure 2.12. They were chosen strategically in order to maximize the potential for discovering a high affinity molecule based on docking results, and also for their synthetic similarity to each other in order to maximize the size of the library and minimize synthetic effort required to make them. The analogues with one phenyl ring missing (YW12-Alkyl-3, YW10-Alkyl-1, YW9-Alkyl, YW11-Alkyl-2) were discarded, due to their inconsistent irrational binding conformations when docked to HDAC3. The ineffectiveness of shorter alkyl chain hydroxamic acids were observed previously by Ben Williams, so with the exception of compound **1**, the chosen molecules contained at least 4-atom alkyl linkers. The oxygen-linked analogues would have the same number of atoms in the alkyl linker as those in the carbon-linked molecules, with one carbon being replaced with oxygen. The remainder of this thesis will focus on the synthesis and biological evaluation of the hybrid candidates shown in Figure 2.12. However, further investigations into other hybrids (e.g. those incorporating SERD pharmacophores) will be considered for future projects.

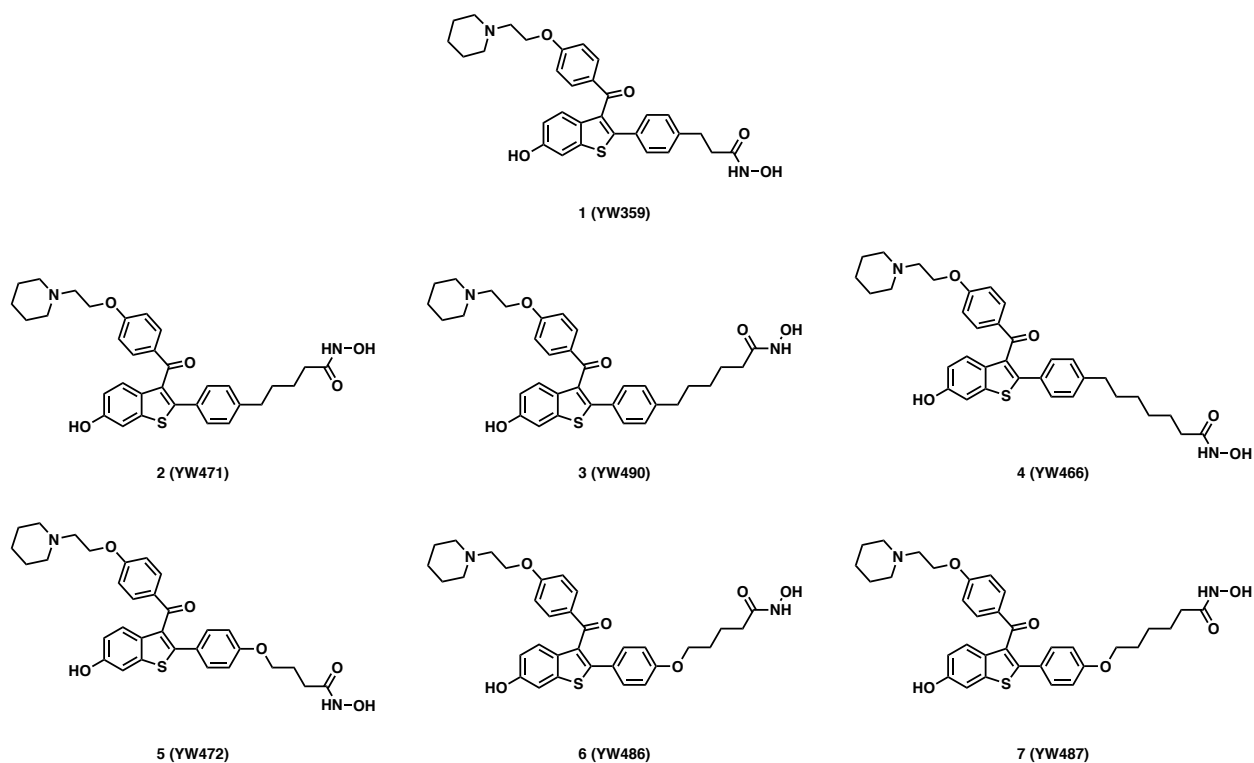


Figure 2.12 Hybrids selected for synthesis.

2.3 Design of SERM/HDACi hybrids

A plethora of raloxifene and raloxifene analogue syntheses have been published, with several representative examples.^{8, 12-28} In general, there are two commonly-employed strategies to construct raloxifene and related analogues (Figure 2.13). The first approach uses either acylation, or nucleophilic aromatic substitution, or both as key step(s). The second approach uses a Grignard addition on to a condensed dialkylamine unit on the benzothiazole. Given that the former has greater literature precedent, the initial retrosynthetic analysis was based on the first approach.

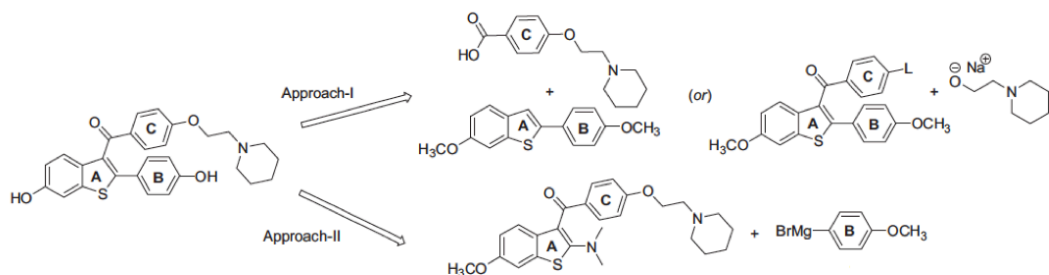
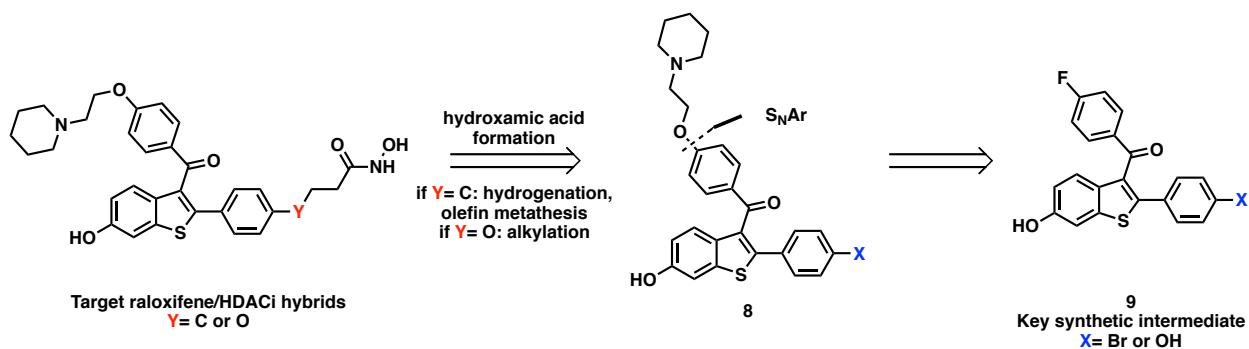


Figure 2.13 Common retrosynthetic strategies towards the raloxifene.²⁹

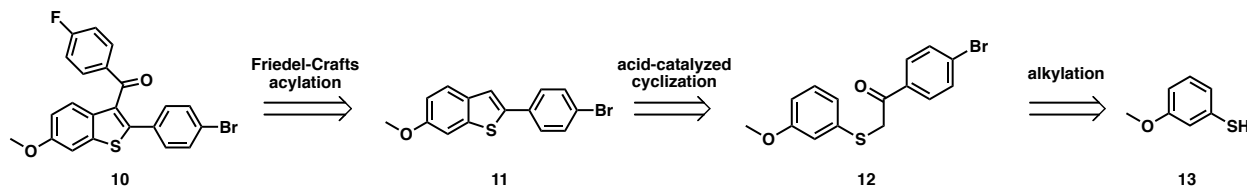
2.4 Synthesis of SERM/HDACi hybrids

Retrosynthetic analysis revealed both the carbon-linked and oxygen-linked hybrids could be made from a similar synthetic route (Scheme 2.1). Given the practical difficulty with which hydroxamic acids are to manipulate due to their high polarity, it was anticipated that the hydroxamic acid formation from the corresponding ester would have to occur last. For the oxygen-linked hybrids, the ester could be attached directly via alkylation with different electrophiles with varying chain length. For the carbon-linked hybrids, the requisite ester could come from olefin metathesis with the appropriate alkene esters. Hydrogenation of the resulting olefin would give access to the desired alkyl side chain. The piperidine side chain could be attached to the main raloxifene triaryl core via a nucleophilic aromatic substitution (S_NAr), bringing the retrosynthetic analysis back to a key synthetic intermediate **9**.



Scheme 2.1 The retrosynthetic analysis to key intermediate **9**.

In our first strategy, it was conceived the key intermediate **9** could come easily from its methyl-protected equivalent **10** (with X= Br, shown in Scheme 2.2). Friedel-Crafts acylation could be used to install the ketone from the aryl bromide **11**. The benzothiophene was envisioned to come from an acid-catalyzed cyclization of an alkylated 3-methoxythiophenol (**13**), which is commercially-available.



Scheme 2.2 Retrosynthetic analysis of the synthetic intermediate **10**.

The acid-catalyzed cyclization, which was reported to occur with a concomitant phenyl shift, had been well-documented in various syntheses of raloxifene, including in one of the original publications from Eli-Lilly.¹⁵ This cyclization and phenyl shift appeared to work well on both electron-rich substrates³⁰ and electron-poor substrates (Figure 2.14).¹⁸ In fact, this phenyl-shift was reported to occur so easily on the original methoxy-substituted substrate^{15, 31} that methods were expressly developed for the cyclization while avoiding the accompanying phenyl shift.³² Additionally, this strategy was appealing because there had been one previous report of the exact substrate of interest.¹⁴

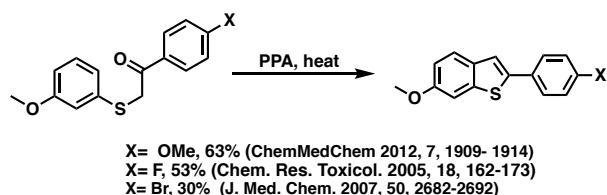
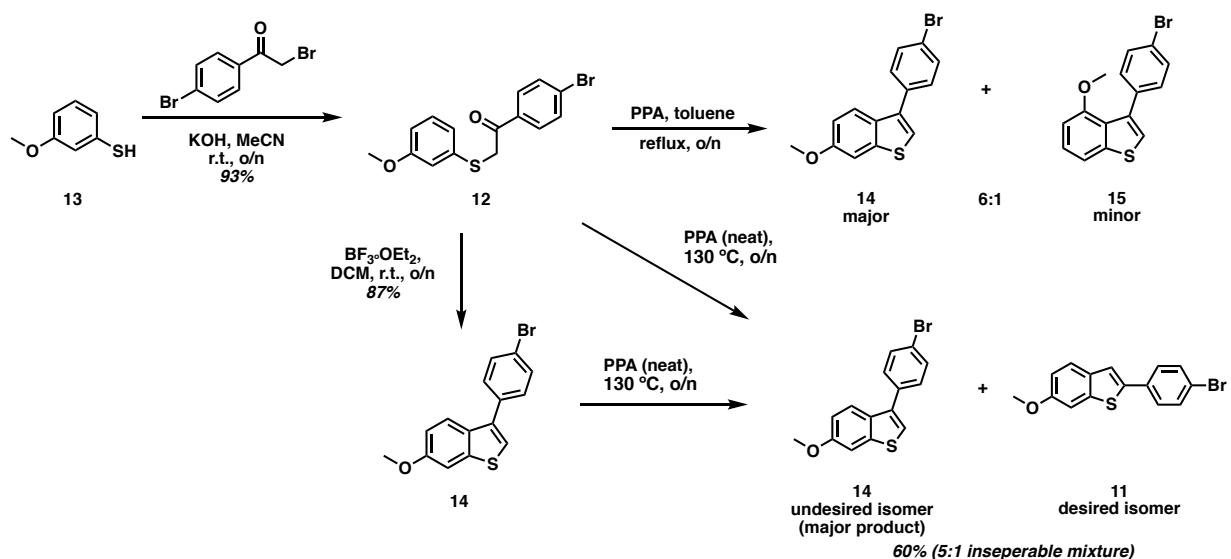


Figure 2.14 Select literature examples of the desired polyphosphoric acid (PPA)-mediated cyclization and phenyl-shift on electron-rich and electron poor substrates.

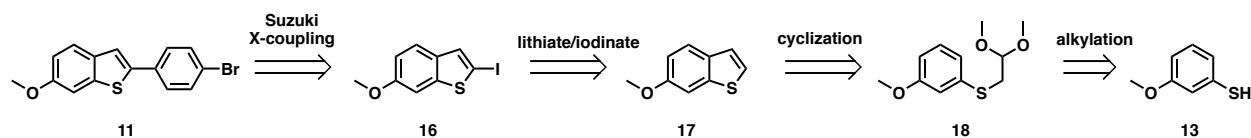
Our synthesis proceeded in the forward sense via the alkylation of commercially-available 3-methoxythiophenol with 2-bromo-1-(4-bromophenyl)ethan-1-one, which

proceed easily (Scheme 2.3). With the alkylated **12** in hand, the ring closure was effected with polyphosphoric acid (PPA) in refluxing toluene. This gave both the *ortho* and *para* ring closure products **14** and **15**. Unfortunately, neither product seemed to have undergone the desired phenyl shift. More forcing conditions were then used, in which **12** was refluxed in neat polyphosphoric acid, at a higher temperature. Even after extensive reaction optimization, only a small amount of the desired 2-aryl isomer was ever formed, giving a 5:1 mixture in favour of the unrearranged 3-aryl product. Not only was the desired product formed in exceedingly low yields, the two isomers were inseparable by standard techniques. Subjecting 3-aryl benzothiophene **14** to the reaction did not improve the yield of the phenyl-shifted product. The desired phenyl shift was not influenced by Lewis acids, nor was it promoted by more acidic Bronsted acids (e.g. TFA).



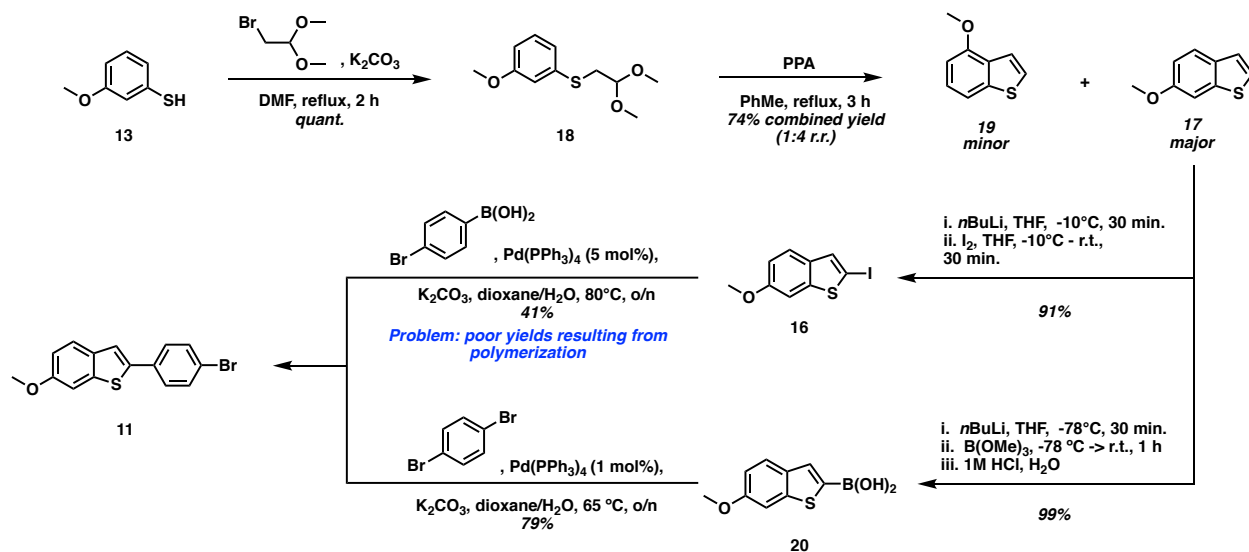
Scheme 2.3 PPA-catalyzed cyclization and phenyl shift approach towards the aryl core.

At this point, the phenyl-shift strategy was abandoned and the construction of the benzothiophene core was redesigned. The second strategy relied on a Suzuki cross-coupling to access to the 2-(*para*-bromo)-phenyl ring (Scheme 2.4). The aryl iodide cross-coupling partner **16** would come from lithiation and iodination of the benzothiophene core **17**, which in turn could come from an acid-catalyzed cyclization of alkylated thiophenol **18**, a well-documented reaction in the literature.³³



Scheme 2.4 A second strategy into aryl bromide **11** via a Suzuki cross-coupling.

In the forward direction (Scheme 2.5), alkylation and acid-catalyzed cyclization of 3-methoxythiophenol gave a mixture of the 4-methoxybenzothiophene and 6-methoxybenzothiophene regioisomers in a 1:4 ratio, with the 6-methoxybenzothiophene being favoured to form due to sterics. The 6-methoxybenzothiophene smoothly underwent a lithiation/iodination sequence in 91% yield. Originally, the iodination was carried out with NIS, but this was later switched to I_2 which gave a cleaner reaction and higher yield. The resulting aryl iodide **16** underwent a Suzuki cross-coupling with 4-bromophenyl boronic acid to give the desired 2-(*para*-bromophenyl)-6-methoxybenzothiophene in 41% yield. A large part of the theoretical yield was lost to undesired polymerization side reactions, where the palladium catalyst would insert into the product aryl bromide bond and proceed to cross-couple with excess equivalents of boronic acid.

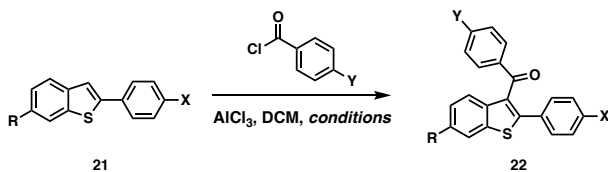


Scheme 2.5 Successful synthesis of **11**.

This route was optimized by taking the 6-methoxybenzothiophene and transforming it into the 2-boronic acid by a lithiation/boration sequence in quantitative yield. The aryl boronic acid was then Suzuki cross-coupled to 1,4-dibromobenzene to give 2-(*para*-bromophenyl)-6-methoxybenzothiophene. This change in route more than doubled the yield over two steps, and was more economical, given the large price difference between 4-bromophenyl boronic acid and 1,4-dibromobenzene.

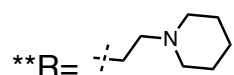
With the biaryl intermediate in hand, attaching the raloxifene C-ring via a Friedel-Crafts acylation was explored. A literature review of this Friedel-Crafts acylation on similar substrates suggested that substitution of the acyl chloride electrophile had a large effect on the overall yield of the reaction (entries 1-3, Table 2.1). Literature precedent revealed the acylation of the electron-rich aryl system **21** would readily give the desired ketone in good yield (entries 4-7, Table 2.1). This method could also be applied towards acylating electron-neutral (entry 10-12, Table 2.1) and electron-poor substrates (entries 8-9, 13-15, Table 2.1). Interestingly, some procedures described the use of excess Lewis acid could be used in conjunction with ethanethiol to effect a one-pot acylation and methyl deprotection (entry 7, 12 Table 2.1), a method first reported by Fujita in 1980.³⁴

Table 2.1 Select literature examples of Friedel-Crafts acylations en route to raloxifene and related compounds.



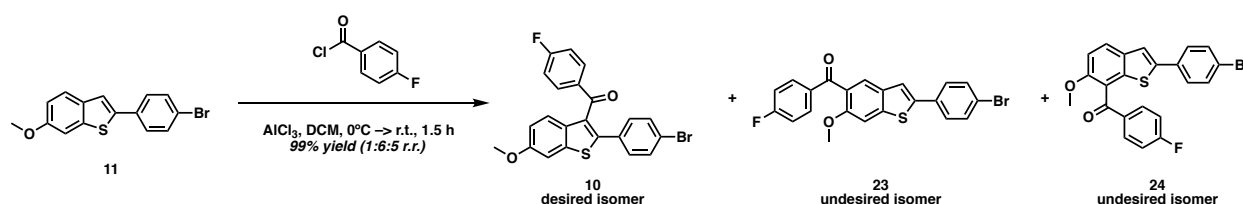
ENTRY ^{REF}	Equiv AlCl ₃	Conditions	R	X	Y	Yield (%)
1 ²⁷	1	5-23 °C, 3-24h	OMe	OMe	F	74
2 ²⁷	1	5-23 °C, 3-24h	OMe	OMe	NO ₂	18
3 ²⁷	1	5-23 °C, 3-24h	OMe	OMe	Br	65
4 ²²	1.3	0°C, 1h	OMe	OMe	OMe	100
5 ²⁰	1.25	50°C	OMe	OMe	OR ^{**}	95
6 ³⁵	1.5	r.t., 24h	OMe	OMe	I	60
7 ²³	1.1	0°C → r.t., o/n	OMe	OMe	F	88*
8 ²⁴	3	r.t.	OMe	F	CF ₃	37
9 ⁸	2.7	reflux, 48h	OMs	F	OR ^{**}	64
10 ⁸	2.7	reflux, 48h	Me	OMs	OR ^{**}	89
11 ⁸	2.7	reflux, 48h	H	H	OR ^{**}	36
12 ⁸	2.7	reflux, 48h	OMe	Me	OR ^{**}	62*
13 ⁸	2.7	reflux, 48h	H	Cl	OR ^{**}	52
14 ⁸	3	0°C, 1.5h	OMs	Cl	OR ^{**}	12
15 ⁸	3	0°C, 1.5h	Cl	OMs	OR ^{**}	15

*with one-pot methyl deprotection



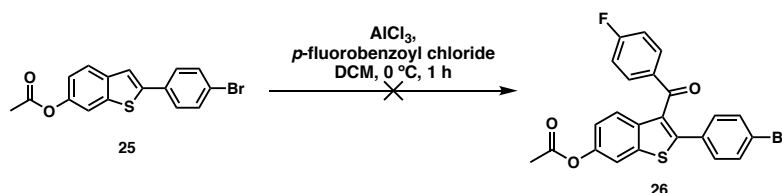
Unfortunately, when actually attempting the Friedel-Crafts acylation on the aryl bromide **11**, extremely poor regioselectivity was observed (Scheme 2.6). While there was

full conversion of the starting material, the desired 3-substituted regioisomer **10** was formed as the minor product in a 1:6:5 regioisomeric mixture, which favoured instead the products **23** and **24** resulting from acylation on the anisole ring of the benzothiophene core. This unacceptably low-yielding reaction severely limited material throughput and became a major bottleneck in the synthetic route. Efforts were then made towards either correcting or circumventing the problematic Friedel-Crafts acylation.



Scheme 2.6. Poor regioselectivity observed in Friedel-Crafts acylation of **11**.

The most obvious adjustment was to deactivate the anisole ring, which was done by replacing the methyl protecting group with an acetyl protecting group (Scheme 2.7). It was hoped that conjugation to the carbonyl group would sufficiently deactivate the anisole ring to favour acylation at the 3-position of the thiophene. Unfortunately, this change seemed to deactivate the whole system, and the substrate did not undergo the desired Friedel-Crafts acylation.



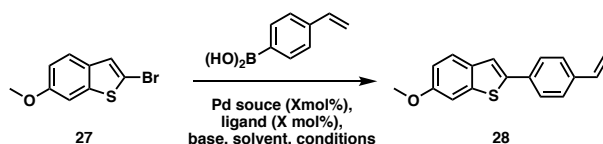
Scheme 2.7. Acetyl-protected aryl bromide does not undergo acylation.

It was suspected that the aryl bromide in **11** was dampening the nucleophilicity of the thiophene ring. It was hoped that its electron-withdrawing effects could be neutralized by replacing the para-bromophenyl ring with a styrene. This styrene was seen as a

synthetic equivalent to the bromide, because the olefin was required at that position for the late-stage Grubbs cross-metathesis. The styrene intermediate could be accessed via Suzuki cross-coupling of 4-vinylphenylboronic acid in lieu of 4-bromophenylboronic acid.

Initial attempts to effect this cross-coupling with Pd(PPh₃)₄ gave solely a mixture of starting material and dehalogenated starting material. Recovery of dehalogenated starting material suggested issues with either transmetalation or reductive elimination. As a result, a variety of bulkier and/or more electron-rich ligands were screened on test-scale (Table 2.2), with Pd(dba)₂ (5 mol%) and XPhos (5 mol%) giving acceptably high yields.

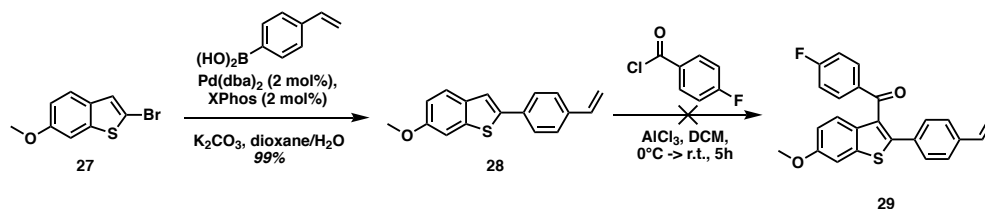
Table 2.2 Screening Suzuki cross-coupling conditions towards intermediate **28**.



ENTRY	Pd source	ligand	base	solvent	temp.	time	yield %
1	Pd(PPh ₃) ₄ (5 mol%)	—	K ₂ CO ₃	DME:H ₂ O (3:1)	80°C	o/n	nd
2	Pd(dba) ₂ (5 mol%)	XPhos (5 mol%)	K ₂ CO ₃	dioxane:H ₂ O (7:3)	80°C	o/n	86
3	Pd(dba) ₂ (5 mol%)	PCy ₃ (10 mol%)	K ₂ CO ₃	dioxane:H ₂ O (7:3)	80°C	o/n	55
4	Pd(dppf)Cl ₂ (5 mol%)	—	K ₂ CO ₃	dioxane:H ₂ O (7:3)	80°C	o/n	55

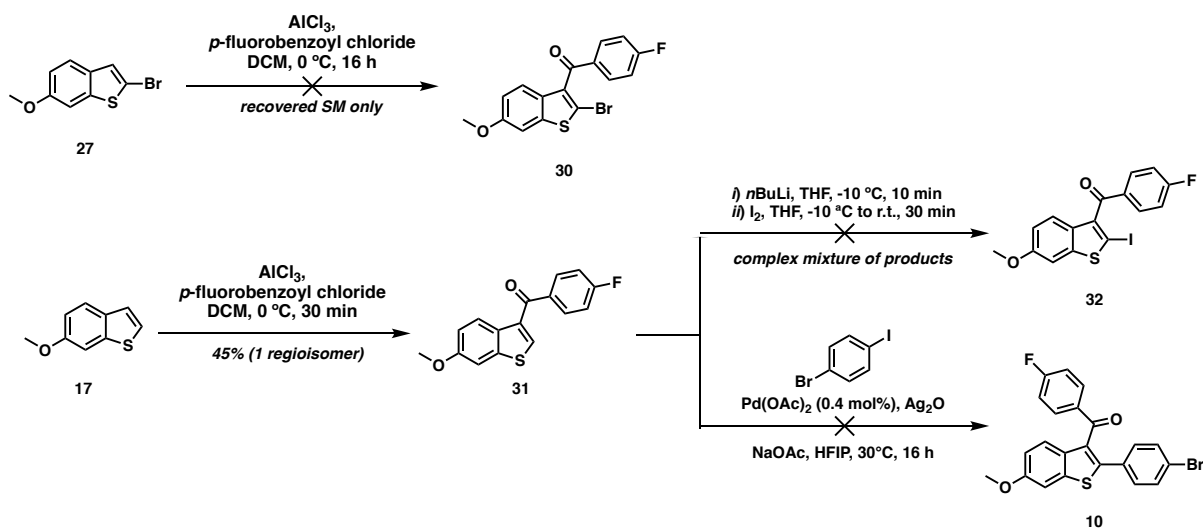
With the styrene in hand, it was discovered that this substrate was not amenable to Friedel-Crafts conditions, giving instead starting material and a complex mixture of inseparable products (Scheme 2.8). Wishing to understand this more, the double bond of the styrene was hydrogenated to the ethyl, and subjected to Friedel-Crafts. This too gave back recovered starting material, along with a complex mixture of products, none of which

appeared to be the desired product. The incorporation of styrene **29** in the synthetic route was abandoned, and other strategies then explored.



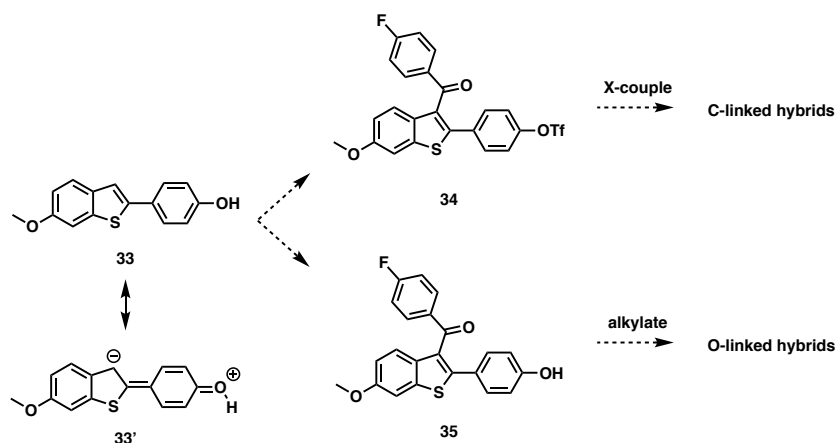
Scheme 2.8 Styrene intermediate not amenable to Friedel-Crafts acylation.

As shown in Scheme 2.9, the acylation of **27** was prohibited by electronic deactivation of the thiophene ring by the bromide. However, the acylation of the C2-unfunctionalized benzothiophene **17** promisingly gave the desired regioisomer **31** as the sole product (albeit in 45% yield). Unfortunately, the intermediate **31** was not amenable to introduction of functional groups at the 2-position. A lithiation/iodination, which would have given a synthetic handle to cross-couple in the desired raloxifene B-ring, failed to give any discernably useful products. A promising method of selectively functionalizing at the 2-position of benzothiophenes using a dual palladium/silver catalyst system³⁶ was unfortunately also not fruitful.



Scheme 2.9 Acylation of **27** (top) and **17** and attempts to functionalize **31** (bottom).

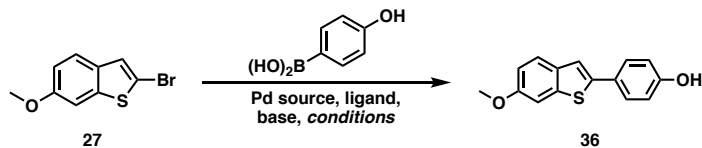
It was thought perhaps an oxygen-containing substituent on the *para*-position of the B-ring would better mimic the electronics of the original raloxifene scaffold, and increase the nucleophilicity of the 3-position (Scheme 2.10). This strategy was additionally attractive because an oxygen-containing substituent could potentially give way into both the oxygen- and carbon-linked hybrids, via alkylation and triflation/cross-coupling, respectively. As a result, methods of putting more electron rich substituents on the B-ring were considered.



Scheme 2.10 Oxygen-containing functionality at the *para* position of the B-ring would confer nucleophilic character to thiophene and can be manipulated into both C- and O-linked hybrids.

Literature conditions to effect the Suzuki cross-coupling of 4-hydroxyphenylboronic acid to 2-bromo-6-methoxybenzothiophene under standard cross-coupling conditions were not fruitful (entry 1, Table 2.3). Another microwave-assisted small-scale procedure gave encouraging results (entry 2, Table 2.3). However, this procedure faced problems when scaling up, and could not be adapted using standard bench-top equipment (entries 3-4, Table 2.3). It became eventually clear that this strategy would not give synthetically viable amounts of material, and a different approach was used to access 2-(4-hydroxyphenyl)-6-methoxybenzothiophene.

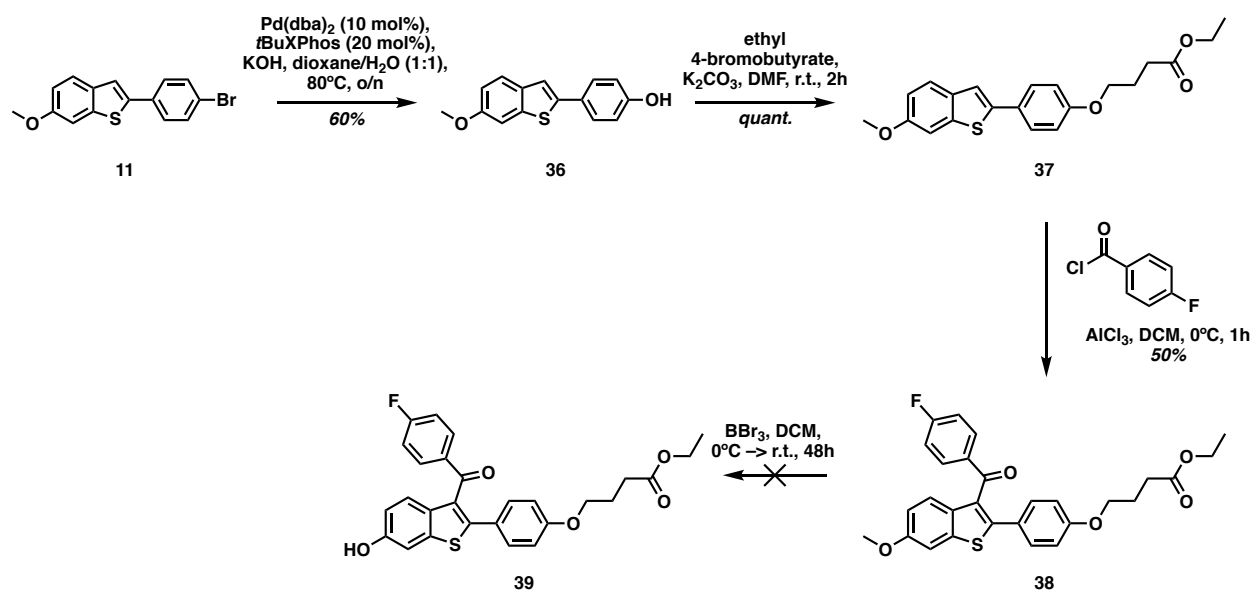
Table 2.3 Screening conditions to effect the Suzuki cross-coupling of **27** with 4-hydroxyphenylboronic acid.



ENTRY	Pd source	ligand	base	solvent	temp. (°C)	time	yield (%)
1	Pd(dba) ₂ (2 mol%)	XPhos (2 mol%)	KF	THF	45	o/n	–
2*	Pd(PPh ₃) ₂ Cl ₂ (3 mol%)	–	Na ₂ CO ₃	DME/EtOH	150	20 min	68%
3	Pd(PPh ₃) ₂ Cl ₂ (3 mol%)	–	Na ₂ CO ₃	DME/EtOH	105°C	o/n	5%
4	Pd(PPh ₃) ₂ Cl ₂ (3 mol%)	–	Na ₂ CO ₃	DME/EtOH	150°C	30 min	–

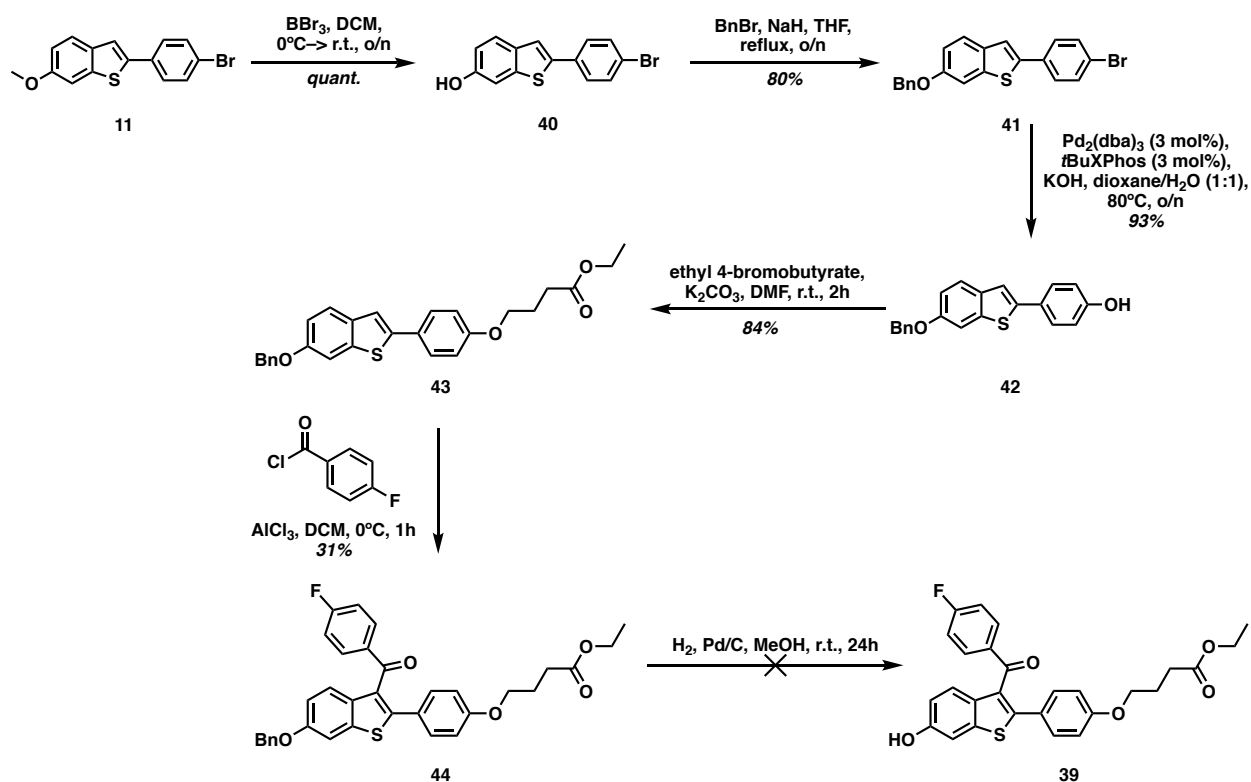
*microwave assisted, small-scale

The phenol **36** was accessed via a Buchwald-Hartwig cross-coupling with **11** and KOH (Scheme 2.11). The resulting phenol underwent alkylation to give the ester **37**, which smoothly underwent Friedel-Crafts acylation, giving the exclusive formation of the correct regioisomer in 50% yield. Unfortunately, deprotection of the methyl aryl ether proved to be difficult with the ester in place, with BBr₃ preferentially cleaving the ester and alkyl chain. Other protecting group strategies were then evaluated.



Scheme 2.11 Regioselective acylation with oxygen-containing substituent on B-ring.

It was postulated that a benzyl protecting group would be more easily removed than the methyl aryl ether of **38**. The benzyl-protected intermediate **43** was made from **11** via demethylation, benzyl-protection, Buchwald-Hartwig cross-coupling, and alkylation (Scheme 2.12). Interestingly, when intermediate **43** underwent Friedel-Crafts acylation, other regioisomers were observed in the crude material, in contrast to the ether **37**, which had been more selective for C3-acylation. Nonetheless, the major product was the desired regioisomer **44**, which was isolated in 31% yield. Unfortunately, the benzyl group was difficult to remove under standard hydrogenolysis conditions. More forcing conditions were tested, but also failed to cleave the benzyl group. Ultimately, this strategy too was abandoned, and the original Friedel-Crafts acylation was revisited.



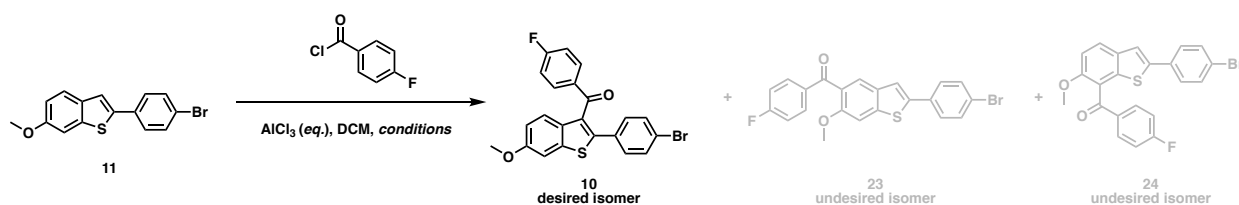
Scheme 2.12 Synthesis and acylation of benzyl-protected intermediate.

Finally, after these unfruitful attempts to circumvent the original Friedel-Crafts acylation, the original acylation of **11** was revisited as it gave the most direct entry to the desired key synthetic intermediate **9**. A successful strategy for the selective acylation of **11** was inspired by the paper mentioned previously, published by Fujita and co-workers³⁴ which described the deprotection of methyl aryl ethers using excess equivalents of Lewis acid. In this methyl aryl ether deprotection, the excess equivalents of a Lewis acid coordinate the oxygen of the anisole ring, and renders it susceptible to nucleophilic attack by the thiol, producing a free phenol upon workup.

An excess of Lewis acid was discovered to work in a similar manner when adapted towards the Friedel-Crafts acylation of **11**. The addition of excess equivalents of aluminum chloride in the acylation of **11** formed the desired regioisomer as the sole product in 73% yield (entry 3, Table 2.4). Presumably in the Friedel-Crafts acylation, the excess aluminum chloride coordinates and deactivates the anisole ring oxygen, thereby leaving the thiophene as the only nucleophilic location in the system. While this Friedel-

Crafts is much slower than those reported in the literature, it is relatively high-yielding for an electron-deficient system, giving the desired product in 74% yield. Interestingly, it would appear that the system is highly sensitive to exactly how much excess Lewis acid is present. With 8 equivalents of aluminum chloride, the reaction goes to completion at 36 hours (entry 3, Table 2.4). When 10 equivalents of aluminum chloride are added, the reaction does not reach completion after 5 days (entry 4, Table 2.4). In the latter case, only 34% of the expected product is observed, and only 15% of starting material is recovered. These observations suggest that the product was likely decomposing under extended exposure to the reaction conditions.

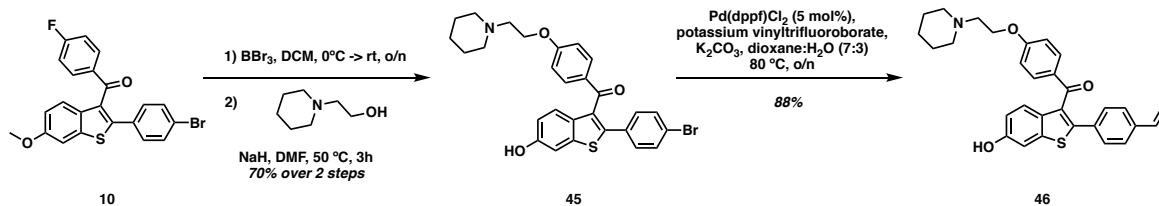
Table 2.4 Effect of AlCl₃ in Friedel-Crafts acylation.



ENTRY NO.	EQUIV ALCL ₃	TEMP.	TIME	YIELD	OBSERVATIONS
1	1.1-1.5	0°C	1.5 h	14%	undesired regioisomers predominate
2	3	0°C	2 h	36%	reduced formation of 2 other regioisomers, 30% recovered S.M.
3	8	0°C -> r.t.	36 h	74%	single regioisomer
4	10	0°C -> r.t.	5 days	34%	15% recovered S.M.

With adequate amounts of aryl fluoride **10** in hand, the rest of the synthesis could be completed with relative ease (Scheme 2.13). For the carbon-linked molecules, the

methyl aryl ether of **10** was deprotected with boron tribromide (BBr₃). This is followed by S_NAr to install the piperidine side chain to give **45** in 70% yield over 2 steps. A vinylation of **45** under Molander's conditions³⁷ for Suzuki cross-coupling of vinyl trifluoroborates gave the styrene **46** in 88% yield. The styrene **46** then underwent Grubbs olefin metathesis.

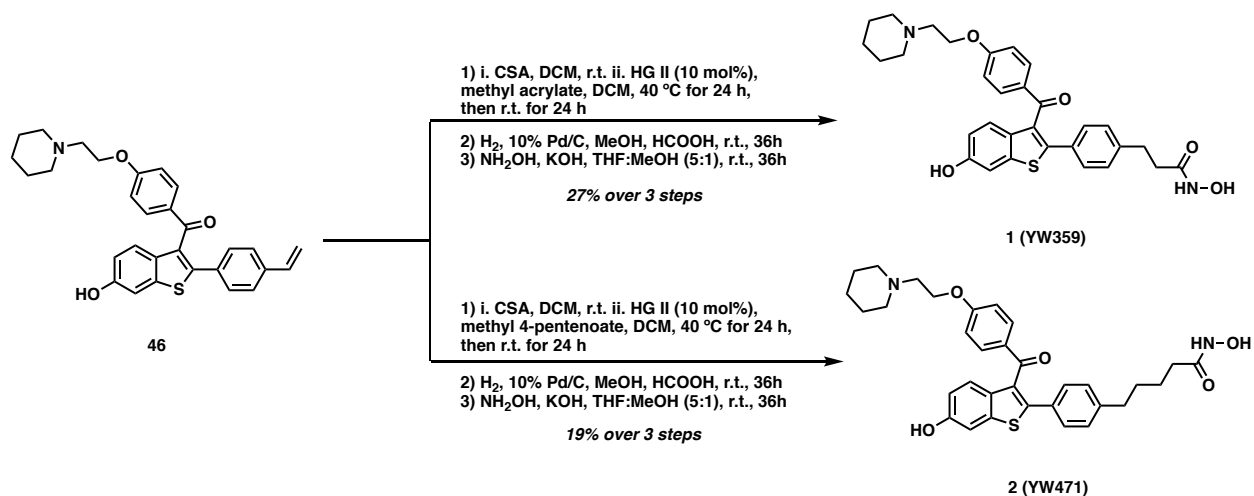


Scheme 2.13 Synthesis of styrene **46**.

The Grubbs olefin metathesis between the styrene and alkene esters was complicated by the tertiary amine present on the styrene. Basic nitrogens are known for displacing phosphine ligands on both the 1st and 2nd generation Grubbs catalysts, and thereby promoting their decomposition.³⁸ Tertiary amines are more well-tolerated than primary or secondary amines due to their steric bulk, preventing them from displacing ligands on the ruthenium centre, but nonetheless require specialized metathesis conditions. Formation of the corresponding ammonium salt has been reported to work well generally,³⁹ and has been used successfully for similar substrates in previous work from the Gleason lab.³

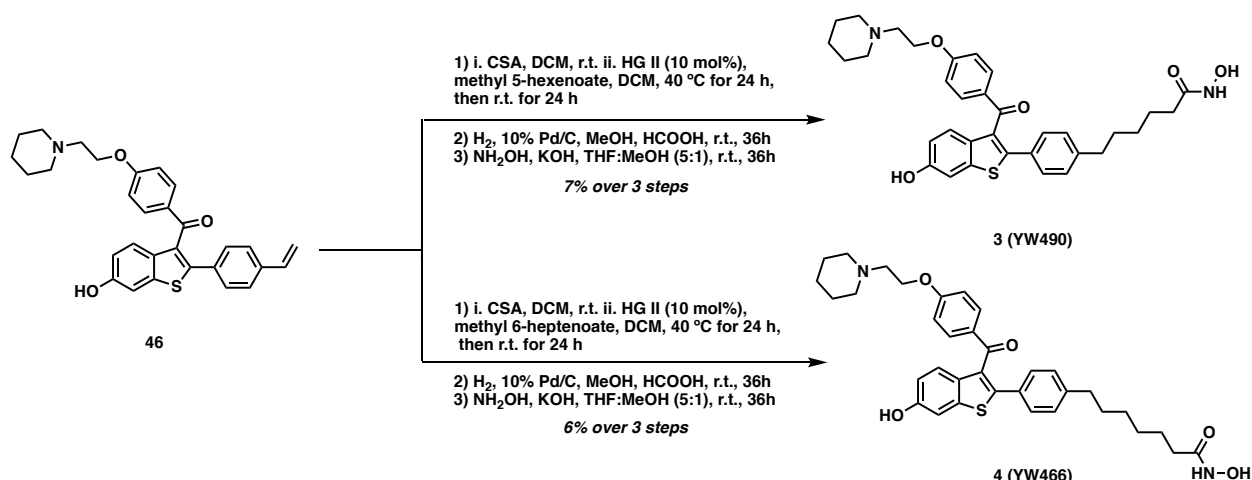
The Grubbs olefin metathesis of styrene **46** with methyl acrylate was completed successfully in the presence of equimolar camphorsulfonic acid (CSA). This afforded the desired methyl ester with a minor inseparable impurity of the corresponding carboxylic acid, which was carried through the remainder of the synthesis. This mixture underwent a subsequent hydrogenation of the olefin resulting from the Grubbs metathesis. The hydrogenated ester was reacted with hydroxylamine to form the corresponding hydroxamic acid **1** (YW359) in 27% yield over three steps. Styrene **46** also underwent Grubbs olefin metathesis with methyl 4-pentenoate in the presence of CSA, again affording the desired methyl ester with a minor inseparable impurity of the corresponding

carboxylic acid, which was carried through the remainder of the synthesis. The mixture underwent hydrogenation and hydroxamic acid formation to give **2** (YW471) in 19% yield over three steps.



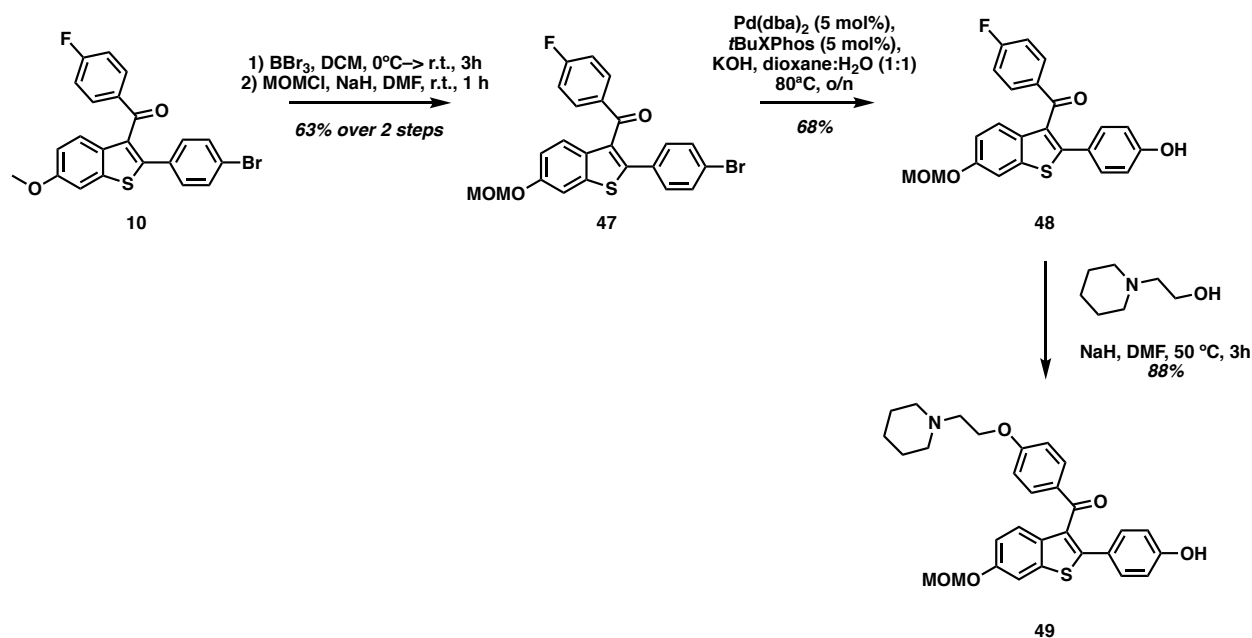
Scheme 2.14 Completion of **1** (YW359) and **2** (YW471).

The five- and six- carbon analogues were made in a similar fashion (Scheme 2.15). Grubbs cross metathesis of styrene **46** with methyl 5-hexenoate or methyl 6-heptenoate in the presence of CSA gave the corresponding methyl esters. Again, the products of both reactions were contaminated with the inseparable carboxylic acid impurity, which was carried through subsequent hydrogenation and hydroxamic acid formation to ultimately give **3** (YW490) and **4** (YW466), respectively.



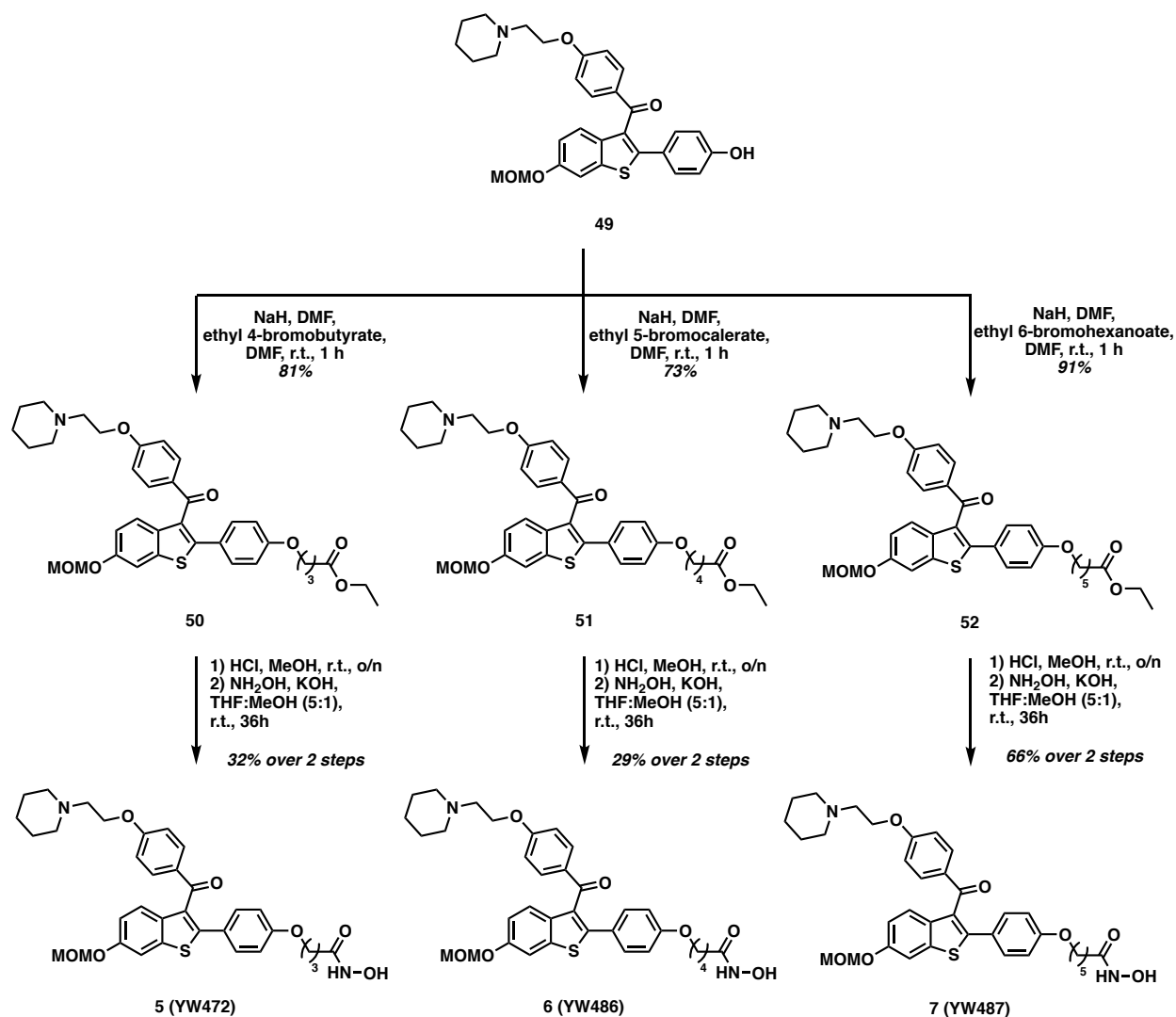
Scheme 2.15 Completion of **3** (YW490) and **4** (YW466).

To prepare oxygen-linked hybrids, a BBr₃ deprotection of the methyl aryl ether in **10** was followed by methoxymethyl ether (MOM) protection of the free phenol **47** in 63% yield over two steps (Scheme 2.16). Subsequent Buchwald-Hartwig cross-coupling with KOH giving **48** in 68% yield. A S_NAr of **47** installed the piperidine to give **49** in 88% yield. The MOM-protected piperidine then underwent alkylation with various alkyl bromides with terminal esters.



Scheme 2.16 Synthesis of O-linked intermediate **49**.

The chain length of the alkyl bromide chosen for alkylation with **49** determined the final chain length for each oxygen-linked hybrid (Scheme 2.17). Alkylation of **49** with ethyl 4-bromobutyrate gave ethyl ester **50** in 81% yield. Intermediate **50** underwent MOM deprotection and hydroxamic acid formation to give **5** (YW472) in 32% yield over two steps. Alkylation of phenol **49** with ethyl 5-bromovalerate gave ethyl ester **51** in 73% yield. The ethyl ester **51** was treated with HCl in methanol to MOM deprotect, then hydroxylamine to form **6** (YW486) in 29% yield over two steps. Finally, **49** underwent alkylation with ethyl 6-bromohexanoate to give **52** in 91% yield. The ethyl ester **52** was MOM deprotected, and transformed into the corresponding hydroxamic acid **7** (YW487) in 66% yield over two steps.



Scheme 2.17 Completion of O-linked targets **5** (YW472), **6** (YW486), **7** (YW487).

Following the synthesis of raloxifene/HDACi hybrids **1**, **2**, **3**, **4**, **5**, **6**, and **7**, these compounds underwent purification by either preparative or semi-preparative HPLC to give the desired >95% purity. The purified compounds underwent testing to determine biological activity, as detailed in the subsequent section.

2.5 Biological Assays

Fluorogenic HDACi assays of compounds **1**, **2**, **3**, **4**, **5**, **6**, and **7** were conducted by the author of this thesis. Samples of these compound were also given to collaborators

in the Mader Lab at the Université de Montréal for cell-based BRET (Bioluminescence Resonance Energy Transfer) and luciferase transactivation assays in order to determine ER affinity and antagonism, respectively. The ER assays have not yet been completed at the time of the submission of this thesis.

2.5.1 Fluorogenic HDACi Assay

The fluorogenic *in vitro* HDACi assay developed by Schweinhorst et al.⁴⁰ involves a two-step enzymatic process (Figure 2.15). The peptide-derived substrate contains an acetylated lysine residue (highlighted in red) and 7-amino-4-methylcoumarin (AMC). This substrate is incubated with the HDAC of interest. Uninhibited HDAC will deacetylate the lysine residue, which produces a compound that is recognized and digested by trypsin. Trypsin cleaves the AMC-lysine bond, releasing Boc-protected lysine giving rise to free AMC, a fluorescent molecule. The amount of free AMC is quantified by measuring fluorescence using a standard 96-well plate reader ($\lambda_{\text{ex}} = 390 \text{ nm}$ and $\lambda_{\text{em}} = 460 \text{ nm}$). The fluorescence emitted is directly proportional to the amount of substrate that has been deacetylated by active HDAC, and thusly related to HDAC enzyme activity. The inhibition concentration 50 (IC_{50}) can be derived from measuring the attenuation of fluorescence as a result of enzyme inhibition, at different concentrations of the inhibitor.

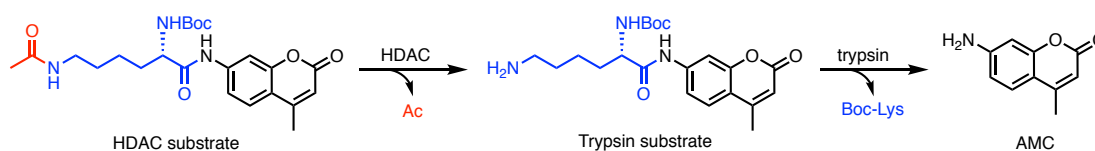


Figure 2.15 Two-stage enzymatic HDAC assay to measure HDAC activity.

The peptide substrate originally used by Schweinhorst et al. was later modified by Mazitschek et al.⁴¹ in order to improve HDAC affinity by replacing the Boc group with an Ac-Leu-Gly dipeptide (Figure 2.16). This allows for less enzyme to be used per well, thus lowering the cost of running the assay. The improved substrate was chosen for the evaluation of previous SERM/HDACi hybrids for this reason, and will continue to be used for the HDAC assays described (*vide infra*).

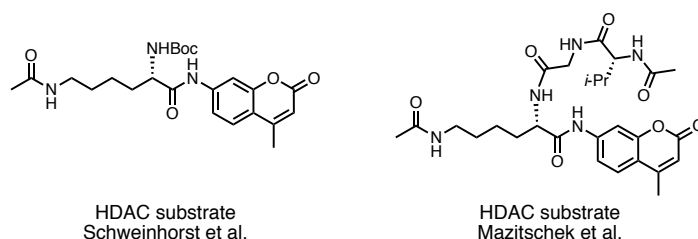


Figure 2.16 Original HDAC substrate (left) and modified HDAC substrate (right).

2.5.2 ER Assays

The hybrids will be tested in two cell-based assays to assess ER antagonism by collaborators in the Mader lab at the Université de Montréal.

Bioluminescence Resonance Energy Transfer (BRET) is a cell-based assay for studying protein-protein interactions. BRET is a naturally occurring phenomenon which results from the non-radioactive energy transfer between a donor-acceptor protein pair in close proximity to one another (less than 100 Å apart).⁴² The donor protein is derived from a luciferase that catalyzes the oxidation of coelenterazine, resulting in the emission at 480 nm. This light then excites the proximal acceptor protein, which emits a second photon with a wavelength greater than the light emitted by the donor protein, resulting from a phenomena called Stoke's shift. This detectable change in emission wavelength is thereby proximity-based and corresponds to the occurrence of a protein-protein association.⁴³ When the donor protein is fused to one protein of interest, and the acceptor protein is fused to another protein of interest, their physical interaction can be detected by the fluorescence emitted by the acceptor protein.

When activated, the ER must interact with various transcription coactivators in order to effect DNA transcription of ER-responsive genes. One such coactivator is SRC1, a LXXLL motif-containing nuclear coactivator known to interact with the ER upon activation by agonists such as E2.⁴⁴ To detect the activation of the ER, the interaction between the ER and SRC1 can be evaluated via BRET. In this assay, HEK93 cells were transfected with Renilla luciferase (RLucII) fused to ER and yellow fluorescent protein (YFP) fused to SRC1, respectively. RLucII emits at 480 nm upon oxidation of a molecule

of coelenterazine which results in the excitation of YFP and the subsequent emission at 530 nm. The BRET ratio of emitted light at 530 nm vs. 480 nm directly corresponds to the degree of which protein-protein interaction is occurring. Using BRET, a dose-response analysis of ER affinity by the hybrid SERM/HDACi's in the presence of E2 will be used to determine the IC₅₀.

A second luciferase transactivation assay will determine ER transcription antagonism. Reporter assays are used to track the transcription of (a) gene(s) downstream of a promoter in question. In this assay, a cell line is engineered to incorporate a reporter gene downstream of a response element of interest. Most commonly, the reporter gene is luciferase, which catalyzes the oxidation of luciferins leading to the emission of light following its transcriptional activation.⁴⁵ This measured light allows direct quantification of the activation of the promoter in question. With respect to the specific ER system in question, T47DKBLuc human mammary epithelial carcinoma cells will be transfected with an ER vector, a ERE3-TATA-Luc reporter vector, and a cytomegalovirus (CMV)- β -galactosidase vector which will serve as an internal control. Competitive and non-competitive transcription activation assays involving the raloxifene/HDACi hybrids and E2 will be conducted to determine whether or not the hybrids exhibit antagonistic character. It is expected that potent antagonists will prevent the activation of the ER whether in the absence or presence of E2, and thereby attenuate fluorescence.

2.6 Biological Activity and Discussion

2.6.1 HDAC inhibition

All synthesized hybrids (**1-7**) were evaluated in enzymatic assays against HDAC1 and HDAC6 to determine their IC₅₀ values. SAHA and E2 were used as positive and negative controls. Each hybrid was tested at 10 different concentrations ranging from 20 μ M – 1 nM in order to generate a dose-response curve. As expected, the bulky raloxifene capping groups of these hybrids were well-tolerated by both HDAC1 and HDAC6. This is unsurprising, given the wide variety of capping groups that HDACi's are known to

posses,⁴⁶⁻⁴⁷ and precedent from the Gleason lab^{3, 6, 48} has shown that steroidal and SERM pharmacophores are well-tolerated as HDACi capping groups.

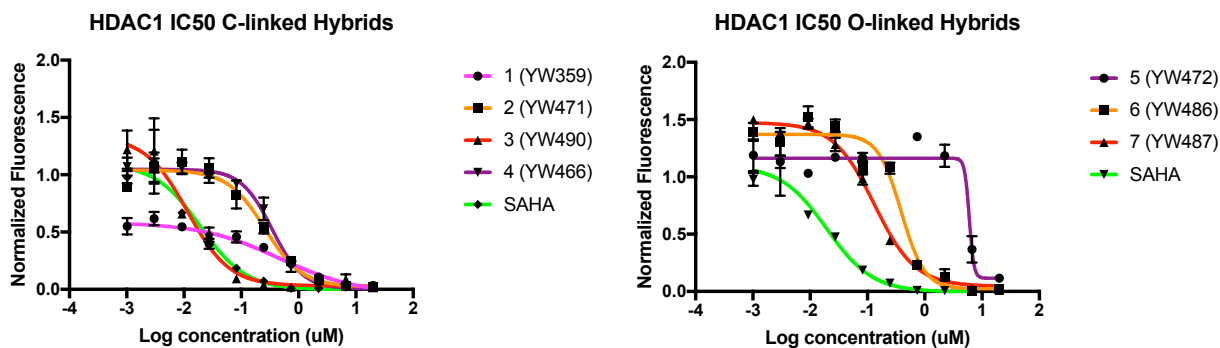
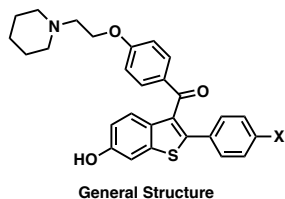
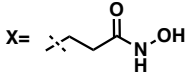
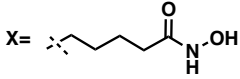
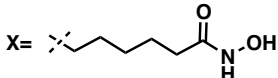
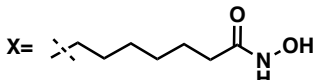
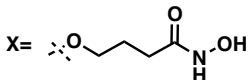
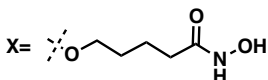
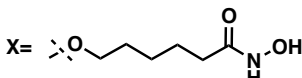


Figure 2.17 Dose-response curves of C-linked hybrids (left) and O-linked hybrids (right) against HDAC1. Values represent the means of three independent experiments and error bars denote standard error.

In HDAC1 assays, all inhibitors except for **5** demonstrated sub-micromolar IC_{50} values. The dose-response curves of these molecules are shown in Figure 2.17. The carbon-linked series were especially potent, with **3** having an IC_{50} within one order of magnitude as that of SAHA (Table 2.5). Interestingly, **3** also seemed to have an optimal carbon chain length of five carbons; hybrids **2** (four carbon linker) and **4** (six carbon linker) were both less potent. As expected, **1** (two carbon linker) was the least potent of these hybrids, presumably resulting from the linker being too short to properly extend into the hydrophobic tunnel of the HDAC enzyme.

Table 2.5 HDAC1 IC₅₀ values (\pm standard error) of all inhibitors tested.



COMPOUND	HDAC1 IC ₅₀ (μ M)
 1 (YW359)	0.464 (\pm 0.311)
 2 (YW471)	0.257 (\pm 0.0567)
 3 (YW490)	0.0115 (\pm 0.0439)
 4 (YW466)	0.344 (\pm 0.0424)
 5 (YW472)	5.99 (\pm 2.82E+30)
 6 (YW486)	0.389 (\pm 0.0536)
 7 (YW487)	0.132 (\pm 0.0124)
SAHA	0.0194 (\pm 0.00719)
E2	<i>n/a</i>

From previous work done on SERM/HDACi hybrid molecules by the Gleason lab, weak inhibition of HDAC enzymes arises from hybrids possessing not only a short alkyl linker, but also in compounds with oxygen in the alkyl linker.³ Ether bridges in the alkyl chain are thought to participate in H-bonding interactions at the ridge of the hydrophobic tunnel, stabilizing the molecules in a conformation such that the Zn²⁺ binding moiety does not reach into the tunnel to bind the Zn²⁺ atom. Molecules possessing all-carbon linkers lack polar functionality and thus cannot form H-bonds with residues at the apex of the tunnel. These reasons may point towards why the with oxygen-containing series tested against HDAC1 were far less potent than all-carbon alkyl linkers (Figure 2.17). The least potent of all hybrids tested was **5**, which had an IC₅₀ value of 5.992 μM. This low potency may be attributed to the combination of its comparatively short chain and ether linkage. Gratifyingly, an increase in potency was correlated to an increase in chain length between the oxygen-linked molecules. **5** (five atom linker) was more potent than **6** (four atom linker), and **7** (six atom linker) was more potent than either of them (Figure 2.17).

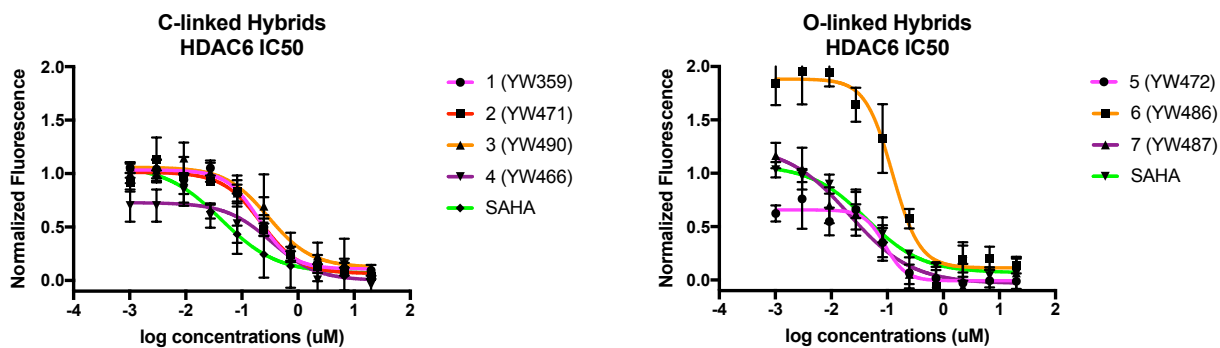


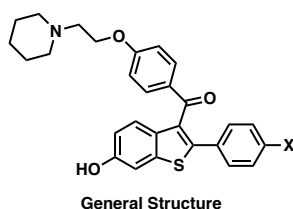
Figure 2.18 Dose-response curves of C-linked hybrids (left) and O-linked hybrids (right) against HDAC6. Values represent the means of three independent experiments and error bars denote standard error.

In HDAC6 assays, all inhibitors had sub-micromolar IC₅₀ values (Figure 2.18). Interestingly, a reversal in HDAC inhibition trends relative to the HDAC1 data was observed, with oxygen-linked molecules performing better than carbon-linked molecules. The carbon-linked molecules had IC₅₀ values ranging from 0.202 μM to 0.333 μM, while

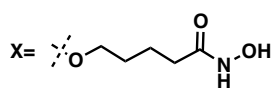
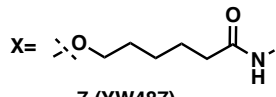
the oxygen-linked molecules had IC₅₀ values ranging from 0.0211 μM to 0.123 μM (Table 2.6). This reversal in potency trends is surprising, but not improbable given the observation that small modifications in the cap group can have elicit subtle changes in HDAC isoform selectivity,⁴⁹ and the inclusion of an oxygen may change the conformation of these molecules at the apex of the hydrophobic tunnel.

Within the carbon-linked molecules, the most potent of the carbon-linked hybrids was **1**, with a two-carbon alkyl linker. The other two-, four-, and six-carbon linker hybrids had somewhat similar IC₅₀ values. This observation was quite surprising, given the short chain-length of **1**.

Table 2.6 HDAC6 IC₅₀ (± standard error) values of all inhibitors tested.



COMPOUND	HDAC6 IC ₅₀ (μM)
<p>1 (YW359)</p>	0.202 (±0.0280)
<p>2 (YW471)</p>	0.221 (±0.0365)
<p>3 (YW490)</p>	0.297 (±0.0496)
<p>4 (YW466)</p>	0.333 (±0.237)
<p>5 (YW472)</p>	0.0910 (±0.216)

 <p>6 (YW486)</p>	0.123 (± 0.0166)
 <p>7 (YW487)</p>	0.0211 (± 0.0104)
SAHA	0.0424 ($\pm 8.46e-3$)
E2	<i>n/a</i>

Within the oxygen-linked series, no clear correlation between chain length and potency was observed. While **7** (six atom linker) was more potent than both **6** (five atom linker) and **5** (four atom linker), **6** appears to be less potent than **5**. It is worth noting that while **5** was not a very potent inhibitor of HDAC1, in HDAC6 it demonstrates potent inhibition of HDAC6, with an IC_{50} value within one order of magnitude of SAHA's IC_{50} .

2.6.2 ER antagonism

The hybrid drug molecules underwent a preliminary single-dose BRET assay to determine their ability to antagonize the ER. The assay was conducted using 4-OHT and raloxifene as positive controls, SAHA was used as negative control, and E2 as the competitive agonist. The inhibitors were assayed at a single concentration of 10 μ M, and E2 was administered at 5 nM.

As shown in Figure 2.19, all the inhibitors showed antagonistic behaviour against the ER, both in the absence and in the presence of E2. In the absence of E2, all the inhibitors exhibited a similar ER inhibition, comparable to that of the parent molecule, raloxifene. In the presence of E2, all hybrids demonstrated antiestrogenic behaviour relative to the negative control, but some to a lesser extent than the positive controls. These included **5**, **1**, and **4**. The other hybrids, **2**, **3**, **6**, and **7** remained antiestrogenic at a level comparable to raloxifene, in the presence of E2. Most importantly, these results indicate that the raloxifene/HDACi hybrids do bind and inhibit the ER. A more conclusive

statement on the antiestrogenic ability of these hybrids relative to each other can only be made once BRET dose-response curves have been obtained.

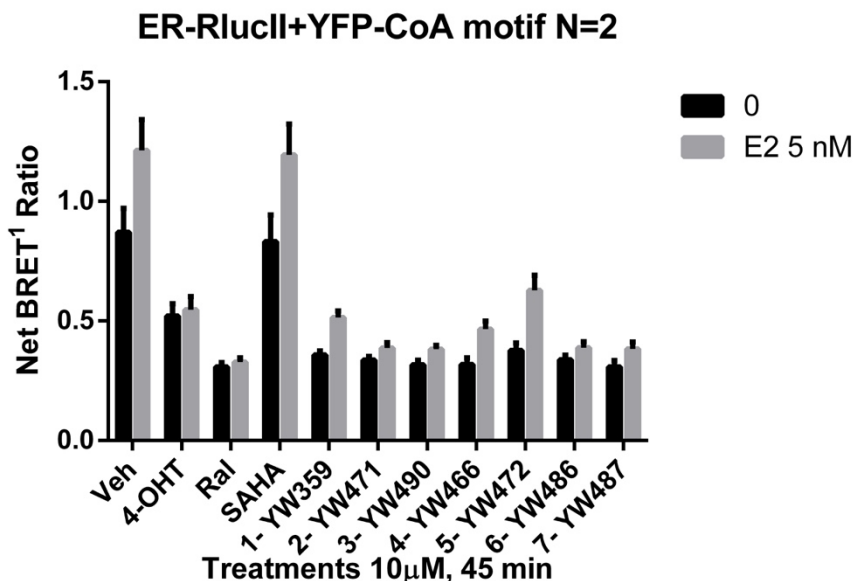


Figure 2.19 Single-dose BRET assay results for the hybrids either in the absence or presence of E2. Veh was DMSO.

2.7 Summary and Conclusion

SERMs have played a significant role in mitigating and managing breast cancer, but fall short once endocrine resistance develops, driving the development of other strategies for combatting this problem. Several projects within the Gleason laboratory have focused specifically on the development of SERM/HDACi hybrid molecules that target two distinct proteins which are implicated in endocrine resistant breast cancer. ‘

Initial work on 4-OHT/HDACi hybrids resulted in very promising compounds, but further efforts towards their modification would be extremely laborious, as intermediates and final compounds were prone to E/Z isomerization. As a result, a synthetic route towards raloxifene/HDACi hybrids was developed, optimized, and successfully executed to give seven novel hybrid molecules. The hybrids were made using a regioselective Friedel-Crafts acylation to give a common synthetic intermediate which gave rise to a set

of C-linked and O-linked hybrids. The C-linked molecules **1**, **2**, **3**, and **4** were made through a Grubbs olefin metathesis. The O-linked molecules **5**, **6**, and **7** were made through O-alkylation with the respective alkyl halide.

Fluorogenic HDACi assays were conducted by the author within the Gleason laboratory using the purified hybrids. In HDAC1 inhibition assays, C-linked molecules tended to be more potent than O-linked hybrids, with **3** being the most potent inhibitor ($IC_{50} = 0.0115 \pm 0.0439$). In contrast, O-linked molecules were more potent than C-linked molecules in HDAC6 assays, with **7** being the most potent inhibitor ($IC_{50} = 0.0211 \pm 0.0104$). These differences in hybrid potency between HDAC1 and HDAC6 is not surprising, given the observation that small changes in cap groups can elicit subtle differences in selectivity between HDAC isoforms.

BRET and luciferase transactivation assays for determining the antiestrogenic activity of the hybrids are ongoing in the Mader lab at the Université de Montréal. Preliminary findings in single-dose BRET assays suggest that all hybrids have antiestrogenic properties at the low-micromolar level. All the inhibitors exhibited a similar ER inhibition in the absence of E2, comparable to that of the parent molecule, raloxifene. Conclusions about the potencies between hybrids can only be drawn once BRET dose-response curves have been obtained. Taken together, these findings suggest promising results will be obtained in further biological work.

Further modification of the raloxifene/HDACi hybrids to improve their potency against endocrine-resistant breast cancer cells will be undertaken by future students in the Gleason lab. Future goals of this ongoing project include: 1) obtain a dose-response curve for antagonism of the ER, 2) observe the effects of these hybrids on a SERM-resistant cell line, and 3) modification of the raloxifene/HDACi hybrids, including the incorporation of a SERD long alkyl side chain (in place of the piperidine chain) to improve cytotoxicity.

References

1. Lim, L. Effects Towards the Design and Synthesis of Small Molecule Inhibitors of the Estrogen Receptor. McGill University, Montreal, Canada, 2011.
2. Williams, B. Design, synthesis and evaluation of selective estrogen receptor modulator/histone deacetylase inhibitor merged bifunctional ligands. McGill University, Montreal, Canada, 2014.
3. Palermo, A. F.; Diennet, M.; El Ezzy, M.; Williams, B. M.; Cotnoir-White, D.; Mader, S.; Gleason, J. L., *Bioorg. Med. Chem.* **2018**, *26* (15), 4428-4440.
4. Cesco, S. p. D.; Deslandes, S. b.; Therrien, E.; Levan, D.; Cueto, M. I.; Schmidt, R.; Cantin, L.-D.; Mittermaier, A.; Juillerat-Jeanneret, L.; Moitessier, N., *J. Med. Chem.* **2012**.
5. Lawandi, J.; Toumieux, S.; Seyer, V.; Campbell, P.; Thielges, S.; Juillerat-Jeanneret, L.; Moitessier, N., *J. Med. Chem.* **2009**, *52* (21), 6672-84.
6. Mendoza-Sanchez, R.; Cotnoir-White, D.; Kulpa, J.; Jutras, I.; Pottel, J.; Moitessier, N.; Mader, S.; Gleason, J. L., *Bioorg. Med. Chem.* **2015**, *23* (24), 7597-606.
7. Englebienne, P.; Moitessier, N., *Journal of Chemical Information and Modeling* **2009**, *49*, 2564–2571.
8. Grese, T. A.; Cho, S.; Finley, D. R.; Godfrey, A. G.; Jones, C. D.; Lugar, C. W. I.; Martin, M. J.; Matsumoto, K., J. G.; Pennington, L. D.; Winter, M. A.; Adrian, M. D.; Cole, H. W.; Magee, D. E.; Phillips, D. L.; Rowley, E. R.; Short, L. L.; Glasebrook, A. L.; Bryant, H. U., *J. Med. Chem.* **1997**, *40*, 146-167.
9. Brzozowski, A. M.; Pike, A. C. W.; Dauter, Z.; Hubbard, R. E.; Bonn, T.; Engstro, O.; Ohman, L.; Greene, G. L.; Gustafsson, J.-A.; Carlquistumoto, M., *Nature* **1997**, *389*, 753-758.
10. Lauffer, B. E.; Mintzer, R.; Fong, R.; Mukund, S.; Tam, C.; Zilberleyb, I.; Flicke, B.; Ritscher, A.; Fedorowicz, G.; Vallero, R.; Ortwine, D. F.; Gunzner, J.; Modrusan, Z.; Neumann, L.; Koth, C. M.; Lupardus, P. J.; Kaminker, J. S.; Heise, C. E.; Steiner, P., *J Biol Chem* **2013**, *288* (37), 26926-43.
11. Hai, Y.; Christianson, D. W., *Nat Chem Biol* **2016**, *12* (9), 741-7.
12. Schmid, C. R.; Sluka, J. P.; Duke, K. M., *Tetrahedron Lett.* **1999**, *40*, 675-678.
13. Wen, S.-M.; Lin, C.-H.; Chen, C.-C.; Wu, M.-J., *Tetrahedron* **2018**, *74* (20), 2493-2499.
14. Qin, Z.; Kastrati, I.; Chandrasena, R. E. P.; Liu, H.; Yao, P.; Petukhov, P. A.; Bolton, J. L.; Thatcher, G. R. J., *J. Med. Chem.* **2007**, *50* (11), 2682-2692.
15. Jones, C. D.; Jevnikar, M. G.; Pike, A. J.; Peters, M. K.; Black, L. J.; Thompson, A. R.; Falcone, J. F.; Clemens, J. A., *J. Med. Chem.* **1984**, *27*, 1057-1066.
16. Sall, D. J.; Bailey, D. L.; Bastian, J. A.; Buben, J. A.; Chirgadze, N. Y.; Clemens-Smith, A. C.; Denney, M. L.; Fisher, M. J.; Giera, D. D.; Gifford-Moore, D. S.; Harper, R. W.; Johnson, L. M.; Klimkowski, V. J.; Kohn, T. J.; Lin, H.-S.; McCowan, J. R.; Palkowitz, A. D.; Richett, M. E.; Smith, G. F.; Snyder, D. W.; Takeuchi, K.; Toth, J. E.; Zhang, M., *The Journal of Medicinal Chemistry* **2000**, *43*, 649-663.
17. Tria, G. S.; Abrams, T.; Baird, J.; Burks, H. E.; Firestone, B.; Gaither, L. A.; Hamann, L. G.; He, G.; Kirby, C. A.; Kim, S.; Lombardo, F.; Macchi, K. J.; McDonnell, D. P.; Mishina, Y.; Norris, J. D.; Nunez, J.; Springer, C.; Sun, Y.; Thomsen, N. M.; Wang,

- C.; Wang, J.; Yu, B.; Tiong-Yip, C. L.; Peukert, S., *J Med Chem* **2018**, *61* (7), 2837-2864.
18. Yu, L.; Liu, H. L.; Li, W.; Zhang, F.; Luckie, C.; van Breemen, R. B. T., Gregory R. J.; Bolton, J. L., *Chem. Res. Toxicol.* **2005**, *17* (7), 879-888.
19. Pinney, K. G.; Katzenellenbogen, J. A., *Synthesis of a Tetrafluoro-Substituted Aryl Azide and Its Protio Analogue as Photoaffinity Labeling Reagents for the Estrogen Receptor* **1991**, *56* (9), 3125-3133.
20. Yang, Y.; Zhang, T.; Huang, W.; Shen, Z., *Synth. Commun.* **2014**, *44* (22), 3271-3276.
21. Shinde, P. S.; Shinde, S. S.; Renge, A. S.; Patil, G. H.; Rode, A. B.; Pawar, R. R., *Lett. Org. Chem.* **2009**, *6*, 8-10.
22. Liu, J.; Li, Q.; Yang, X.; van Breemen, R. B.; Bolton, J. L.; Thatcher, G. R. J., *Chem. Res. Toxicol.* **2005**, *18*, 162-173.
23. Yu, B.; Qin, Z. Q.; Wijewickrama, G. T.; Edirisinghe, P.; Bolton, J. L.; Thatcher, G. R. J., *Bioconjugate Chem.* **2009**, *20* (4), 728-741.
24. Xiong, R.; Patel, H. K.; Gutgesell, L. M.; Zhao, J.; Delgado-Rivera, L.; Pham, T. N. D.; Zhao, H.; Carlson, K.; Martin, T.; Katzenellenbogen, J. A.; Moore, T. W.; Tonetti, D. A.; Thatcher, G. R. J., *J. Med. Chem.* **2016**, *59* (1), 219-237.
25. Liu, H.; Liu, J.; van Breemen, R. B.; Thatcher, G. R. J.; Bolton, J. L., *Chem. Res. Toxicol.* **2005**, *18*, 162-173.
26. Takeuchi, K.; Kohn, T. J.; Sail, D. J.; Delmeyer, M. L.; McCowan, J. R.; Smith, G. F.; Gifford-Moore, D. S., *Bioorg. Med. Chem. Lett.* **1999**, *9*, 759-764.
27. Schmid, C. R.; Sluka, J. P.; Duke, K. M., *Tetrahedron Lett.* **1999**, *40*.
28. Schmid, C. R.; Glasebrook, A. L.; Misner, J. W.; Stephenson, G. A., *Biological and Medicinal Chemistry Letters* **1999**, *9*, 1137-1140.
29. Dadiboyena, S., *Eur. J. Med. Chem.* **2012**, *51*, 17-34.
30. Rey, J.; Hu, H.; Kyle, F.; Lai, C. F.; Buluwela, L.; Coombes, R. C.; Ortlund, E. A.; Ali, S.; Snyder, J. P.; Barrett, A. G., *ChemMedChem* **2012**, *7* (11), 1909-14.
31. Iddon, B.; Scrowston, R. M., In *Advances in Heterocyclic Chemistry*, 1970; Vol. 11, pp 177-381.
32. Kim, S.; Yang, J.; DiNinno, F., *Tetrahedron Lett.* **1999**, *40*, 2909-2912.
33. Cerminara, I.; D'Alessio, L.; D'Auria, M.; Funicello, M.; Guarnaccio, A., *Helv. Chim. Acta* **2016**, *99* (5), 384-392.
34. Node, M.; Nishide, K.; Fujii, K.; Fujita, E., *JOC* **1980**, *45*, 4275-4277.
35. Patel, H. K.; Siklos, M. I.; Abdelkarim, H.; Mendonca, E. L.; Vaidya, A.; Petukhov, P. A.; Thatcher, G. R., *ChemMedChem* **2014**, *9* (3), 602-13.
36. Colletto, C.; Panigrahi, A.; Fernandez-Casado, J.; Larrosa, I., *J. Am. Chem. Soc.* **2018**, *140* (30), 9638-9643.
37. Molander, G. A.; Rivero, M. R., *Org. Lett.* **2002**, *4* (1), 107-109.
38. Wilson, G. O.; Porter, K. A.; Weissman, H.; White, S. R.; Sottos, N. R.; Moore, J. S., *Advanced Synthesis & Catalysis* **2009**, *351* (11-12), 1817-1825.
39. Woodward, C. P.; Spiccia, N. D.; Jackson, W. R.; Robinson, A. J., *Chem. Commun.* **2011**, *47* (2), 779-781.

40. Wegener, D.; Wirsching, F.; Riester, D.; Schwienhorst, A., *Chemistry & Biology* **2003**, *10* (1), 61-68.
41. Bradner, J. E.; West, N.; Grachan, M. L.; Greenberg, E. F.; Haggarty, S. J.; Warnow, T.; Mazitschek, R., *Nat Chem Biol* **2010**, *6* (3), 238-243.
42. Dacres, H.; Wang, J.; Dumancic, M. M.; Trowell, S. C., *Anal. Chem.* **2010**, *82*, 432-435.
43. Breton, B.; Sauvageau, E.; Zhou, J.; Bonin, H.; Le Gouill, C.; Bouvier, M., *Biophys J* **2010**, *99* (12), 4037-46.
44. Kalkhoven, E.; Valentine, J. E.; Heery, D. M.; Parker, M. G., *EMBO* **1998**, *17* (1), 232-243.
45. Naylor, L. H., *Biochem. Pharmacol.* **1999**, *58*, 749-757.
46. Bertrand, P., *Eur J Med Chem* **2010**, *45* (6), 2095-116.
47. Falkenberg, K. J.; Johnstone, R. W., *Nat. Rev. Drug Discov.* **2014**, *13* (9), 673-91.
48. Lamblin, M.; Dabbas, B.; Spingarn, R.; Mendoza-Sanchez, R.; Wang, T. T.; An, B. S.; Huang, D. C.; Kremer, R.; White, J. H.; Gleason, J. L., *Bioorg. Med. Chem.* **2010**, *18* (11), 4119-37.
49. Khan, N.; Jeffers, M.; Kumar, S.; Hackett, C.; Boldog, F.; Khramtsov, N.; Qian, X.; Mills, E.; Berghs, S. C.; Carey, N.; Finn, P. W.; Collins, L. S.; Tumber, A.; Ritchie, J. W.; Jensen, P. B.; Lichenstein, H. S.; Sehested, M., *Biochem J* **2008**, *409* (2), 581-9.

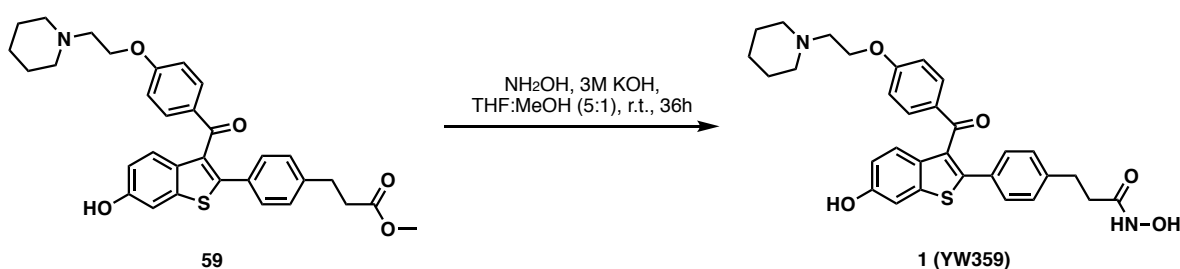
Chapter 3: Experimental Procedures

3.1 Chemical Syntheses

Materials and Instruments

All reactions were performed using magnetic stirring. Reactions employing dry solvents were conducted using oven or flame-dried round bottom flasks. Reactions requiring controlled atmospheres were fitted with rubber septa unless otherwise stated. Oil baths were used for reactions performed at temperatures in excess of room temperature. The cooling of reactions below room temperature was accomplished using one of the following techniques: ice/water bath (0 °C), ice/NaCl bath (-10 °C), or dry ice/acetone bath (-78 °C). Liquids and solutions were transferred via glass syringe or stainless-steel cannula under inert conditions. Thin-layer chromatography (TLC) was carried out on glass plates, coated with 250 μm of 230 – 400 mesh silica gel that had been saturated with F-254 indicator. TLC plates were visualised using ultraviolet light and/or by exposure to an acidic solution of cerium (IV) ammonium molybdate followed by heating, a basic solution of potassium permanganate followed by heating, an acidic solution of p-anisaldehyde, or an acidic iron (III) chloride solution, followed by heating. Flash column chromatography was carried out using 230 – 400 mesh silica gel (Silicycle) with reagent grade solvents. Room temperature (r.t.) indicates a temperature of 22 °C. THF and diethyl ether were purified by distillation over Na metal and benzophenone under nitrogen atmosphere. Toluene and DMF were purified by distillation over CaH₂ under an air atmosphere. DMF and methanol were stored over 4.0 Å molecular sieves and kept under argon atmosphere. All other commercial solvents and reagents were used as received from Sigma-Aldrich, Fisher Scientific, Chem Impex, CombiBlocks, Strem Chemicals, and Alfa Aesar unless otherwise specified. Infrared (IR) spectra were obtained using a Perkin-Elmer Spectrum One FT-IR spectrophotometer. NMR spectra were recorded on a 500 MHz Varian or 400, 500 MHz Bruker spectrometers. Chemical shifts (δ) were internally referenced to the residual solvent resonance; CDCl₃ (δH 7.26 ppm, δC 77.0 ppm), CD₃OD (δH 3.31, δC 49.00 ppm) DMSO-d₆ (δH 2.50 ppm, δC 39.5 ppm). The following abbreviations were used to

describe NMR signal multiplicities: singlet (s), doublet (d), triplet (t), quartet (q), and multiplet (m). Coupling constants (J) are reported in Hertz (Hz). High resolution mass spectrometry (HRMS) was conducted by Dr. Alexander Wahba or Dr. Nadim Saadé in the Mass Spectrometry Facility in the Department of Chemistry, McGill University. High resolution, accurate mass measurements were made using the a Thermo Exactive Plus Orbitrap-API or Bruker Maxis API QqTOF mass spectrometer. Low resolution mass spectrometry (LRMS) were measured on a Thermo Polaris Q CI quadrupole in trap mass spectrometer. Semi-preparative HPLC was performed using Agilent Zorbax SB-C18 and Agilent Infinity 1260 system.



***N*-hydroxy-3-(4-(6-hydroxy-3-(4-(2-(piperidin-1-yl)ethoxy)benzoyl)benzo[*b*]thiophen-2-yl)phenyl)propenamide (1):** Hydroxylamine (50 % w/w in H₂O, 3.40 mL, 110.0 mmol, 500.0 equiv) was added to a 1 M solution of methyl ester **59** (120 mg, 0.20 mmol, 1 equiv) in 5:1 THF:MeOH. Cold 3 M KOH (0.47 mL, 1.40 mmol, 7.0 equiv) was added dropwise to the mixture at 0 °C. The reaction was then warmed to room temperature and stirred for 36 hours. The reaction was neutralized with 1 M HCl solution, extracted with EtOAc (3 x 10 mL), dried over Na₂SO₄, filtered, and concentrated in vacuo. The crude mixture was purified by chromatography on silica using 0-20% MeOH:DCM as eluent. The product was purified over C18-functionalized silica using reverse-phase preparative HPLC using 20-100% ACN:H₂O to give 60 mg (55%) of the hydroxamic acid **1** as a yellow solid

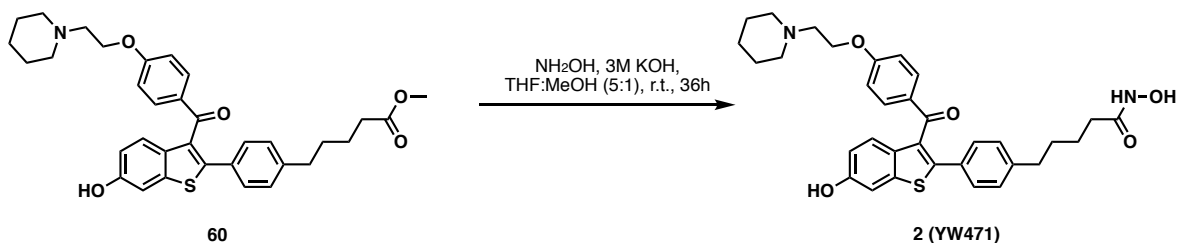
¹H NMR (500 MHz, CD₃OD) δ 8.53 (s, 1H), 7.77 – 7.72 (m, 2H), 7.42 (d, *J* = 8.7 Hz, 1H), 7.32 – 7.28 (m, 3H), 7.10 (d, *J* = 7.9 Hz, 2H), 6.93 – 6.87 (m, 3H), 4.31 (t, *J* = 5.0 Hz, 2H),

3.31 (s, 2H), 3.10 (s, 4H), 2.85 (t, $J = 7.5$ Hz, 2H), 2.34 (t, $J = 7.5$ Hz, 2H), 1.81 (p, $J = 5.7$ Hz, 4H), 1.63 (d, $J = 6.3$ Hz, 2H).

^{13}C NMR (126 MHz, CD_3OD) δ 193.84, 170.18, 162.34, 155.72, 141.57, 141.14, 140.34, 132.72, 132.06, 131.48, 130.89, 130.86, 128.68, 128.34, 123.52, 114.89, 114.09, 106.52, 62.98, 56.06, 53.82, 33.63, 30.58, 23.30, 21.81.

HRMS (ESI) calc. for $\text{C}_{31}\text{H}_{33}\text{N}_2\text{O}_5\text{S}$ ($\text{M} + \text{H}$) $^+$: 545.2093. Found: 545.2105.

IR (thin film) $\nu = 3261, 2940, 2829, 1647, 1595, 1252, 1167, 1022, 907, 816$ cm^{-1} .



N-hydroxy-5-(4-(6-hydroxy-3-(4-(2-(piperidin-1-yl)ethoxy)benzoyl)benzo[b]thiophen-2-yl)phenyl)pentanamide (2): Hydroxylamine (50 % w/w in H_2O , 1.13 mL, 37.0 mmol, 500 equiv) was added to a 1 M solution of methyl ester **60** (42.0 mg, 0.0700 mmol, 1 equiv) in 5:1 THF:MeOH. Cold 3 M KOH (0.170 mL, 0.500 mmol, 7.00 equiv) was added dropwise to the mixture at 0 °C. The reaction was then warmed to room temperature and stirred for 36 hours. The reaction was neutralized with 1 M HCl solution, extracted with EtOAc (3 x 10.0 mL), dried over Na_2SO_4 , filtered, and concentrated in vacuo. The crude mixture was purified by chromatography on silica using 0-20% MeOH:DCM as eluent. The product was purified over C18-functionalized silica using reverse-phase semi-preparative HPLC using 20-100% ACN: H_2O to give 16.0 mg (22%) of the hydroxamic acid **2** as a yellow solid.

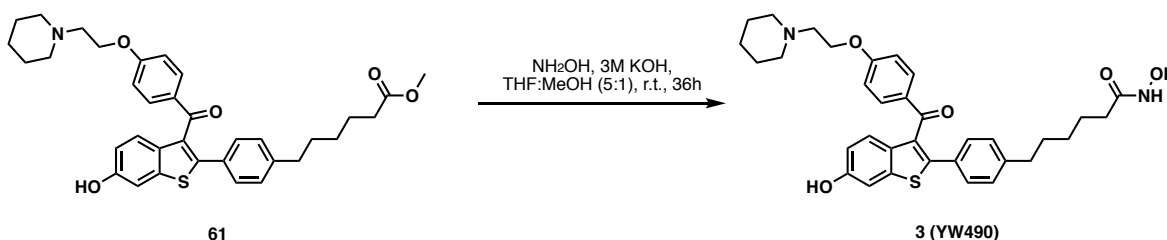
^1H NMR (800 MHz, CD_3OD) δ 8.53 (s, 3H), 7.71 (d, $J = 7.8$ Hz, 2H), 7.46 (d, $J = 8.7$ Hz, 1H), 7.29 (d, $J = 2.2$ Hz, 1H), 7.26 (d, $J = 7.6$ Hz, 2H), 7.05 (d, $J = 7.8$ Hz, 2H), 6.89 (dt,

$J = 12.8, 6.4$ Hz, 3H), 4.31 (s, 2H), 3.44 – 3.37 (m, 2H), 3.28 – 3.12 (m, 4H), 2.55 (q, $J = 6.9, 5.0$ Hz, 2H), 2.04 (tdt, $J = 8.2, 6.8, 1.4$ Hz, 2H), 1.84 (s, 4H), 1.64 (s, 2H), 1.58 (s, 2H), 1.50 – 1.44 (m, 2H).

^{13}C NMR (201 MHz, CD_3OD) δ 193.77, 168.41, 162.10, 155.70, 142.68, 142.23, 140.36, 132.73, 132.04, 131.06, 131.04, 130.70, 128.68, 128.36, 123.52, 114.87, 113.97, 106.51, 62.63, 55.91, 53.78, 39.03, 34.38, 31.66, 29.95, 22.98, 21.52.

HRMS (ESI) calc. for $\text{C}_{33}\text{H}_{37}\text{N}_2\text{O}_5\text{S}$ ($\text{M} + \text{H}$) $^+$: 573.2405. Found: 573.2418.

IR (thin film) $\nu = 3190, 2928, 2853, 1595, 1379, 1357, 1252, 1167$ cm^{-1} .



***N*-hydroxy-6-(4-(6-hydroxy-3-(4-(2-(piperidin-1-**

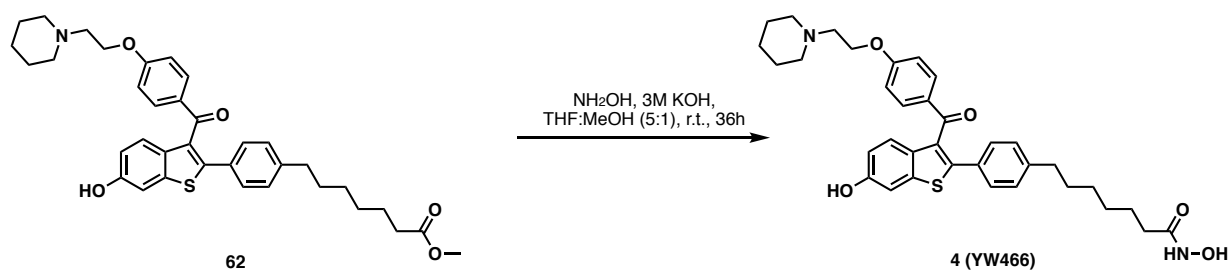
yl)ethoxy)benzoyl)benzo[*b*]thiophen-2-yl)phenyl)hexanamide: Hydroxylamine (50 % w/w in H_2O , 3.70 mL, 122 mmol, 500 equiv) was added to a 1 M solution of methyl ester **61** (143 mg, 0.200 mmol, 1 equiv) in 5:1 THF:MeOH. Cold 3 M KOH (0.470 mL, 1.40 mmol, 7.00 equiv) was added dropwise to the mixture at 0 °C. The reaction was then warmed to room temperature and stirred for 36 hours. The reaction was neutralized with 1 M HCl solution, extracted with EtOAc (3 x 10.0 mL), dried over Na_2SO_4 , filtered, and concentrated in vacuo. The crude mixture was purified by chromatography on silica using 0-20% MeOH:DCM as eluent. The product was purified over C18-functionalized silica using reverse-phase semi-preparative HPLC using 20-100% ACN: H_2O to give 13.0 mg (11%) of the hydroxamic acid **3** as a yellow solid.

¹H NMR (500 MHz, CD₃OD) δ 8.49 (s, 3H), 7.75 – 7.71 (m, 2H), 7.43 (d, *J* = 8.8 Hz, 1H), 7.29 (d, *J* = 2.3 Hz, 1H), 7.28 – 7.26 (m, 2H), 7.05 (d, *J* = 8.1 Hz, 2H), 6.92 – 6.87 (m, 3H), 4.31 (t, *J* = 5.1 Hz, 2H), 3.36 (t, *J* = 5.2 Hz, 2H), 3.15 (d, *J* = 13.7 Hz, 4H), 2.53 (t, *J* = 7.5 Hz, 2H), 2.04 (t, *J* = 7.4 Hz, 2H), 1.81 (p, *J* = 5.8 Hz, 4H), 1.58 (ddq, *J* = 24.3, 15.2, 7.4 Hz, 7H), 1.24 (p, *J* = 8.1 Hz, 2H).

¹³C NMR (201 MHz, CD₃OD) δ 193.89, 168.35, 162.19, 155.68, 143.10, 141.97, 140.34, 132.74, 132.06, 131.02, 130.95, 130.69, 128.56, 128.40, 123.45, 114.84, 114.02, 106.51, 62.75, 55.90, 53.72, 39.02, 34.74, 32.15, 30.44, 27.94, 25.03, 23.16.

HRMS (ESI) calc. for C₃₄H₃₉N₂O₅S (M + H)⁺: 587.2568. Found: 587.2574.

IR (thin film) ν = 3226, 2932, 2857, 1597, 1466, 1353, 1252, 1020 cm⁻¹.



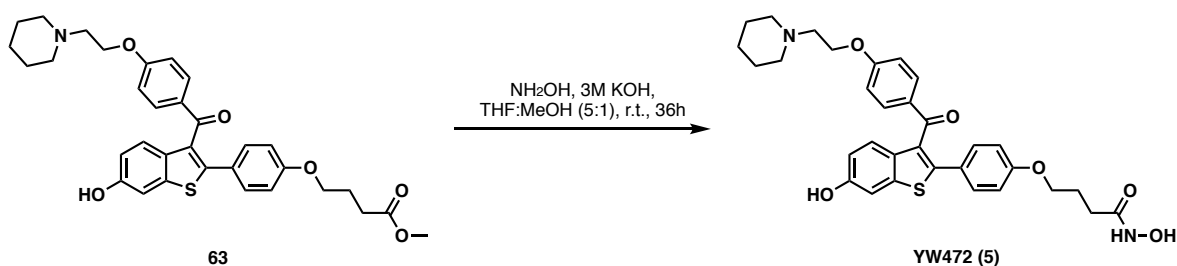
***N*-hydroxy-7-(4-(6-hydroxy-3-(4-(2-(piperidin-1-yl)ethoxy)benzoyl)benzo[*b*]thiophen-2-yl)phenyl)heptanamide (**4**):** Hydroxylamine (50 % w/w in H₂O, 1.20 mL, 40.0 mmol, 500 equiv) was added to a 1 M solution of methyl ester **62** (46.0 mg, 0.0800 mmol, 1 equiv) in 5:1 THF:MeOH. Cold 3 M KOH (0.190 mL, 0.560 mmol, 7.00 equiv) was added dropwise to the mixture at 0 °C. The reaction was then warmed to room temperature and stirred for 36 hours. The reaction was neutralized with 1 M HCl solution, extracted with EtOAc (3 x 10.0 mL), dried over Na₂SO₄, filtered, and concentrated in vacuo. The crude mixture was purified by chromatography on silica using 0-20% MeOH:DCM as eluent. The product was purified over C18-functionalized silica using 7-reverse-phase semi-preparative HPLC using 20-100% ACN:H₂O to give 10.0 mg (21%) of the hydroxamic acid **4** as a yellow solid.

¹H NMR (500 MHz, Methanol-*d*₄) δ 8.51 (s, 3H), 7.74 (d, *J* = 8.3 Hz, 2H), 7.42 (d, *J* = 8.8 Hz, 1H), 7.31 – 7.24 (m, 3H), 7.05 (d, *J* = 7.8 Hz, 2H), 6.92 – 6.85 (m, 3H), 4.31 (s, 2H), 3.36 (d, *J* = 8.5 Hz, 2H), 3.15 (d, *J* = 10.7 Hz, 4H), 2.53 (t, *J* = 7.5 Hz, 2H), 2.05 (s, 2H), 1.81 (d, *J* = 5.9 Hz, 4H), 1.63 (s, 2H), 1.54 (t, *J* = 7.5 Hz, 4H), 1.23 (d, *J* = 7.8 Hz, 2H).

¹³C NMR (201 MHz, MeOD) δ 193.96, 168.53, 162.22, 155.67, 143.19, 141.87, 140.34, 132.74, 132.06, 130.99, 130.90, 130.69, 128.52, 128.38, 123.42, 114.84, 114.04, 106.52, 62.75, 55.88, 53.69, 39.03, 34.80, 30.55, 28.43, 28.15, 25.24, 23.15, 21.66.

HRMS (ESI) calc. for C₃₅H₄₁N₂O₅S (M + H)⁺: 601.2732. Found: 601.2731.

IR (thin film) ν = 3186.50, 2928.57, 2857.14, 1597.57, 1466.74, 1353.74, 1252.64, 1167.40, 1036.36 cm⁻¹.



***N*-hydroxy-4-(4-(6-hydroxy-3-(4-(2-(piperidin-1-**

yl)ethoxy)benzoyl)benzo[*b*]thiophen-2-yl)phenoxy)butanamide (5**):** Hydroxylamine (50 % w/w in H₂O, 0.960 mL, 31.0 mmol, 500 equiv) was added to a 1 M solution of methyl ester **63** (36.0 mg, 0.0600 mmol, 1 equiv) in 5:1 THF:MeOH. Cold 3 M KOH (0.15 mL, 0.400 mmol, 7.00 equiv) was added dropwise to the mixture at 0 °C. The reaction was then warmed to room temperature and stirred for 36 hours. The reaction was neutralized with 1 M HCl solution, extracted with EtOAc (3 x 10 mL), dried over Na₂SO₄, filtered, and concentrated in vacuo. The crude mixture was purified by chromatography on silica using 0-20% MeOH:DCM as eluent. The product was purified over C18-functionalized silica

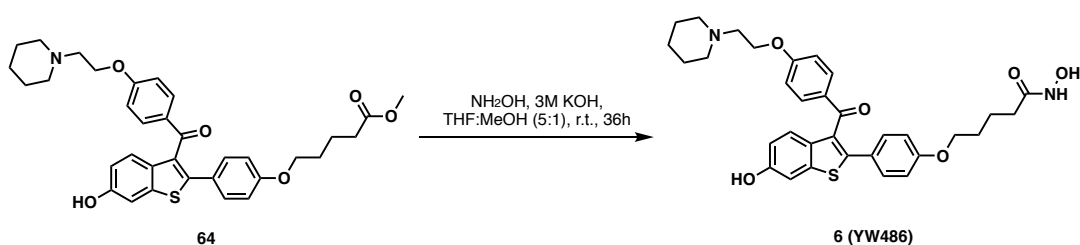
using reverse-phase semi-preparative HPLC using 20-100% ACN:H₂O to give 11.0 mg (32%) of the hydroxamic acid **6** as a yellow solid.

¹H NMR (500 MHz, CD₃OD) δ 8.39 (s, 1H), 7.72 (d, *J* = 7.2 Hz, 2H), 7.45 (d, *J* = 7.6 Hz, 1H), 7.26 (d, *J* = 8.0 Hz, 3H), 6.89 (s, 3H), 6.77 (d, *J* = 7.9 Hz, 2H), 4.34 (s, 2H), 3.94 (s, 2H), 3.49 (s, 2H), 3.26 (s, 4H), 2.24 (s, 2H), 1.99 (s, 2H), 1.86 (s, 4H), 1.66 (s, 2H).

¹³C NMR (201 MHz, (CD₃)₂SO) δ 193.03, 168.97, 163.39, 159.16, 156.02, 139.89, 139.82, 132.66, 132.29, 130.73, 130.04, 130.03, 125.81, 123.85, 115.78, 115.34, 115.09, 107.61, 67.38, 66.36, 57.50, 54.75, 29.10, 25.91, 25.14, 24.28.

HRMS (ESI) calc. for C₃₂H₃₅N₂O₆S (M + H)⁺: 575.2195. Found: 575.2210.

IR (thin film) ν = 3412, 2940, 2253, 1659, 1050, 1022, 1000, 822, 761 cm⁻¹.



***N*-hydroxy-5-(4-(6-hydroxy-3-(4-(2-(piperidin-1-yl)ethoxy)benzoyl)benzo[*b*]thiophen-2-yl)phenoxy)pentanamide (**6**):** Hydroxylamine (50 % w/w in H₂O, 1.00 mL, 33.0 mmol, 500 equiv) was added to a 1 M solution of methyl ester **64** (39.0 mg, 0.0700 mmol, 1 equiv) in 5:1 THF:MeOH. Cold 3 M KOH (0.150 mL, 0.500 mmol, 7.00 equiv) was added dropwise to the mixture at 0 °C. The reaction was then warmed to room temperature and stirred for 36 hours. The reaction was neutralized with 1 M HCl solution, extracted with EtOAc (3 x 10.0 mL), dried over Na₂SO₄, filtered, and concentrated in vacuo. The crude mixture was purified by chromatography on silica using 0-20% MeOH:DCM as eluent. The product was purified over C18-functionalized

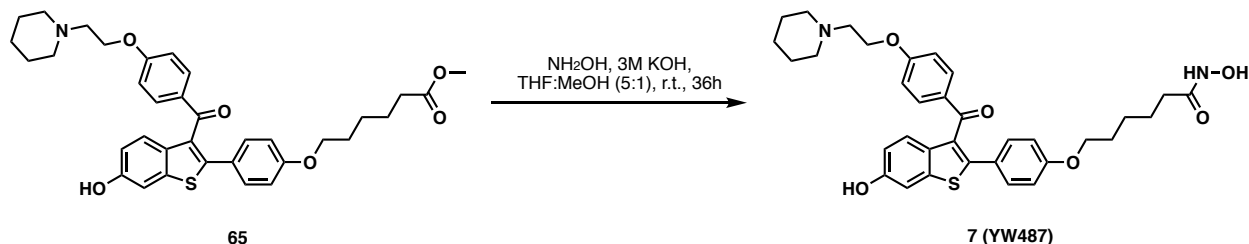
silica using reverse-phase semi-preparative HPLC using 20-100% ACN:H₂O to give 12.0 mg (29%) of the hydroxamic acid **6** as a yellow solid.

¹H NMR (500 MHz, (CD₃)₂SO) δ 10.38 (s, 1H), 8.39 (s, 2H), 7.69 – 7.65 (m, 2H), 7.36 (d, *J* = 2.3 Hz, 1H), 7.30 – 7.26 (m, 2H), 7.22 (d, *J* = 8.7 Hz, 1H), 6.96 – 6.92 (m, 2H), 6.89 – 6.84 (m, 3H), 4.09 (t, *J* = 5.9 Hz, 2H), 3.91 (t, *J* = 6.0 Hz, 2H), 2.61 (t, *J* = 5.9 Hz, 2H), 2.39 (s, 4H), 1.99 (t, *J* = 7.0 Hz, 2H), 1.63 (dtt, *J* = 16.4, 8.2, 5.3 Hz, 4H), 1.46 (p, *J* = 5.6 Hz, 4H), 1.36 (q, *J* = 6.8, 6.3 Hz, 2H).

¹³C NMR (201 MHz, (CD₃)₂SO) δ 193.06, 169.27, 165.51, 163.41, 159.23, 156.23, 139.81, 132.56, 132.28, 130.73, 130.04, 130.00, 125.74, 123.81, 115.84, 115.31, 115.08, 107.61, 67.62, 66.44, 57.56, 54.79, 32.30, 28.50, 25.99, 24.35, 22.17.

HRMS (ESI) calc. for C₃₃H₃₇N₂O₆S (M + H)⁺: 589.2374. Found: 589.2367.

IR (thin film) ν = 3373, 2940, 2908, 2817, 2250, 1054, 1024, 1004, 820, 757 cm⁻¹.



N-hydroxy-6-(4-(6-hydroxy-3-(4-(2-(piperidin-1-yl)ethoxy)benzoyl)benzo[b]thiophen-2-yl)phenoxy)hexanamide (7): Hydroxylamine (50 % w/w in H₂O, 0.760 mL, 25.0 mmol, 500 equiv) was added to a 1 M solution of methyl ester **65** (30 mg, 0.0500 mmol, 1 equiv) in 5:1 THF:MeOH. Cold 3 M KOH (0.100 mL, 0.30 mmol, 7.0 equiv) was added dropwise to the mixture at 0 °C. The reaction was then warmed to room temperature and stirred for 36 hours. The reaction was neutralized with 1 M HCl solution, extracted with EtOAc (3 x 10.0 mL), dried over Na₂SO₄, filtered, and concentrated in vacuo. The crude mixture was purified by chromatography on silica using

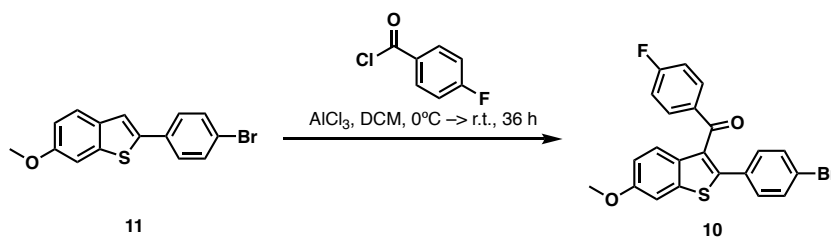
0-20% MeOH:DCM as eluent. The product was purified over C18-functionalized silica using reverse-phase semi-preparative HPLC using 20-100% ACN:H₂O to give 20.0 mg (66%) of the hydroxamic acid **7** as a yellow solid.

¹H NMR (500 MHz, (CD₃)₂SO) δ 10.34 (s, 1H), 8.32 (s, 1H), 7.69 – 7.63 (m, 2H), 7.35 (d, *J* = 2.2 Hz, 1H), 7.30 – 7.25 (m, 2H), 7.23 (d, *J* = 8.7 Hz, 1H), 6.95 – 6.91 (m, 2H), 6.86 (dq, *J* = 8.8, 2.7, 2.2 Hz, 3H), 4.08 (t, *J* = 5.9 Hz, 2H), 3.89 (t, *J* = 6.5 Hz, 2H), 2.61 (t, *J* = 5.8 Hz, 2H), 2.42 – 2.35 (m, 4H), 1.94 (t, *J* = 7.3 Hz, 2H), 1.65 (p, *J* = 6.6 Hz, 2H), 1.52 (q, *J* = 7.5 Hz, 2H), 1.48 (s, 4H), 1.34 (dtt, *J* = 15.2, 9.5, 4.9 Hz, 4H).

¹³C NMR (201 MHz, (CD₃)₂SO) δ 193.03, 169.41, 164.97, 163.39, 159.27, 156.12, 139.90, 139.81, 132.61, 132.28, 130.70, 130.03 (d), 125.70, 123.83, 115.80, 115.30, 115.07, 107.61, 67.92, 66.43, 57.55, 54.79, 32.66, 28.76, 25.99, 25.56, 25.32, 24.35.

HRMS (ESI) calc. for C₃₄H₃₉N₂O₆S (M + H)⁺: 603.2523. Found: 603.2523.

IR (thin film) ν = 3373, 2940, 2908, 2817, 2250, 1054, 1024, 1004, 820, 757 cm⁻¹.



(2-(4-bromophenyl)-6-methoxybenzo[*b*]thiophen-3-yl)(4-fluorophenyl)methanone

(10): AlCl₃ (960 mg, 7.20 mmol, 8.00 equiv) was added to a stirring solution of aryl bromide **11** (285 mg, 0.900 mmol, 1 equiv) in anhydrous DCM (9 mL) at 0 °C. 4-fluorobenzoyl chloride (0.120 mL, 1.00 mmol, 1.10 equiv) was added dropwise at 0 °C. The reaction was allowed to gradually reach room temperature, and was stirred for 36 h, at which point TLC analysis indicated the complete consumption of starting material. The reaction was quenched by dropwise addition of 30.0 mL 1 M HCl at 0°C. The organic

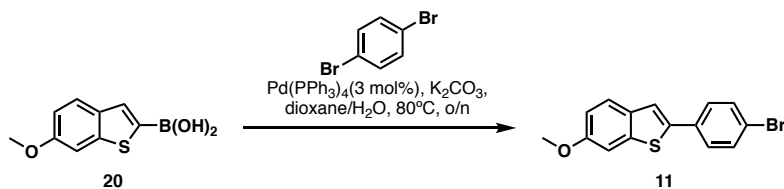
layer was separated from the aqueous layer, and the product was extracted with DCM (3 x 10.0 mL). The combined organic layers were washed with brine, dried over MgSO₄, filtered, and concentrated to give a yellow oil. The crude material was purified via chromatography on silica using 5% EtOAc:hexanes as eluent to afford 281 mg of the aryl fluoride **10** as a yellow foam.

¹H NMR (500 MHz, CDCl₃) δ 7.82 – 7.76 (m, 2H), 7.59 (d, *J* = 8.9 Hz, 1H), 7.37 – 7.33 (m, 2H), 7.32 (d, *J* = 2.4 Hz, 1H), 7.26 – 7.22 (m, 2H), 7.00 (dd, *J* = 8.9, 2.4 Hz, 1H), 6.98 – 6.93 (m, 2H), 3.88 (s, 3H).

¹³C NMR (126 MHz, CDCl₃) δ 192.44, 166.90, 164.87, 158.13, 142.03, 140.43, 133.72, 133.70, 133.51, 132.58, 132.50, 132.25, 131.83, 131.28, 130.51, 124.37, 123.01, 115.80, 115.62, 115.38, 104.48, 55.66.

HRMS (ESI) *m/z* calc. for C₂₂H₁₄BrFNaO₂S (M + Na)⁺: 462.9759. Found: 462.9774.

IR (thin film) ν = 3067, 3003, 2960, 2936, 2837, 1649, 1595, 1522, 1472, 1437, 1409, 1349, 1324, 1228, 1254, 1212, 1151, 1072, 1044, 1010, 893, 826, 816, 755, 729, 683 cm⁻¹.



2-(4-bromophenyl)-6-methoxybenzo[*b*]thiophene (11): Boronic acid **20** (301 mg, 1.40 mmol, 1 equiv), 1,4-dibromobenzene (1.01 g, 4.30 mmol, 3.00 equiv), Pd(PPh₃)₄ (32.0 mg, 0.0200 mmol, 0.0200 equiv), and K₂CO₃ (60.0 mg, 4.30 mmol, 3.00 equiv) were suspended in 7:3 dioxane:H₂O (14.0 mL). The mixture was stirred at 80 °C overnight. In the morning, TLC analysis indicated the complete consumption of the starting material. The reaction was cooled to room temperature and 30 mL H₂O was added, followed by

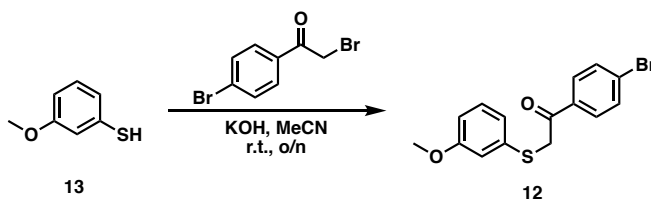
10.0 mL DCM. The organic layer was separated from the aqueous layer and DCM was used to extract the product (5 x 10.0 mL). The combined organic layers were washed with brine, dried over MgSO₄, filtered, and concentrated in vacuo to give an orange solid. The crude material was purified by trituration from EtOAc:hexanes and filtered to afford 337 mg of the aryl bromide **11** as a white solid, which was sufficiently pure for use without further purification.

¹H NMR (500 MHz, CDCl₃) δ 7.65 (d, *J* = 8.7 Hz, 1H), 7.53 (s, 4H), 7.44 (s, 1H), 7.30 (d, *J* = 2.4 Hz, 1H), 6.99 (dd, *J* = 8.7, 2.3 Hz, 1H), 3.89 (s, 3H).

¹³C NMR (126 MHz, CDCl₃) δ 157.67, 141.02, 140.18, 134.60, 133.47, 132.00, 127.58, 124.34, 121.67, 119.51, 114.75, 104.84, 55.64.

HRMS (APCI) *m/z* calc. for C₁₅H₁₁OBrS (M + H)⁺: 318.9785. Found: 318.9787.

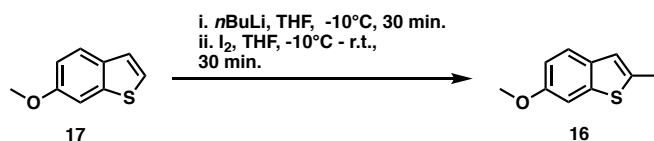
IR (thin film) ν = 3019, 1601, 1478, 1262, 1214 cm⁻¹.



1-(4-bromophenyl)-2-((3-methoxyphenyl)thio)ethan-1-one (12): 2-bromo-1-(4-bromophenyl)-ethanone (218 mg, 0.790 mmol, 1.00 equiv) was added dropwise to a 10.0-mL solution of 3-methoxythiophenol (100 mg, 0.790 mmol, 1.00 equiv) and KOH (44.0 mg, 0.790 mmol, 1.00 equiv) in EtOH:H₂O (7:3) at 0 °C. The reaction was brought to room temperature and stirred overnight. In the morning, TLC analysis indicated the complete consumption of starting material and the reaction was quenched by addition of 10.0 mL H₂O and the product was extracted with EtOAc (5 x 10.0 mL). The combined organic layers were washed with brine, dried over Na₂SO₄, filtered, and concentrated to give a yellow oil. The crude material was purified by chromatography on silica using 10%

EtOAc:hexanes as eluent to afford 248 mg (93%) of the alkylated product **12** as a yellow solid.

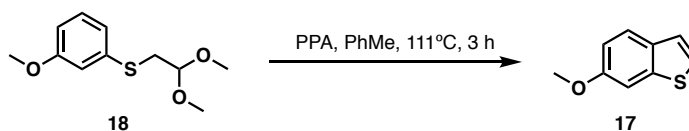
¹H NMR (400 MHz, CDCl₃) δ 7.81 – 7.77 (m, 2H), 7.61 – 7.57 (m, 2H), 7.19 (t, *J* = 8.0 Hz, 1H), 6.94 (ddd, *J* = 7.6, 1.8, 0.9 Hz, 1H), 6.91 (dd, *J* = 2.5, 1.8 Hz, 1H), 6.77 (ddd, *J* = 8.3, 2.5, 0.9 Hz, 1H), 4.22 (s, 2H), 3.77 (s, 3H).



2-iodo-6-methoxybenzo[b]thiophene (16): *n*BuLi (2.55 M in hexanes, 2.20 mL, 5.70 mmol, 1.20 equiv) was added dropwise to a 40.0-mL solution of **17** (0.782 g, 4.70 mmol, 1 equiv) in anhydrous THF at -78 °C. The dark red solution was stirred for 30 min, then I₂ (1.45 g, 5.70 mmol, 1.20 equiv) was added via cannula as a 15.0-mL solution in anhydrous THF. The mixture turned yellow, then dark red, and was stirred for 30 min before quenching with 10% Na₂S₂O₃. The product was extracted with EtOAc (5 x 10.0 mL), and the combined organic layers were washed with sat. NaHCO₃, dried over MgSO₄, filtered, and evaporated. The crude was purified by chromatography on silica using 5% EtOAc:hexanes to give 1.26 g (92%) of the aryl iodide **16** as a white solid.

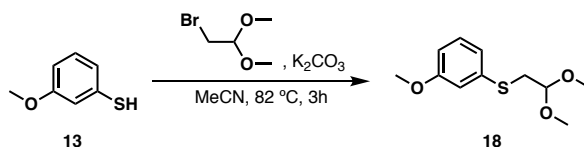
¹H NMR (500 MHz, CDCl₃) δ 7.58 (d, *J* = 8.7 Hz, 1H), 7.42 (d, *J* = 0.7 Hz, 1H), 7.24 (d, *J* = 2.3 Hz, 1H), 6.93 (dd, *J* = 8.7, 2.4 Hz, 1H), 3.86 (s, 3H).

¹³C NMR (126 MHz, CDCl₃) δ 157.44, 145.70, 134.97, 133.26, 122.83, 114.43, 103.94, 74.10, 55.62.

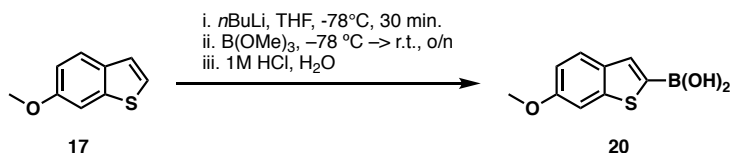


6-methoxybenzothiophene (17): Polyphosphoric acid (3.59 g, 36.7 mmol, 1.00 equiv) was added to a stirring solution of acetal **18** (10.6 g, 36.7 mmol, 1 equiv) in toluene (200

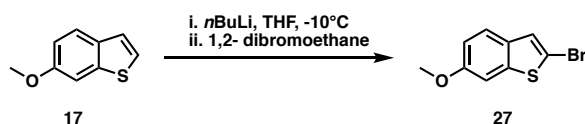
mL). The mixture was stirred at reflux for 3 h, at which point TLC analysis indicated the complete consumption of the starting material. The reaction was cooled to room temperature before the mixture was neutralized with 2.67 M KOH. The organic layer was separated from the aqueous layer, and EtOAc (3 x 50.0 mL) was used to extract the product from the aqueous layer. The combined organic layers were washed with brine, dried over MgSO₄, filtered, and concentrated to give an orange oil. The crude was chromatographed over silica using 100% hexanes as eluent to afford 4.30 g (71%) of the desired benzothiophene **17** as a clear oil, and 1.43 g (24%) of the minor 4-methoxybenzothiophene was also isolated as a clear oil. The spectroscopic data is in agreement with that published in literature.²



(2,2-dimethoxyethyl)(3-methoxyphenyl)sulfane (18): Potassium carbonate (7.04 g, 51.0 mmol, 3.00 equiv.) was added in one portion to a stirring solution of 3-methoxythiophenol (1.50 mL, 17.0 mmol, 1 equiv) and bromoacetaldehyde dimethylacetal (2.32 mL, 17.0 mmol, 1.00 equiv) in ACN (170 mL). The mixture was stirred at reflux for 3 h, at which point TLC analysis indicated the complete consumption of the starting material. The reaction mixture was cooled to room temperature and filtered through celite. The filtrate was washed with 60.0 mL brine, dried over MgSO₄, filtered, and concentrated to give the crude as a brown oil. The crude material was purified by chromatography on silica using 5% EtOAc:hexanes as eluent to give 3.20 g (88%) of the acetal **18** as a clear oil. The spectroscopic data is in agreement with that published in the literature.¹



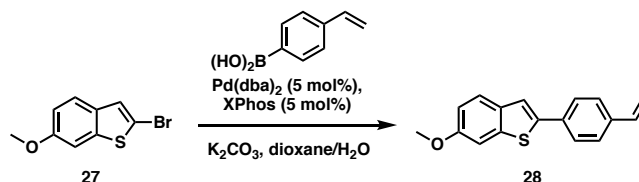
(6-methoxybenzo[*b*]thiophen-2-yl)boronic acid (20): *n*BuLi (2.4 M in hexanes, 3.90 mL, 9.40 mmol, 1.10 equiv) was added dropwise to a stirring solution of 6-methoxybenzothiophene (1.40 g, 8.50 mmol, 1 equiv) in THF (85.0 mL) at -78°C . The mixture was stirred at -78°C for 30 min before trimethyl borate (1.90 mL, 17.0 mmol, 2.00 equiv) was added dropwise, turning the solution from dark red to clear light yellow. The reaction was allowed to reach room temperature gradually overnight. In the morning, 20.0 mL 1 M HCl was added. The organic layer was separated from the aqueous layer, and EtOAc (3 x 50.0 mL) was used to extract the product from the aqueous layer. The combined organic layers were washed with brine, dried over MgSO_4 , filtered, and concentrated in vacuo to give a white solid. The crude material was purified by trituration from Et_2O :hexanes and filtered to provide 1.76 g (89%) of boronic acid **20** as a white solid which was used without further purification. The spectroscopic data is in agreement with that published in literature.³



2-bromo-6-methoxybenzo[*b*]thiophene (27): *n*BuLi (2.5 M in hexanes, 3.56 mL, 8.90 mmol, 1.70 equiv) was added dropwise to a solution of **17** (0.857 g, 5.20 mmol, 1 equiv) in anhydrous THF (50-mL) at -10°C . The dark red solution was stirred for five minutes, then 1,2-dibromoethane (2.93 g, 15.6 mmol, 3.00 equiv) was added dropwise. The orange mixture was stirred for 1 h before quenching with sat. NH_4Cl . The product was extracted with Et_2O (3 x 50.0 mL), and the combined organic layers were washed with sat. NaHCO_3 , dried over Na_2SO_4 , filtered, and evaporated to give a brown oil. The crude was purified by chromatography on silica using hexanes to give 0.756 g (60%) of the aryl bromide **27** as a white solid.

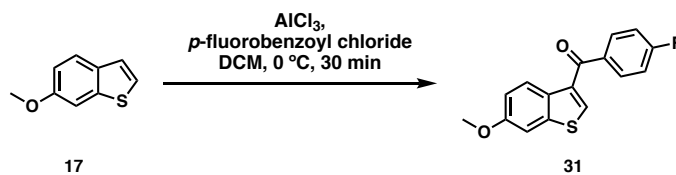
¹H NMR (400 MHz, CDCl₃) δ 7.56 (d, *J* = 8.7 Hz, 1H), 7.22 (d, *J* = 0.7 Hz, 1H), 7.20 (d, *J* = 2.4 Hz, 1H), 6.95 (dd, *J* = 8.7, 2.4 Hz, 1H), 3.86 (s, 3H).

¹³C NMR (101 MHz, CDCl₃) δ 157.38, 141.17, 133.65, 124.09, 123.66, 123.39, 114.40, 104.80, 55.61.



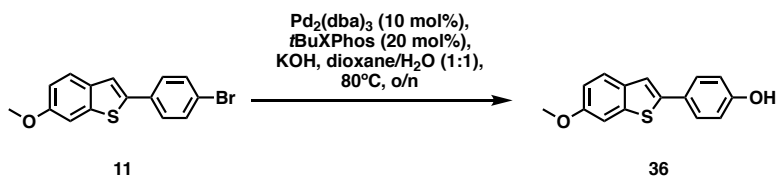
6-methoxy-2-(4-vinylphenyl)benzo[*b*]thiophene (28): Aryl bromide **27** (54.0 mg, 0.220 mmol, 1 equiv), 4-vinylphenylboronic acid (56.0 mg, 0.370 mmol, 1.70 equiv), Pd(dba)₂ (10.0 mg, 0.011 mmol, 0.050 equiv), XPhos (5.00 mg, 0.0110 mmol, 1.70 equiv), K₂CO₃ (61.0 mg, 0.440 mmol, 2.00 equiv) were suspended in 2.00 mL dioxane:H₂O (7:3). The mixture was stirred at 80 °C overnight. In the morning, TLC analysis indicated the complete consumption of starting material, and the reaction was diluted at room temperature with 1.00 mL EtOAc and 1.00 mL H₂O. The product was extracted with EtOAc (3 x 10.0 mL), and the combined organic layers were washed with brine, dried over Na₂SO₄, filtered, and evaporated to give an orange oil. The crude material was purified by chromatography on silica using 5% EtOAc:hexanes to give 62.0 mg (quant.) of the styrene **28** as a white solid.

¹H NMR (400 MHz, CDCl₃) δ 7.67 – 7.61 (m, 3H), 7.46 (d, *J* = 2.2 Hz, 2H), 7.44 (d, *J* = 1.9 Hz, 1H), 7.30 (d, *J* = 2.3 Hz, 1H), 6.98 (dd, *J* = 8.7, 2.4 Hz, 1H), 6.74 (dd, *J* = 17.6, 10.9 Hz, 1H), 5.79 (dd, *J* = 17.6, 0.9 Hz, 1H), 5.28 (dd, *J* = 10.9, 0.9 Hz, 1H), 3.89 (s, 3H).



(4-fluorophenyl)(6-methoxybenzo[*b*]thiophen-3-yl)methanone (31): AlCl₃ (320 mg, 2.40 mmol, 1.10 equiv) was added to a 20.0-mL solution of **17** (368 mg, 2.19 mmol, 1 equiv) in anhydrous DCM at 0 °C, followed by the dropwise addition of 4-fluorobenzoylchloride (0.29 mL, 2.40 mmol, 1.10 equiv). The mixture was stirred at 0 °C for 30 min, at which point TLC analysis indicated the complete consumption of starting material. The reaction was quenched by dropwise addition of 3.00 mL 1 M HCl, which turned the mixture from green to yellow. The product was extracted with DCM (3 x 10.0 mL), and the combined organic layers were washed with sat. NaHCO₃, brine, dried over Na₂SO₄, filtered, and evaporated to give a yellow solid. The crude was purified by chromatography on silica using 5-10% EtOAc:hexanes to give 291 mg (46%) of the aryl fluoride **31** as a yellow solid.

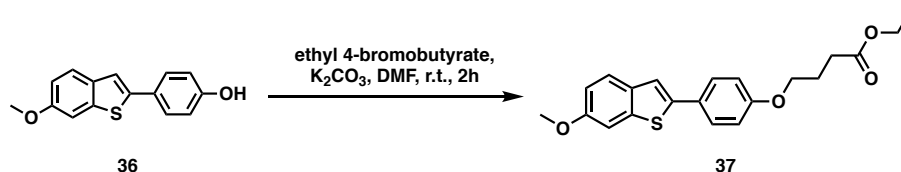
¹H NMR (500 MHz, CDCl₃) δ 7.96 – 7.91 (m, 2H), 7.75 (dd, *J* = 4.8, 4.0 Hz, 2H), 7.34 (d, *J* = 2.3 Hz, 1H), 7.23 – 7.18 (m, 2H), 7.04 (dd, *J* = 8.8, 2.3 Hz, 1H), 3.92 (s, 3H).



4-(6-methoxybenzo[*b*]thiophen-2-yl)phenol (36): Aryl bromide **11** (23.0 mg, 0.100 mmol, 1 equiv), Pd₂(dba)₃ (9.00 mg, 0.01 mmol, 0.100 equiv), tBuXPhos (8.00 mg, 0.020 mmol, 0.200 equiv), and KOH (36.0 mg, 0.110 mmol, 1.10 equiv) were suspended in 1.00 mL dioxane:H₂O (1:1). The mixture was stirred at 80 °C overnight. In the morning, TLC analysis indicated the complete consumption of starting material, and the mixture was diluted at room temperature with 1.00 mL EtOAc and 1.00 mL H₂O. The product was extracted with EtOAc (3 x 10.0 mL) and the combined organic layers were washed with brine, dried over MgSO₄, filtered, and evaporated to give a beige solid. The crude material

was purified by chromatography on silica using 20% EtOAc:hexanes to give 16.0 mg (60%) of the phenol **36** as a white solid.

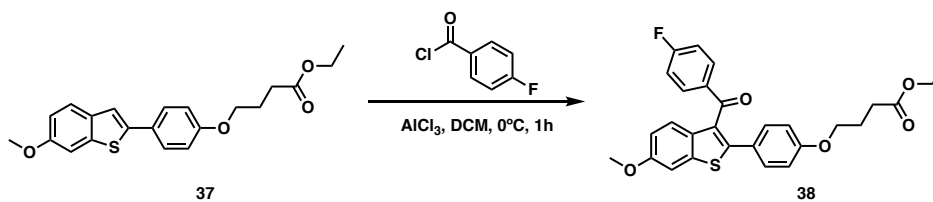
¹H NMR (500 MHz, CDCl₃) δ 7.62 (d, *J* = 8.6 Hz, 1H), 7.54 – 7.50 (m, 2H), 7.31 (s, 1H), 7.29 (d, *J* = 2.5 Hz, 1H), 6.96 (dd, *J* = 8.6, 2.4 Hz, 1H), 6.84 – 6.80 (m, 2H), 3.88 (s, 3H).



ethyl 4-(4-(6-methoxybenzo[b]thiophen-2-yl)phenoxy)butanoate (37): Ethyl 4-bromobutyrate (0.010 mL, 0.0700 mmol, 1.10 equiv) was added to a 2.0-mL solution of phenol **36** (16.0 mg, 0.0600 mmol, 1 equiv) and K₂CO₃ (17.0 mg, 0.120 mmol, 2.00 equiv) in anhydrous DMF. The mixture was stirred at room temperature for 2 hours, at which point TLC analysis indicated the complete consumption of starting material. The mixture was washed with 20.0 mL H₂O, and the product was extracted with EtOAc (3 x 5.00 mL). The combined organic layers were washed with brine, dried over MgSO₄, filtered, and evaporated to give a white solid and a yellow oil. The crude material was purified by washing with hexanes (3 x 5.00 mL) to give 23.0 mg (quant.) of the alkylated product **37** as a white solid.

¹H NMR (500 MHz, CDCl₃) δ 7.61 (d, *J* = 8.7 Hz, 1H), 7.60 – 7.56 (m, 2H), 7.33 (d, *J* = 0.7 Hz, 1H), 7.29 (d, *J* = 2.4 Hz, 1H), 6.96 (dd, *J* = 8.7, 2.4 Hz, 1H), 6.94 – 6.90 (m, 2H), 4.16 (q, *J* = 7.2 Hz, 2H), 4.05 (t, *J* = 6.1 Hz, 2H), 3.88 (s, 3H), 2.53 (t, *J* = 7.3 Hz, 2H), 2.14 (tt, *J* = 7.3, 6.1 Hz, 2H), 1.27 (t, *J* = 7.1 Hz, 3H).

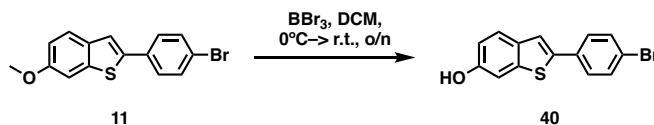
¹³C NMR (126 MHz, CDCl₃) δ 173.18, 158.74, 157.19, 141.52, 140.62, 134.91, 127.41, 127.33, 123.89, 117.76, 114.87, 114.35, 104.92, 66.88, 60.49, 55.64, 30.79, 24.63, 14.26.



ethyl 4-(4-(3-(4-fluorobenzoyl)-6-methoxybenzo[*b*]thiophen-2-yl)phenoxy)butanoate (38): AlCl₃ (23.0 mg, 0.180 mmol, 2.20 equiv) was added to a 2-mL solution of benzothiophene **37** (30.0 mg, 0.0800 mmol, 1 equiv) in anhydrous DCM at 0 °C. 4-fluorobenzoyl chloride (0.0100 mL, 0.0900 mmol, 1.10 equiv) was added to the dark red solution. The reaction was stirred at 0 °C for 1 hour, at which point TLC analysis indicated the complete consumption of starting material. The reaction was quenched by dropwise addition of 5.00 mL 1 M HCl at 0 °C. The product was extracted with DCM (3 x 10.0 mL) and the combined organic layers were washed with brine, dried over MgSO₄, filtered, and evaporated to give a yellow oil. The crude material was purified by chromatography on silica using 20% EtOAc:hexanes to give 20.0 mg (50%) of the aryl fluoride **38** as a gold oil.

¹H NMR (500 MHz, CDCl₃) δ 7.82 – 7.77 (m, 2H), 7.63 (d, *J* = 8.9 Hz, 1H), 7.34 (d, *J* = 2.4 Hz, 1H), 7.31 – 7.27 (m, 2H), 7.01 (dd, *J* = 8.9, 2.4 Hz, 1H), 6.97 – 6.91 (m, 2H), 6.75 – 6.71 (m, 2H), 4.15 (q, *J* = 7.1 Hz, 2H), 3.95 (t, *J* = 6.1 Hz, 2H), 3.91 (s, 3H), 2.49 (t, *J* = 7.3 Hz, 2H), 2.11 – 2.05 (m, 2H), 1.26 (t, *J* = 7.1 Hz, 3H).

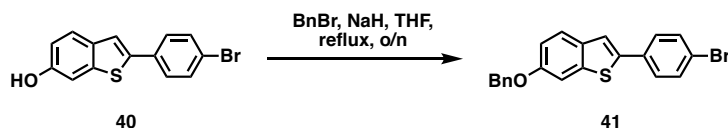
¹³C NMR (101 MHz, CDCl₃) δ 192.77, 173.09, 159.18, 157.77, 144.19, 140.10, 132.57, 132.47, 130.46, 129.87, 127.42, 125.81, 124.10, 115.56, 115.35, 114.99, 114.58, 104.50, 66.77, 60.47, 55.66, 30.68, 24.48, 14.22.



2-(4-bromophenyl)benzo[*b*]thiophen-6-ol (40): BBr₃ (1.29 mL, 13.4 mmol, 1.10 equiv.) was added dropwise at 0 °C to a 120-mL solution of methyl aryl ether **11** (3.90 g, 12.2 mmol, 1 equiv) in anhydrous DCM. The reaction was stirred at 0 °C for 2 hours before

being allowed to warm gradually to room temperature overnight. In the morning, TLC analysis indicated the complete consumption of starting material. The reaction was quenched by addition of 50.0 mL sat. NaHCO₃, and stirred until the formation of a biphase. The product was extracted with THF (3 x 50.0 mL), and the combined organic layers were washed with brine, dried over MgSO₄, filtered, and evaporated to give a grey solid. The crude material was purified by recrystallization with minimal hot EtOAc to give 3.72 g (quant.) of the phenol **40** as a white solid.

¹H NMR (500 MHz, CDCl₃) δ 7.63 (d, *J* = 8.5 Hz, 1H), 7.53 (s, 4H), 7.44 (d, *J* = 0.7 Hz, 1H), 6.90 (dd, *J* = 8.5, 2.4 Hz, 1H).

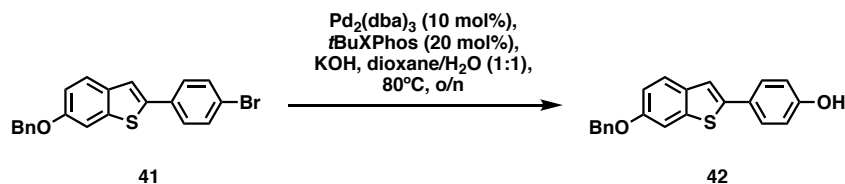


6-(benzyloxy)-2-(4-bromophenyl)benzo[*b*]thiophene (41): NaH (480 mg, 20.0 mmol, 2.00 equiv) was added to a 60.0-mL solution of phenol **40** (1.96 g, 6.00 mmol, 1 equiv) in anhydrous THF. Benzyl bromide (0.840 mL, 7.10 mmol, 1.10 equiv) was added, and the reaction was stirred at reflux overnight. In the morning, TLC analysis indicated the complete consumption of starting material. The reaction was quenched at room temperature by addition of 20.0 mL H₂O. The product was extracted with EtOAc (5 x 10.0 mL) and the combined organic layers were washed with brine, dried over MgSO₄, filtered, and evaporated to give a red solid. The crude material purified by trituration from EtOAc:hexanes and filtered to give 1.84 g (78%) of the alkylated product **41** as a yellow solid.

¹H NMR (500 MHz, CDCl₃) δ 7.66 (d, *J* = 8.8 Hz, 1H), 7.53 (s, 4H), 7.47 (ddt, *J* = 7.6, 1.5, 0.7 Hz, 2H), 7.45 (d, *J* = 0.8 Hz, 1H), 7.41 (ddd, *J* = 7.5, 6.7, 1.2 Hz, 2H), 7.37 (d, *J* = 2.3 Hz, 1H), 7.37 – 7.33 (m, 1H), 7.07 (dd, *J* = 8.7, 2.3 Hz, 1H), 5.14 (s, 2H).

^{13}C NMR (126 MHz, CDCl_3) δ 156.81, 140.94, 140.39, 136.78, 134.82, 133.45, 132.01, 128.65, 128.08, 127.59, 127.51, 124.39, 121.71, 119.49, 115.34, 106.18, 77.27, 77.02, 76.77, 70.48.

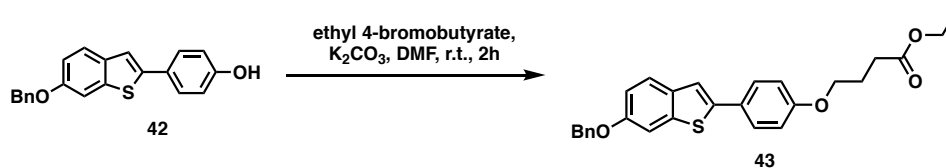
HRMS (ESI) calc. for $\text{C}_{21}\text{H}_{15}\text{BrNaOS}$ ($\text{M} + \text{Na}$) $^+$: 416.9901. Found: 416.9919.



4-(6-(benzyloxy)benzo[*b*]thiophen-2-yl)phenol (42): Aryl bromide **41** (1.84 g, 4.70 mmol, 1 equiv), $\text{Pd}(\text{dba})_2$ (80.0 mg, 0.140 mmol, 0.0300 equiv), *t*BuXPhos (60.0 mg, 0.140 mmol, 0.0300 equiv), and KOH (791 mg, 14.1 mmol, 3.00 equiv) were suspended in 200 mL dioxane: H_2O (1:1) and stirred at 80°C overnight. In the morning, TLC analysis indicated the complete consumption of starting material. The reaction was diluted with 50.0 mL H_2O and 30.0 mL EtOAc. The product was extracted with EtOAc (5 x 10.0 mL) and the combined organic layers were washed with brine, dried over MgSO_4 , filtered, and evaporated to give a peach solid. The crude material was purified by trituration from EtOAc:hexanes and filtered to provide 1.45 g (93%) of the product as a yellow solid.

^1H NMR (500 MHz, CDCl_3) δ 7.63 (d, $J = 8.7$ Hz, 1H), 7.57 – 7.53 (m, 2H), 7.49 – 7.45 (m, 2H), 7.43 – 7.33 (m, 5H), 7.33 (s, 1H), 7.05 (dd, $J = 8.6, 2.4$ Hz, 1H), 6.90 – 6.85 (m, 2H), 5.15 (d, $J = 7.8$ Hz, 2H).

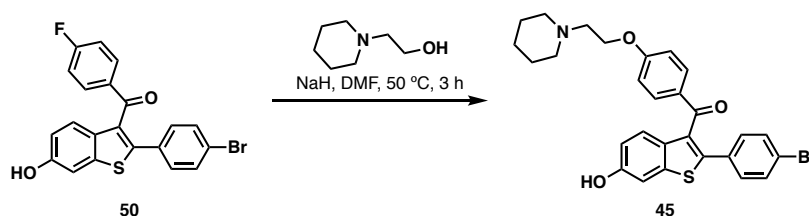
HRMS (ESI) calc. for $\text{C}_{21}\text{H}_{15}\text{O}_2\text{S}$ ($\text{M} - \text{H}$) $^-$: 331.0814. Found: 331.0798.



ethyl 4-(4-(6-(benzyloxy)benzo[*b*]thiophen-2-yl)phenoxy)butanoate (43): Ethyl 4-bromobutyrate (0.390 mL, 2.70 mmol, 1.10 equiv) was added to a 25.0-mL solution of phenol **42** (827 mg, 2.50 mmol, 1 equiv) and K₂CO₃ (1.04 g, 7.50 mmol, 3.00 equiv) in anhydrous DMF. The mixture was stirred at room temperature for 24 hours, at which point TLC analysis indicated the complete consumption of starting material. The mixture was washed with 250 mL H₂O, and the product was extracted with EtOAc (5 x 10.0 mL). The combined organic layers were washed with brine, dried over MgSO₄, filtered, and evaporated to give an orange solid. The crude material was purified by trituration from EtOAc:hexanes and filtered to provide 942 mg (84%) of the product as an orange solid.

¹H NMR (500 MHz, CDCl₃) δ 7.62 (d, *J* = 8.7 Hz, 1H), 7.60 – 7.56 (m, 2H), 7.47 (d, *J* = 7.2 Hz, 2H), 7.44 – 7.31 (m, 5H), 7.05 (dd, *J* = 8.7, 2.3 Hz, 1H), 6.95 – 6.90 (m, 2H), 5.14 (s, 2H), 4.17 (q, *J* = 7.1 Hz, 2H), 4.05 (t, *J* = 6.1 Hz, 2H), 2.54 (t, *J* = 7.3 Hz, 2H), 2.18 – 2.10 (m, 2H), 1.28 (t, *J* = 7.1 Hz, 3H).

¹³C NMR (126 MHz, CDCl₃) δ 173.19, 158.77, 156.36, 141.74, 140.54, 136.94, 135.16, 128.63, 128.03, 127.52, 127.43, 127.30, 123.93, 117.75, 114.98, 114.88, 106.29, 70.49, 66.88, 60.49, 30.80, 24.64, 14.27.



(2-(4-bromophenyl)-6-hydroxybenzo[*b*]thiophen-3-yl)(4-(2-(piperidin-1-

yl)ethoxy)phenyl)methanone (45): 2-hydroxyethyl piperidine (0.0700 mL, 0.530 mmol, 1.10 equiv) was added to a solution of NaH (60% in mineral oil, 100 mg, 2.50 mmol, 5.00 equiv) in anhydrous DMF (2.00 mL). H₂ was allowed to evolve before the aryl fluoride **50** (206 mg, 0.480 mmol, 1 equiv) was added via cannula as a 1.00-mL solution in DMF. The reaction was stirred at 50 °C for 3 h, at which point TLC analysis indicated the complete consumption of the starting material. The mixture was cooled to room temperature and

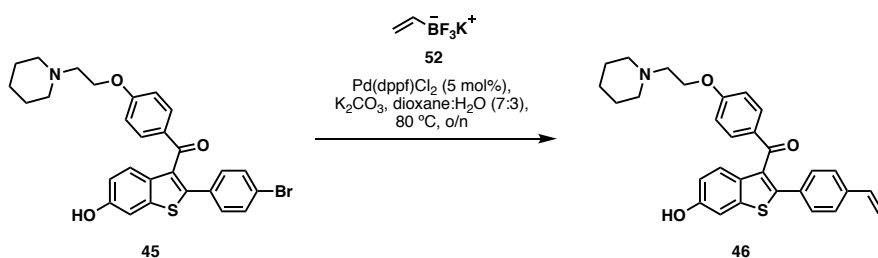
washed with 50.0 mL H₂O. The product was extracted with EtOAc (5 x 10.0 mL), and the combined organic layers were washed with brine, dried over MgSO₄, filtered, and evaporated to give a brown oil. The crude material was purified by chromatography over silica using 0-5% MeOH:DCM as eluent to give 256 mg (99%) of the piperidine **45** as a yellow oil.

¹H NMR (500 MHz, CDCl₃) δ 7.66 – 7.62 (m, 2H), 7.35 (d, *J* = 8.8 Hz, 1H), 7.34 – 7.31 (m, 2H), 7.22 – 7.19 (m, 2H), 7.16 (d, *J* = 2.2 Hz, 1H), 6.77 (dd, *J* = 8.8, 2.3 Hz, 1H), 6.60 – 6.57 (m, 2H), 4.12 (t, *J* = 5.6 Hz, 2H), 2.83 (t, *J* = 5.6 Hz, 2H), 2.61 (s, 4H), 1.67 (p, *J* = 5.6 Hz, 4H), 1.47 (s, 1H).

¹³C NMR (126 MHz, CDCl₃) δ 193.01, 163.06, 154.51, 140.37, 140.19, 133.42, 132.42, 132.21, 131.94, 131.77, 130.30, 128.94, 124.43, 122.63, 115.44, 114.25, 107.37, 65.60, 57.75, 55.10, 25.48, 24.00.

HRMS (ESI) *m/z* calc. for C₂₈H₂₇BrNO₃S (M + H)⁺: 536.0871. Found: 536.0890.

IR (neat) *ν* = 3015, 2936, 1645, 1597, 1254, 1214, 1167, 1036, 1008, 848, 832, 816, 751, 667 cm⁻¹.



(6-hydroxy-2-(4-vinylphenyl)benzo[*b*]thiophen-3-yl)(4-(2-(piperidin-1-

yl)ethoxy)phenyl)methanone (46): Aryl bromide **45** (239 mg, 0.400 mmol, 1 equiv), potassium vinyltrifluoroborate (101 mg, 0.700 mmol, 1.70 equiv), Pd(dppf)Cl₂ (33.0 mg, 0.0400 mmol, 0.100 equiv), and K₂CO₃ (110 mg, 0.800 mmol, 2.00 equiv) were suspended in 4.00 mL 7:3 dioxane:H₂O. The mixture was stirred at 80 °C overnight. In the morning, the reaction was cooled to room temperature and diluted with 10.0 mL H₂O,

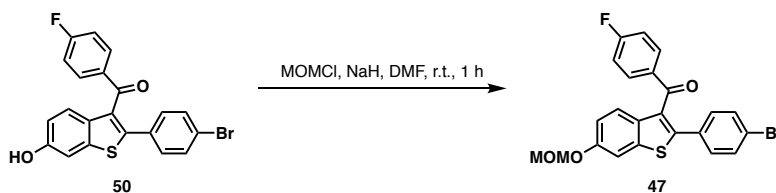
followed by 5.00 mL EtOAc. The organic layer was separated from the aqueous layer and the product was extracted with EtOAc (5 x 10.0 mL). The combined organic layers were washed with 50.0 mL brine, dried over MgSO₄, filtered, and evaporated to give a brown oil. The crude material was purified by chromatography on silica using 0-5% MeOH:DCM as eluent to give 170 mg (88%) of the styrene **46** as a brown oil.

¹H NMR (500 MHz, CDCl₃) δ 8.85 (s, 1H), 7.72 – 7.64 (m, 2H), 7.35 (d, *J* = 8.8 Hz, 1H), 7.33 – 7.29 (m, 2H), 7.25 – 7.20 (m, 2H), 7.18 (d, *J* = 2.3 Hz, 1H), 6.76 (dd, *J* = 8.8, 2.3 Hz, 1H), 6.63 – 6.56 (m, 3H), 5.68 (d, *J* = 17.6 Hz, 1H), 5.21 (d, *J* = 10.9 Hz, 1H), 4.10 (t, *J* = 5.5 Hz, 2H), 2.83 (t, *J* = 5.6 Hz, 2H), 2.61 (s, 4H), 1.67 (p, *J* = 5.6 Hz, 4H), 1.47 (q, *J* = 5.6 Hz, 2H).

¹³C NMR (126 MHz, CDCl₃) δ 193.51, 162.72, 154.89, 141.19, 140.34, 137.37, 136.10, 133.24, 132.87, 132.28, 131.33, 130.46, 128.96, 126.41, 124.16, 115.50, 114.53, 114.17, 107.44, 65.13, 57.57, 54.95, 25.08, 23.73.

HRMS (ESI) calc. for C₃₀H₂₈NO₃S (M – H)⁻: 482.1812. Found: 482.1795.

IR (thin film) ν = 3019, 1597, 1254, 1214, 1167, 745, 667 cm⁻¹.



(2-(4-bromophenyl)-6-(methoxymethoxy)benzo[*b*]thiophen-3-yl)(4-

fluorophenyl)methanone (47): NaH (60% in mineral oil, 58.0 mg, 2.40 mmol, 2.00 equiv) was added to a solution of phenol **47** (849 mg, 2.00 mmol, 1 equiv) in anhydrous DMF (20.0 mL). Chloromethyl methyl ether (0.170 mL, 2.20 mmol, 1.10 equiv) was added, and the mixture was stirred for 1 h at which point TLC analysis indicated the complete consumption of the starting material. 10.0 mL MeOH was added and the mixture was

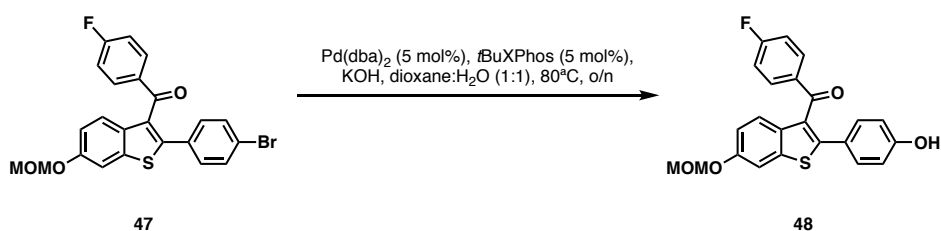
stirred for 6 h. The reaction was washed with 200 mL H₂O and the product was extracted with EtOAc (4 x 10.0 mL). The combined organic layers were washed with brine, dried over MgSO₄, filtered, and concentrated to give a yellow solid. The crude was chromatographed over silica using 15% EtOAc:hexanes as eluent to give 834 mg (90%) of the ether **47** as a white solid.

¹H NMR (500 MHz, CDCl₃) δ 7.83 – 7.76 (m, 2H), 7.61 (d, *J* = 8.9 Hz, 1H), 7.57 (d, *J* = 2.3 Hz, 1H), 7.39 – 7.34 (m, 2H), 7.29 – 7.23 (m, 2H), 7.11 (dd, *J* = 8.9, 2.3 Hz, 1H), 6.97 (t, *J* = 8.6 Hz, 2H), 5.26 (s, 2H), 3.52 (s, 3H).

¹³C NMR (126 MHz, CDCl₃) δ 192.38, 166.91, 164.87, 155.60, 142.76, 140.18, 134.38, 133.70, 133.68, 132.56, 132.49, 132.19, 131.84, 131.22, 130.53, 124.37, 123.11, 116.57, 115.80, 115.63, 107.92, 94.83, 56.13.

HRMS (ESI) calc. for C₂₃H₁₆BrFNaO₃S (M + Na)⁺: 492.9879. Found: 492.9880.

IR (thin film) ν = 3067, 2932, 1637, 1597, 1504, 1468, 1242, 1149, 1072, 1038, 992, 846, 828, 792, 770 cm⁻¹.



(4-fluorophenyl)(2-(4-hydroxyphenyl)-6-(methoxymethoxy)benzo[*b*]thiophen-3-yl)methanone (48**):** Aryl bromide **47** (734 mg, 1.60 mmol, 1 equiv), Pd(dba)₂ (45.0 mg, 0.0800 mmol, 0.0500 equiv), tBuXPhos (33.0 mg, 0.0800 mmol, 0.0500 equiv), and KOH (269 mg, 4.80 mmol, 3.00 equiv) were suspended in 1:1 dioxane:H₂O (20.0 mL). The mixture was brought to 80 °C and stirred overnight. In the morning, the mixture was cooled to room temperature and diluted with 10.0 mL H₂O followed by 5.0 mL EtOAc. The mixture was neutralized with 1 M HCl, and the organic layer was separated from the aqueous

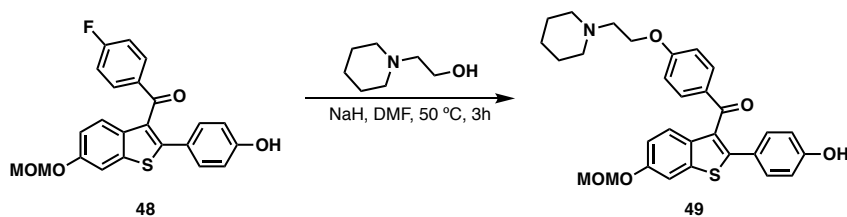
layer. The product was extracted with EtOAc (3 x 10.0 mL) and the combined organic layers were washed with brine, dried over MgSO₄, filtered, and concentrated to give a yellow oil. The crude material was chromatographed over silica using 20% EtOAc:hexanes as eluent to afford 513 mg (68%) of the phenol **48** as a yellow solid.

¹H NMR (500 MHz, CDCl₃) δ 7.80 – 7.74 (m, 2H), 7.62 (d, *J* = 8.9 Hz, 1H), 7.54 (d, *J* = 2.3 Hz, 1H), 7.25 – 7.21 (m, 2H), 7.08 (dd, *J* = 8.8, 2.3 Hz, 1H), 6.96 – 6.90 (m, 2H), 6.68 – 6.64 (m, 2H), 5.25 (s, 2H), 3.52 (s, 3H).

¹³C NMR (126 MHz, CDCl₃) δ 192.81, 166.72, 164.69, 156.12, 155.25, 145.03, 139.87, 134.56, 133.88, 132.59, 132.51, 130.73, 129.86, 125.90, 124.13, 116.33, 115.60, 115.58, 115.41, 107.98, 94.88, 56.10.

HRMS (ESI) calc. for C₂₃H₁₇FN₄O₄S (M + Na)⁺: 431.0711. Found: 431.0724.

IR (thin film) ν = 3369, 3071, 3015, 2956, 2900, 2829, 1643, 1607, 1595, 1534, 1502, 1470, 1409, 1353, 1272, 1246, 1151, 1082, 1038, 1000, 834, 755 cm⁻¹.



(2-(4-hydroxyphenyl)-6-(methoxymethoxy)benzo[*b*]thiophen-3-yl)(4-(2-(piperidin-1-yl)ethoxy)phenyl)methanone (49): 2-hydroxyethyl piperidine (0.150 mL, 1.20 mmol, 1.10 equiv) was added to a stirring solution of NaH (220 mg, 5.50 mmol, 5.00 equiv). H₂ gas was allowed to evolve before aryl fluoride **48** (496 mg, 1.10 mmol, 1 equiv) was added via cannula as a 5.00-mL solution in anhydrous DMF. The resulting bright red solution was stirred at 50 °C for 3 hours before TLC analysis indicated the complete consumption of the starting material. The reaction was at room temperature by dropwise addition of 10.0 mL H₂O. The mixture was washed with 100 mL H₂O and the product was extracted

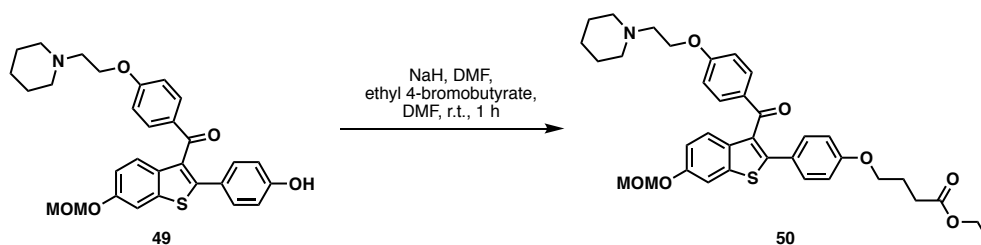
with EtOAc (5 x 10.0 mL). The combined organic layers were washed with brine, dried over MgSO₄, filtered, and concentrated to give a yellow oil. The crude material was purified chromatography on silica using 0-5% MeOH:DCM as eluent to give 501 mg (88%) of the piperidine **49** as a yellow crystalline solid.

¹H NMR (500 MHz, CDCl₃) δ 8.46 (s, 1H), 7.71 – 7.64 (m, 2H), 7.20 – 7.09 (m, 2H), 7.05 (dd, *J* = 8.9, 2.3 Hz, 1H), 6.64 – 6.59 (m, 2H), 6.59 – 6.54 (m, 2H), 5.24 (s, 2H), 4.06 (t, *J* = 5.7 Hz, 2H), 3.51 (s, 3H), 2.76 (t, *J* = 5.7 Hz, 2H), 2.55 (s, 4H), 1.62 (p, *J* = 5.6 Hz, 4H), 1.45 (t, *J* = 7.9 Hz, 2H).

¹³C NMR (126 MHz, CDCl₃) δ 193.41, 162.53, 157.22, 155.08, 144.60, 139.74, 134.85, 132.36, 130.55, 130.53, 129.99, 125.01, 124.07, 116.10, 115.99, 114.20, 107.99, 94.91, 65.40, 57.40, 56.08, 54.86, 25.16, 23.76.

HRMS (ESI) calc. for C₃₀H₃₂NO₅S (M + H)⁺: 518.1975. Found: 518.1996.

IR (thin film) ν = 3353, 3019, 1645, 1597, 1532, 1502, 1468, 1214, 1000, 747, 667 cm⁻¹.



Ethyl 4-(4-(6-(methoxymethoxy)-3-(4-(2-(piperidin-1-yl)ethoxy)benzoyl)benzo[*b*]thiophen-2-yl)phenoxy)butanoate (50): NaH (60% in mineral oil, 10.0 mg, 0.400 mmol, 2.00 equiv) was added to a stirring solution of phenol **49** (61.0 mg, 0.120 mmol, 1 equiv) in anhydrous DMF (2.00 mL). Ethyl 4-bromobutyrate (0.0200 mL, 0.140 mmol, 1.20 equiv) was added, and the mixture was stirred at room temperature for 1 h at which point TLC analysis indicated the complete consumption of the starting material. The mixture was washed with 50.0 mL H₂O and the product was

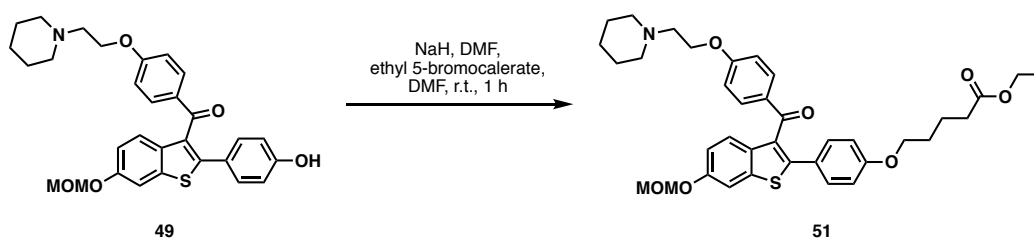
extracted with EtOAc (3 x 10.0 mL). The combined organic layers were washed with brine, dried over MgSO₄, filtered, and concentrated to give a yellow oil. The crude material was purified by chromatography on silica using 0-5% MeOH:DCM as eluent to afford 51.0 mg (67%) of the ethyl ester **50** as a yellow oil.

¹H NMR (500 MHz, CDCl₃) δ 7.78 – 7.73 (m, 2H), 7.54 – 7.49 (m, 2H), 7.36 – 7.31 (m, 2H), 7.04 (dd, *J* = 8.8, 2.3 Hz, 1H), 6.79 – 6.75 (m, 2H), 6.75 – 6.72 (m, 2H), 5.24 (s, 2H), 4.17 – 4.07 (m, 4H), 3.94 (t, *J* = 6.2 Hz, 2H), 3.51 (s, 3H), 2.77 (s, 2H), 2.48 (q, *J* = 9.2, 7.1 Hz, 6H), 2.11 – 2.02 (m, 1H), 1.61 (s, 4H), 1.45 (s, 2H), 1.24 (t, *J* = 7.1 Hz, 3H).

¹³C NMR (126 MHz, CDCl₃) δ 193.18, 173.11, 162.94, 159.06, 155.09, 143.08, 139.83, 134.90, 132.32, 130.49, 130.42, 130.25, 125.99, 124.02, 116.05, 114.60, 114.24, 107.98, 94.91, 66.75, 66.08, 60.46, 57.61, 56.07, 55.05, 30.74, 25.73, 24.54, 24.01, 14.23.

HRMS (ESI) calc. for C₃₆H₄₂NO₇S (M + H)⁺: 632.2688. Found: 632.2677.

IR (thin film) ν = 3023, 2944, 1730, 1595, 1470, 1248, 1214, 749, 567 cm⁻¹.



ethyl 5-(4-(6-(methoxymethoxy)-3-(4-(2-(piperidin-1-yl)ethoxy)benzoyl)benzo[*b*]thiophen-2-yl)phenoxy)pentanoate (51**):** NaH (60% in mineral oil, 9.00 mg, 0.220 mmol, 2.00 equiv) was added to a stirring solution of phenol **49** (58.0 mg, 0.110 mmol, 1 equiv) in anhydrous DMF. Ethyl 5-bromovalerate (0.0200 mL, 0.120 mmol, 1.10 equiv) was added, and the mixture was stirred at room temperature for 1 h at which point TLC analysis indicated the complete consumption of the starting material. The mixture was washed with 50.0 mL H₂O and the product was extracted with

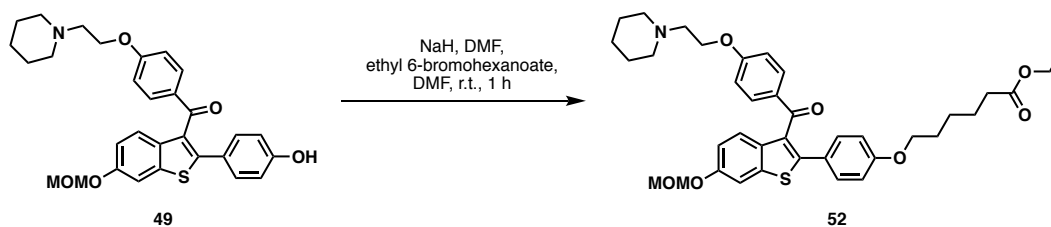
EtOAc (3 x 10.0 mL). The combined organic layers were washed with brine, dried over MgSO₄, filtered, and concentrated to give a yellow oil. The crude material was purified by chromatography on silica using 0-5% MeOH:DCM as eluent to afford 52.0 mg (73%) of the ethyl ester **51** as a yellow oil.

¹H NMR (500 MHz, Chloroform-*d*) δ 7.75 (dd, *J* = 8.7, 1.0 Hz, 2H), 7.55 – 7.49 (m, 2H), 7.35 – 7.31 (m, 2H), 7.03 (ddd, *J* = 8.8, 2.4, 1.0 Hz, 1H), 6.78 – 6.75 (m, 2H), 6.75 – 6.71 (m, 2H), 5.23 (d, *J* = 1.9 Hz, 2H), 4.16 – 4.04 (m, 3H), 3.90 (dt, *J* = 5.9, 2.7 Hz, 2H), 3.51 (d, *J* = 2.0 Hz, 3H), 2.76 (t, *J* = 5.8 Hz, 2H), 2.50 (s, 4H), 2.35 (td, *J* = 5.7, 2.9 Hz, 2H), 1.82 – 1.73 (m, 4H), 1.60 (p, *J* = 5.6 Hz, 4H), 1.44 (d, *J* = 6.7 Hz, 2H), 1.24 (t, *J* = 7.1, 3H).

¹³C NMR (126 MHz, Chloroform-*d*) δ 193.18, 173.37, 162.94, 159.18, 155.08, 143.15, 139.82, 134.91, 132.31, 130.44, 130.41, 130.24, 125.86, 124.01, 116.04, 114.58, 114.23, 107.98, 94.90, 67.39, 66.09, 60.32, 57.62, 56.06, 55.05, 33.92, 28.58, 25.75, 24.01, 21.59, 14.26.

HRMS (ESI) calc. for C₃₇H₄₄NO₇S (M + H)⁺: 646.2856. Found: 646.2833.

IR (thin film) ν = 3063, 3035, 2936, 1730, 1595, 1468, 1244, 1161, 996, 830 cm⁻¹.



Ethyl 6-(4-(6-(methoxymethoxy)-3-(4-(2-(piperidin-1-yl)ethoxy)benzoyl)benzo[*b*]thiophen-2-yl)phenoxy)hexanoate (52): NaH (60% in mineral oil, 8.00 mg, 0.200 mmol, 2.00 equiv) was added to a stirring solution of phenol **49** (51.0 mg, 0.100 mmol, 1 equiv) in anhydrous DMF. Ethyl 6-bromohexanoate (0.0200 mL, 0.110 mmol, 1.10 equiv) was added, and the mixture was stirred at room temperature

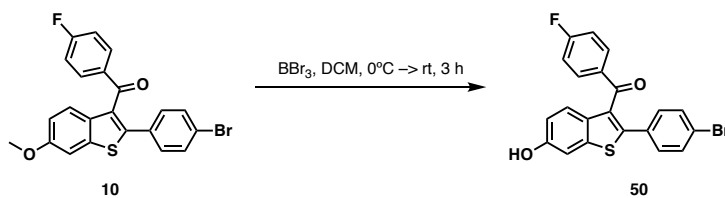
for 1 h at which point TLC analysis indicated the complete consumption of the starting material. The mixture was washed with 50 mL H₂O and the product was extracted with EtOAc (3 x 10.0 mL). The combined organic layers were washed with brine, dried over MgSO₄, filtered, and concentrated to give a yellow oil. The crude material was purified by chromatography on silica using 0-5% MeOH:DCM as eluent to afford 60.0 mg (60%) of the ethyl ester **52** as a yellow oil.

¹H NMR (500 MHz, CDCl₃) δ 7.78 – 7.73 (m, 2H), 7.54 – 7.50 (m, 2H), 7.36 – 7.29 (m, 2H), 7.04 (dd, *J* = 8.8, 2.4 Hz, 1H), 6.78 – 6.74 (m, 2H), 6.74 – 6.71 (m, 2H), 5.23 (s, 2H), 4.12 (q, *J* = 7.1 Hz, 4H), 3.89 (t, *J* = 6.4 Hz, 2H), 3.51 (s, 3H), 2.76 (s, 2H), 2.50 (s, 4H), 2.31 (t, *J* = 7.5 Hz, 2H), 1.76 (p, *J* = 6.6 Hz, 2H), 1.68 (p, *J* = 7.5 Hz, 3H), 1.60 (t, *J* = 5.9 Hz, 4H), 1.47 (tt, *J* = 9.8, 6.3 Hz, 4H), 1.25 (t, *J* = 7.1 Hz, 3H).

¹³C NMR (126 MHz, CDCl₃) δ 193.19, 173.58, 162.94, 159.27, 155.08, 139.82, 134.92, 132.31, 130.42 (d), 130.24, 125.80, 124.01, 116.03, 114.58, 114.23, 107.98, 94.91, 67.66, 66.13, 60.25, 57.63, 56.07, 55.05, 34.22, 28.86, 25.78, 25.61, 24.70, 24.03, 14.26.

HRMS (ESI) calc. for C₃₈H₄₆NO₇S (M + H)⁺: 660.2986. Found: 660.2990.

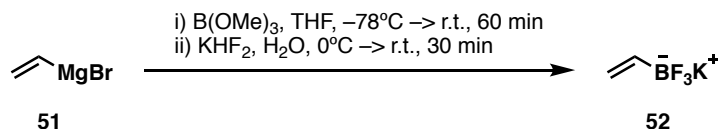
IR (thin film) ν = 3067, 2936, 1732, 1587, 1468, 1248, 1165, 1038, 1000 cm⁻¹.



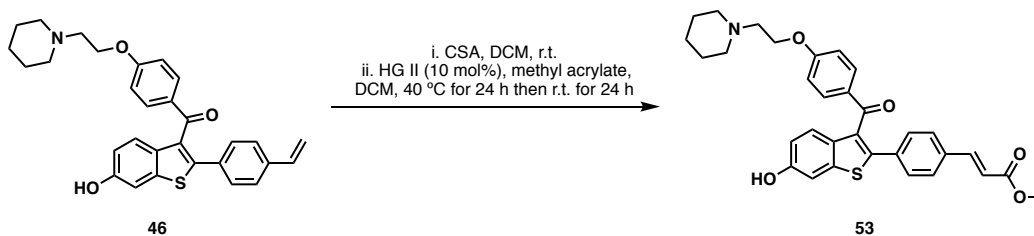
(2-(4-bromophenyl)-6-(4-fluorophenyl)-3-hydroxybenzo[*b*]thiophen-3-yl)(4-fluorophenyl)methanone

(50): BBr₃ (0.0700 mL, 0.750 mmol, 1.10 equiv) was added dropwise to a solution of methyl aryl ether **10** (269 mg, 0.700 mmol, 1 equiv) in DCM (7.00 mL) at 0 °C. The mixture was gradually allowed to reach r.t. over a 3 h period, at which TLC analysis indicated the complete consumption of starting material. The reaction was cooled to 0 °C, and 5.00-mL

of a saturated NaHCO₃ solution was added dropwise. The organic layer was separated from the aqueous layer, and the product was extracted with DCM (3 x 10.0 mL). The combined organic layers were washed with brine, dried over MgSO₄, filtered, and evaporated to give 206 mg (70%) of the free phenol **50** as an orange solid, which was used immediately in the subsequent reaction.

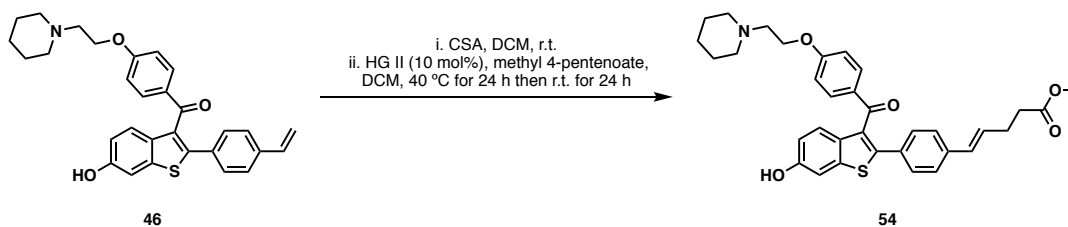


Potassium vinyltrifluoroborate (52): Vinylmagnesium bromide (1 M THF, 12.0 mL, 12.0 mmol, 1 equiv) was added at -78°C to a solution of trimethyl borate (1.61 mL, 14.4 mmol, 1.20 equiv) in THF (15.0 mL). The reaction was stirred at -78°C for 20 min, then at room temperature for 1 h. The reaction was then cooled to 0°C , and potassium difluoride (4.49 g, 60.0 mmol, 5.00 equiv) was added, followed by 7.00 mL H₂O over 30 min using an addition funnel. The mixture was brought to room temperature and stirred for 30 min. The solution was then concentrated in vacuo and lyophilized overnight. The resulting yellow solid was dissolved in acetone, filtered, and concentrated to give a cream solid. The cream solid was purified by dissolving in hot acetone and precipitating with Et₂O, obtaining 980 mg of the trifluoroborate **52** as a white solid (61%). The spectroscopic data is in agreement with that published in literature.⁴



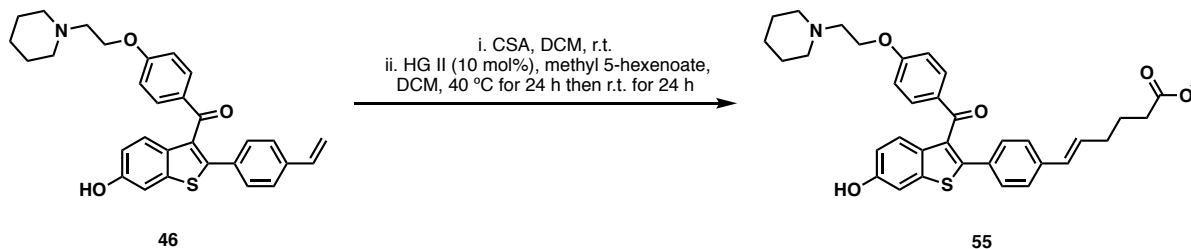
methyl (E)-3-(4-(6-hydroxy-3-(4-(2-(piperidin-1-yl)ethoxy)benzoyl)benzo[*b*]thiophen-2-yl)phenyl)acrylate (53): CSA (95.0 mg, 0.400 mmol, 1.00 equiv) was added to a 1.00-mL solution of the styrene **46** (203 mg, 0.410 mmol, 1.00 equiv) in anhydrous DCM, and stirred for 10 minutes at room temperature. The mixture was concentrated in vacuo to give the amine salt as a yellow foam. The

freshly-distilled methyl acrylate (0.370 mL, 4.90 mmol, 10.0 equiv) was added to the styrene via cannula as a 1.00-mL solution in anhydrous DCM. A half-portion of the HG II catalyst (33.0 mg, 0.0400 mmol, 0.100 equiv) was added via cannula to the solution of olefins as a 1.00-mL solution in anhydrous DCM. The mixture was stirred at reflux for 24 hours, then cooled to room temperature. Another half-portion of the catalyst was added to the reaction via cannula as a 0.500-mL solution in anhydrous DCM. The reaction was stirred at room temperature for another 24 hours, before 5.00 mL of a saturated solution of NaHCO₃ was added. The product was extracted with DCM (3 x 10.0 mL), dried over MgSO₄, filtered, and concentrated in vacuo to give 100 mg of the methyl ester **53** as a green oil, which was used without further purification.

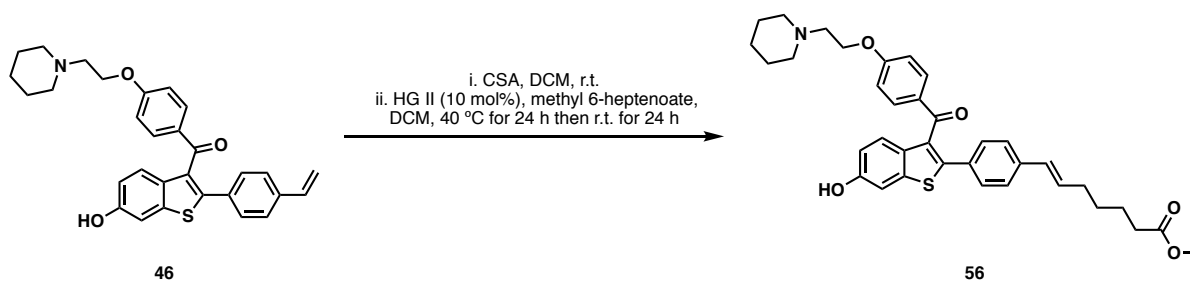


methyl (E)-5-(4-(6-hydroxy-3-(4-(2-(piperidin-1-yl)ethoxy)benzoyl)benzo[*b*]thiophen-2-yl)phenyl)pent-4-enoate (54): CSA (37.0 mg, 0.160 mmol, 1.05 equiv) was added to a 1-mL solution of the styrene **46** (73.0 mg, 0.150 mmol, 1 equiv) in anhydrous DCM, and stirred for 10 minutes at room temperature. The mixture was concentrated in vacuo to give the amine salt as a yellow foam. The freshly-distilled methyl 4-pentenoate (168 mg, 1.50 mmol, 10.0 equiv) was added to the styrene via cannula as a 1.00-mL solution in anhydrous DCM. A half-portion of the HG II catalyst (13.0 mg, 0.0150 mmol, 0.100 equiv) was added via cannula to the solution of olefins as a 1.00-mL solution in anhydrous DCM. The mixture was stirred at reflux for 24 hours, then cooled to room temperature. Another half-portion of the catalyst was added to the reaction via cannula as a 0.500-mL solution in anhydrous DCM. The reaction was stirred at room temperature for another 24 hours, then 5.00 mL of a saturated solution of NaHCO₃ was added, and the product was extracted with DCM (3 x 10.0 mL). The combined organic layers were washed with 10.0 mL brine, dried over MgSO₄, filtered, and concentrated in

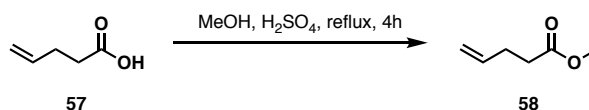
vacuo to give 58 mg of the methyl ester **54** as a green oil, which was used without further purification.



methyl (E)-6-(4-(6-hydroxy-3-(4-(2-(piperidin-1-yl)ethoxy)benzoyl)benzo[*b*]thiophen-2-yl)phenyl)hex-5-enoate (55): CSA (70.0 mg, 0.300 mmol, 1.00 equiv) was added to a 1.00-mL solution of the styrene **46** (150 mg, 0.300 mmol, 1 equiv) in anhydrous DCM, and stirred for 10 minutes at room temperature. The mixture was concentrated in vacuo to give the amine salt as a yellow foam. The freshly-distilled methyl 5-hexenoate (385 mg, 3.00 mmol, 10.0 equiv) was added to the styrene via cannula as a 1.00-mL solution in anhydrous DCM. A half-portion of the HG II catalyst (26.0 mg, 0.0300 mmol, 0.100 equiv) was added via cannula to the solution of olefins as a 1.00-mL solution in anhydrous DCM. The mixture was stirred at reflux for 24 hours, then cooled to room temperature. Another half-portion of the catalyst was added to the reaction via cannula as a 0.500-mL solution in anhydrous DCM. The reaction was stirred at room temperature for another 24 hours, then 5.00 mL of a saturated solution of NaHCO₃ was added, and the product was extracted with DCM (3 x 10.0 mL). The combined organic layers were washed with 10.0 mL brine, dried over MgSO₄, filtered, and concentrated in vacuo to give 124 mg of the methyl ester **55** as a green oil, which was used without further purification.

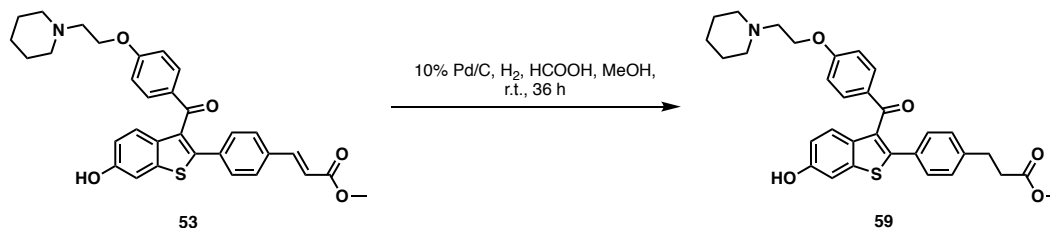


methyl (E)-7-(4-(6-hydroxy-3-(4-(2-(piperidin-1-yl)ethoxy)benzoyl)benzo[*b*]thiophen-2-yl)phenyl)hept-6-enoate (56): CSA (61.0 mg, 0.300 mmol, 1.00 equiv) was added to a 1.00-mL solution of the styrene **46** (131 mg, 0.300 mmol, 1 equiv) in anhydrous DCM, and stirred for 10 minutes at room temperature. The mixture was concentrated in vacuo to give the amine salt as a yellow foam. The freshly-distilled methyl 6-heptenoate (0.400 mL, 3.00 mmol, 10.0 equiv) was added to the styrene via cannula as a 1.00-mL solution in anhydrous DCM. A half-portion of the catalyst (25.0 mg, 0.0300 mmol, 0.100 equiv) was added via cannula to the solution of olefins as a 1.00-mL solution in anhydrous DCM. The mixture was stirred at reflux for 24 hours, then cooled to room temperature. Another half-portion of the catalyst was added to the reaction via cannula as a 0.500-mL solution in anhydrous DCM. The reaction was stirred at room temperature for another 24 hours, then 5.00 mL of a saturated solution of NaHCO₃ was added, and the product was extracted with DCM (3 x 10.0 mL). The combined organic layers were washed with 10.0 mL brine, dried over MgSO₄, filtered, and concentrated in vacuo to give 53.0 mg of the methyl ester **56** as a green oil, which was used without further purification.

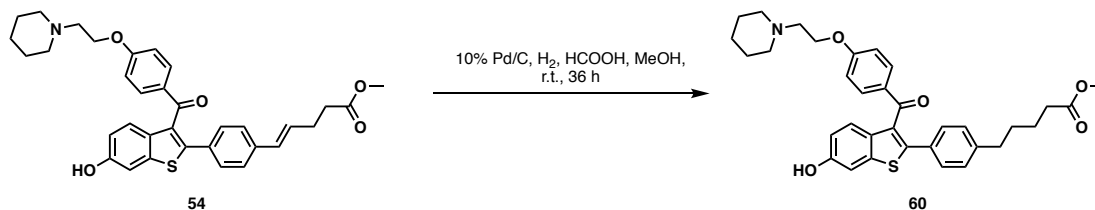


Methyl pent-4-enoate (58): Catalytic concentrated H₂SO₄ (5 drops) was added to a 15.0-mL solution of pent-4-enoic acid **57** (5.10 mL, 50.0 mmol, 1.00 equiv) in anhydrous MeOH. The reaction was stirred at reflux for 4 hours, after which full conversion of starting material was revealed by ¹HNMR analysis. The reaction was cooled to room temperature, and 5.00 mL of H₂O was added directly to the reaction. The product separated into the organic layer, and the top phase was passed through a small plug of MgSO₄ to afford

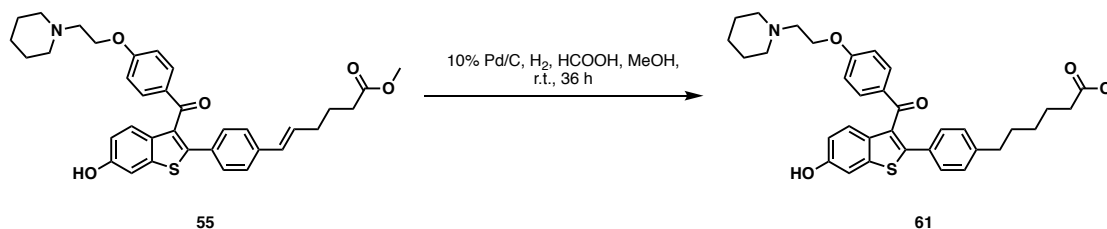
3.63 g (64%) of the ester **58** as a clear oil. The spectroscopic data is in agreement with that reported in the literature.⁵



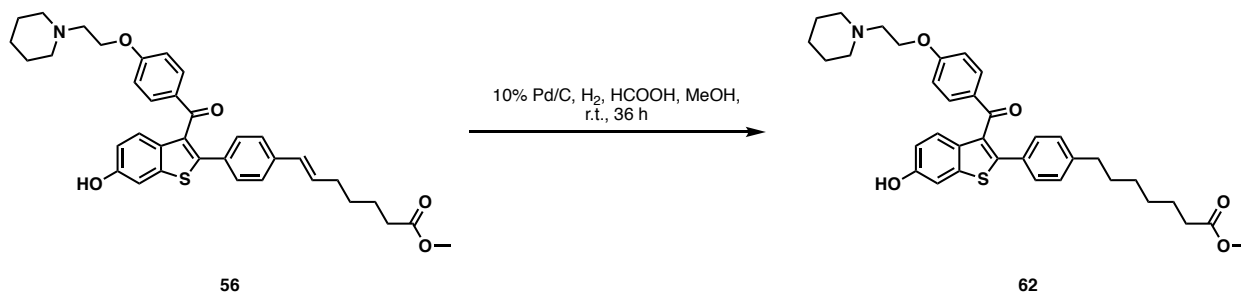
methyl 3-(4-(6-hydroxy-3-(4-(2-(piperidin-1-yl)ethoxy)benzoyl)benzo[b]thiophen-2-yl)phenyl)propanoate (59): 10% Pd/C (21.0 mg, 0.180 mmol, 0.100 equiv) was added to a 1.00-mL solution of alkene **53** (100 mg, 0.180 mmol, 1 equiv) in MeOH. Three drops of formic acid were added, and a balloon charged with H₂ was inserted into the reaction. The mixture was stirred at room temperature for 36 h, then filtered through celite and concentrated in vacuo to give 99.0 mg (99%) of the hydrogenated product **59** as a yellow oil, which was used without further purification.



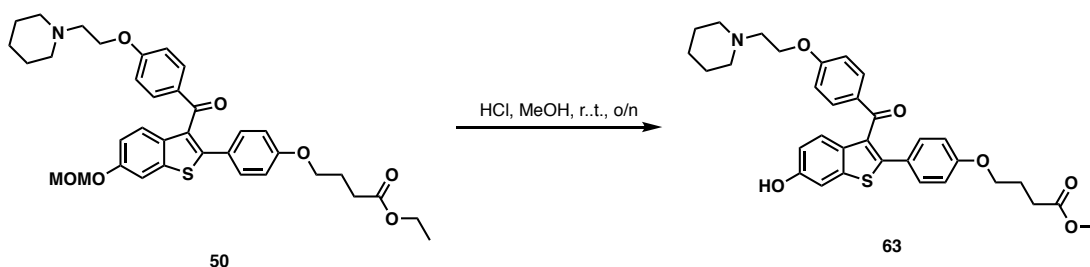
methyl 5-(4-(6-hydroxy-3-(4-(2-(piperidin-1-yl)ethoxy)benzoyl)benzo[b]thiophen-2-yl)phenyl)pentanoate (60): 10% Pd/C (16.0 mg, 0.100 mmol, 0.100 equiv) was added to a 1.00-mL solution of alkene **54** (58.0 mg, 0.100 mmol, 1 equiv) in MeOH. Three drops of formic acid were added, and a balloon charged with H₂ was inserted into the reaction. The mixture was stirred at room temperature for 36 h, then filtered through celite and concentrated in vacuo to give 42.0 mg (73%) of the hydrogenated product **60** as a brown oil, which was used without further purification.



methyl 6-(4-(6-hydroxy-3-(4-(2-(piperidin-1-yl)ethoxy)benzoyl)benzo[*b*]thiophen-2-yl)phenyl)hexanoate (61): 10% Pd/C (21.0 mg, 0.200 mmol, 0.100 equiv) was added to a 2.00-mL solution of alkene **55** (124 mg, 0.200 mmol, 1 equiv) in MeOH. Three drops of formic acid were added, and a balloon charged with H₂ was inserted into the reaction. The mixture was stirred at room temperature for 36 h, then filtered through celite and concentrated in vacuo to give 116 mg (99%) of the hydrogenated product **61** as a yellow oil, which was used without further purification.



methyl 7-(4-(6-hydroxy-3-(4-(2-(piperidin-1-yl)ethoxy)benzoyl)benzo[*b*]thiophen-2-yl)phenyl)heptanoate (62): Prepared according to General Procedure C using alkene (106 mg, 0.180 mmol, 1 equiv) and 10% Pd/C (20.0 mg, 0.180 mmol, 0.100 equiv) in 1.00 mL MeOH to give 46.0 mg (43%) of the hydrogenated product **62** as a yellow oil, which was used without further purification.

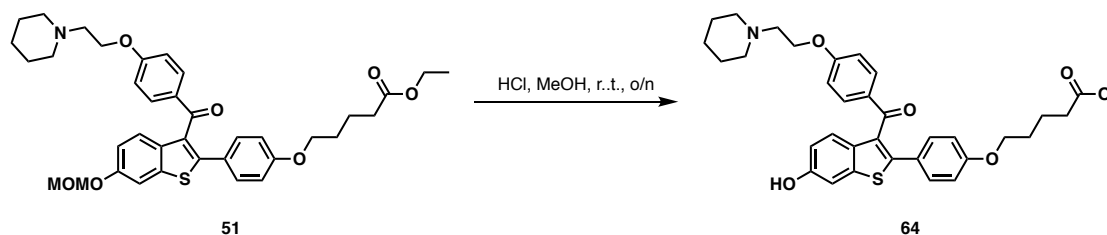


methyl 4-(4-(6-hydroxy-3-(4-(2-(piperidin-1-yl)ethoxy)benzoyl)benzo[b]thiophen-2-yl)phenoxy)butanoate (63): Three drops of concentrated HCl was added to a 1.00-mL solution of ether **50** (51.0 mg, 0.0800 mmol, 1 equiv) in MeOH. The reaction was stirred at room temperature overnight. In the morning, 10.0 mL of H₂O was added and the product was extracted with EtOAc (3 x 5.00 mL). The combined organic layers were washed with brine, dried over MgSO₄, filtered, and concentrated to give the phenol **63** was isolated as a yellow oil and was used immediately without further purification.

¹H NMR (500 MHz, CDCl₃) δ 7.68 (d, *J* = 8.5 Hz, 2H), 7.35 (d, *J* = 8.7 Hz, 1H), 7.28 (s, 2H), 7.20 (d, *J* = 2.3 Hz, 1H), 6.78 (dd, *J* = 8.7, 2.3 Hz, 1H), 6.70 (d, *J* = 8.7 Hz, 2H), 6.62 (d, *J* = 8.5 Hz, 2H), 4.13 (t, *J* = 5.5 Hz, 2H), 3.92 (t, *J* = 6.1 Hz, 2H), 3.67 (s, 3H), 2.86 (t, *J* = 5.6 Hz, 2H), 2.65 (s, 4H), 2.48 (t, *J* = 7.3 Hz, 2H), 2.06 (p, *J* = 6.7 Hz, 2H), 1.69 (p, *J* = 5.7 Hz, 4H), 1.48 (s, 2H).

¹³C NMR (126 MHz, CDCl₃) δ 193.54, 173.68, 162.52, 158.89, 154.51, 141.86, 140.09, 133.37, 132.29, 130.58, 130.43, 130.16, 126.07, 123.99, 115.27, 114.58, 114.13, 107.42, 66.69, 64.99, 57.51, 54.93, 51.69, 30.51, 24.92, 24.53, 23.60.

HRMS (ESI) calc. for C₃₃H₃₆NO₆S (M + H)⁺: 574.2254. Found: 574.2258.

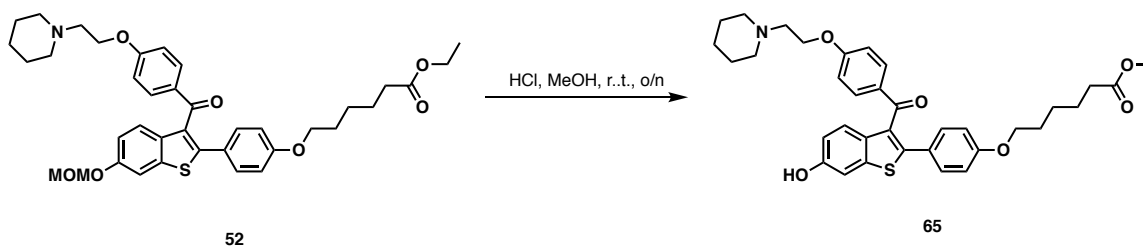


methyl 5-(4-(6-hydroxy-3-(4-(2-(piperidin-1-yl)ethoxy)benzoyl)benzo[b]thiophen-2-yl)phenoxy)pentanoate (64): Three drops of concentrated HCl was added to a 1.00-mL solution of ether **51** (49.0 mg, 0.0700 mmol, 1 equiv) in MeOH. The reaction was stirred at room temperature overnight. In the morning, 10.0 mL of H₂O was added and the product was extracted with EtOAc (3 x 5.00 mL). The combined organic layers were washed with brine, dried over MgSO₄, filtered, and concentrated to give the phenol **64** was isolated as a yellow oil and was used immediately without further purification.

¹H NMR (500 MHz, CDCl₃) δ 7.75 – 7.71 (m, 2H), 7.41 (d, *J* = 8.7 Hz, 1H), 7.32 – 7.28 (m, 2H), 7.24 (d, *J* = 2.3 Hz, 1H), 6.84 (dd, *J* = 8.8, 2.3 Hz, 1H), 6.74 – 6.66 (m, 4H), 4.13 (t, *J* = 5.6 Hz, 2H), 3.92 – 3.88 (m, 2H), 3.66 (s, 3H), 2.80 (t, *J* = 5.8 Hz, 2H), 2.56 (s, 4H), 2.38 (dq, *J* = 5.6, 3.0, 2.2 Hz, 2H), 1.78 (h, *J* = 2.8 Hz, 4H), 1.64 (p, *J* = 5.6 Hz, 4H), 1.46 (s, 2H).

¹³C NMR (126 MHz, CDCl₃) δ 193.17, 173.93, 161.01, 159.11, 154.30, 142.73, 140.08, 133.57, 132.43, 131.48, 130.25, 130.13, 125.87, 124.01, 115.13, 114.63, 114.19, 107.40, 67.43, 62.91, 56.22, 54.18, 51.60, 33.65, 28.57, 22.71, 21.80, 21.58.

HRMS (ESI) calc. for C₃₄H₃₈NO₆S (M + H)⁺: 588.2394. Found: 588.2414.



methyl 6-(4-(6-hydroxy-3-(4-(2-(piperidin-1-yl)ethoxy)benzoyl)benzo[*b*]thiophen-2-yl)phenoxy)hexanoate (65): 3 drops of concentrated HCl was added to a 1.00-mL solution of ether **52** (57.0 mg, 0.0800 mmol, 1 equiv) in MeOH. The reaction was stirred at room temperature overnight. In the morning, 10.0 mL of H₂O was added and the product was extracted with EtOAc (3 x 5.00 mL). The combined organic layers were washed with brine, dried over MgSO₄, filtered, and concentrated to give the phenol **65** was isolated as a yellow oil and was used immediately without further purification.

¹H NMR (500 MHz, CDCl₃) δ 7.71 – 7.67 (m, 2H), 7.36 (d, *J* = 8.7 Hz, 1H), 7.26 (s, 2H), 7.19 (d, *J* = 2.3 Hz, 1H), 6.79 (dd, *J* = 8.7, 2.3 Hz, 1H), 6.71 – 6.68 (m, 2H), 6.65 – 6.62 (m, 2H), 3.86 (t, *J* = 6.4 Hz, 2H), 3.65 (s, 3H), 2.82 (t, *J* = 5.6 Hz, 2H), 2.59 (s, 4H), 2.32 (t, *J* = 7.5 Hz, 3H), 1.77 – 1.61 (m, 9H), 1.49 – 1.42 (m, 4H).

3.2 HDAC Assay Protocol

Assay materials

Human recombinant HDAC1 and HDAC6 were purchased from Cayman Chemical Company with a SDS-PAGE purity of > 90% for both enzymes according to the supplier. HDAC substrate Ac-Leu-Gly-Lys(Ac)-AMC was synthesized as previously described.⁷ A stock solution of the substrate was made by dissolving in DMSO to 8 mM. For the assay, the stock solution was further diluted to with assay buffer (7.5 μM for HDAC1, 60 μM for HDAC6). Trypsin from porcine pancreas (25 g/L in 0.9% NaCl from Sigma-Aldrich) was diluted to 0.4 mg/mL with assay buffer for a stock solution. Assay buffer consisted of 50 mM Tris-OH, 137 mM NaCl, 2.7 mM KCl, 1 mM MgCl₂, and 1.7 vol% DMSO was brought to pH 8.0 before adding 0.5 mg/mL of bovine serum albumin (cold ethanol precipitation,

96-99% by gel electrophoresis, Sigma). The assay buffer was passed through a 0.45 μm filter by syringe and refrigerated. All inhibitors were purified by reverse-phase preparative or semi-preparative HPLC (>95% purity at 254 nm). Stock solutions of inhibitors were made by dissolving 1 mg of inhibitor in 1 mL 50 v%v DMSO: assay buffer. Dilution series (10 concentrations) were prepared with assay buffer.

***In Vitro* HDAC Inhibition Assay Procedure**

For inhibition of recombinant human HDAC1 and HDAC6, dose-response experiments with internal controls were performed in black medium binding Fluorotrac 200 96-well plates from Greiner Bio-One. The appropriate dilution of inhibitor (10 μL at 5x the desired final concentration) was added to each well, followed by assay buffer (15 μL) with HDAC enzyme (HDAC1, 7.5 ng/well; HDAC6, 40 ng/well). Finally, assay buffer (25 μL) containing substrate Ac-Leu-Gly-Lys(Ac)-AMC (synthesized as previously described) was added to each well (3.75 μM for HDAC1; 30 μM for HDAC6). The plate was gently tapped and then developed at room temperature for 30 mins, at which time 50 μL of trypsin solution was added to all wells. The assay was developed for a further 30 mins. HDAC1 assays were performed in triplicate, while HDAC6 assays were performed in quadruplicate. Fluorescence emission was normalized using blanks, run in six replicates per plate, containing substrate (25 μL), assay buffer (25 μL), and trypsin (50 μL). Baseline fluorescence emission was normalized using controls, run in six replicates on each plate containing substrate (25 μL), HDAC (15 μL), assay buffer (10 μL), and trypsin (50 μL). Fluorescence measurements were taken on a Molecular Devices SpectraMax i3x plate reader using 6 scans per well with respective excitation and emission wavelengths of 360 and 460 nm (15 nm bandwidth). IC₅₀ values were calculated by nonlinear regression using a sigmoidal 4PL analysis with GraphPad Prism 8.2.

3.3 ER Assay Protocols

Cell lines, plasmids and reagents:

Cell lines were purchased from the American Type Culture Collection (ATCC) and maintained in a humidified 37°C, 5% CO₂ incubator. HEK293T cells were maintained in Dulbecco's modified Eagle's Media (DMEM, Wisent) supplemented with 10% Fetal Bovine Serum (FBS, Sigma) and 100 UI/mL penicillin-streptomycin (Wisent).

The transfection reagent linear polyethylenimine (PEI) was ordered from Polysciences, Inc. 17 β -estradiol (E2) and suberoylanilide hydroxamic acid (SAHA) were purchased from Sigma, 4-hydroxytamoxifen (4-OHT) and raloxifene were purchased from Tocris.

Vectors for Bioluminescence Resonance Energy Transfer (BRET) assays were generated by David Cotnoir-White at IRIC⁶. Donor pcDNA3.1-ER α -RLucII was obtained by cloning Renilla Luciferase II (RLucII) to the C-terminus of human estrogen receptor α (ER α). Acceptor pEYFP-N2- mVenus-(LXXLL)₂-NLS₂-mVenus was obtained by fusing two copies of YFP (Venus) at the N- and C-termini of a tandem LXXLF motif from aa 641-645 of human NCOA2 (Nuclear Receptor Coactivator 2) and of a tandem of the glucocorticoid receptor nuclear localization signal (NLS, amino acids 467-503).

Cell transfection

Before each experiment, cells were switched for 48 h in DMEM without phenol red, supplemented with 10% charcoal-dextran-stripped FBS and 4 mM L-glutamine. Cells were seeded at 15 million of cells per 15 cm² plates and co-transfected with 150 ng of pcDNA3.1-ER α -RLucII either alone (for background evaluation) or together with 6 μ g of pEYFP-N2- mVenus-(LXXLL)₂-NLS₂-mVenus in 1 ml of PBS and completed to 15 μ g with salmon sperm DNA. Transient transfections were performed using PEI (3 μ g of linear PEI for each μ g of DNA diluted in PBS) that was mixed with DNA (1v/v, 2 mL total) and left for 12 min at room temperature. The PEI:DNA mixture was added to attached cells and changed after 16h. Cells were harvested 2 days after transfection in Hank's Balanced Salt Solution (HBSS) supplemented with 4.5 g/L dextrose, seeded in a 96-well white plate

(Costar, Corning) and immediately co-treated with 5 nM E2 and 10 μ M of tested compounds in triplicates for 45 min before BRET assays.

BRET Assays

Coelenterazine H (Coel-h, Nanolight Technology) was added to each well to a final concentration of 5 μ M and incubated for 5 min at room temperature protected from light. Readings were then collected using a MITHRAS LB940 (Berthold Technology) multidetector plate reader, allowing the sequential integration of the signals detected in the 485/20 nm and 530/25 nm windows, for luciferase and YFP light emissions, respectively. The BRET signal was determined by calculating the ratio of the light intensity emitted by the YFP fusion over the light intensity emitted by the Luc fusion. The values were corrected by subtracting the background BRET signal detected when the Luc fusion construct was expressed alone.

References

1. Robertson, D. W.; Krushinski, J. H.; Beedle, E. E.; Wyss, V.; Pollock, G. D.; Hayes, J. S., *Eur. J. Med. Chem.* **1986**, *21* (3), 223-229.
2. Cerminara, I.; D'Alessio, L.; D'Auria, M.; Funicello, M.; Guarnaccio, A., *Helv. Chim. Acta* **2016**, *99* (5), 384-392.
3. Sall, D. J.; Bailey, D. L.; Bastian, J. A.; Buben, J. A.; Chirgadze, N. Y.; Clemens-Smith, A. C.; Denney, M. L.; Fisher, M. J.; Giera, D. D.; Gifford-Moore, D. S.; Harper, R. W.; Johnson, L. M.; Klimkowski, V. J.; Kohn, T. J.; Lin, H.-S.; McCowan, J. R.; Palkowitz, A. D.; Richett, M. E.; Smith, G. F.; Snyder, D. W.; Takeuchi, K.; Toth, J. E.; Zhang, M., *The Journal of Medicinal Chemistry* **2000**, *43*, 649-663.
4. Molander, G. A.; Felix, L. A., *JOC* **2005**, *70*, 3950-3956.
5. Lambert, J. D.; Rice, J. E.; Hong, J.; Hou, Z.; Yang, C. S., *Bioorg Med Chem Lett* **2005**, *15* (4), 873-6.
6. Cotnoir-White, D.; El Ezzy, M.; Boulay, P. L.; Rozendaal, M.; Bouvier, M.; Gagnon, E.; Mader, S., *Proc Natl Acad Sci U S A* **2018**, *115* (11), E2653-E2662.
7. Bradner, J. E.; West, N.; Grachan, M. L.; Greenberg, E. F.; Haggarty, S. J.; Warnow, T.; Mazitschek, R., *Nat Chem Biol* **2010**, *6* (3), 238-243.